NUREG/CR-3295
MEA-2017
Vol. 1

Light Water Reactor Pressure Vessel Surveillance Dosimetry Improvement Program

Notch Ductility and Fracture Toughness Degradation of A 302-B and A 533-B Reference Plates from PSF Simulated Surveillance and Through-Wall Irradiation Capsules

Prepared by J. R. Hawthorne, B. H. Menke, A. L. Hiser

Materials Engineering Associates, Inc.

ENSA, Inc.

Prepared for
U.S. Nuclear Regulatory Commission

NOTICE

This report was prepared as an account of work sponsored by an agency of the United States Government. Neither the United States Government nor any agency thereof, or any of their employees, makes any warranty, expressed or implied, or assumes any legal liability of responsibility for any third party's use, or the results of such use, of any information, apparatus, product or process disclosed in this report, or represents that its use by such third party would not infringe privately owned rights.

NOTICE

Availability of Reference Materials Cited in NRC Publications

Most documents cited in NRC publications will be available from one of the following sources:

1. The NRC Public Document Room, 1717 H Street, N.W.
   Washington, DC 20555
2. The NRC/GPO Sales Program, U.S. Nuclear Regulatory Commission,
   Washington, DC 20555
3. The National Technical Information Service, Springfield, VA 22161

Although the listing that follows represents the majority of documents cited in NRC publications, it is not intended to be exhaustive.

Referenced documents available for inspection and copying for a fee from the NRC Public Document Room include NRC correspondence and internal NRC memoranda; NRC Office of Inspection and Enforcement bulletins, circulars, information notices, inspection and investigation notices; Licensee Event Reports; vendor reports and correspondence; Commission papers; and applicant and licensee documents and correspondence.

The following documents in the NUREG series are available for purchase from the NRC/GPO Sales Program: formal NRC staff and contractor reports, NRC-sponsored conference proceedings, and NRC booklets and brochures. Also available are Regulatory Guides, NRC regulations in the *Code of Federal Regulations*, and *Nuclear Regulatory Commission Issuances*.

Documents available from the National Technical Information Service include NUREG series reports and technical reports prepared by other federal agencies and reports prepared by the Atomic Energy Commission, forerunner agency to the Nuclear Regulatory Commission.

Documents available from public and special technical libraries include all open literature items, such as books, journal and periodical articles, and transactions. *Federal Register* notices, federal and state legislation, and congressional reports can usually be obtained from these libraries.

Documents such as theses, dissertations, foreign reports and translations, and non-NRC conference proceedings are available for purchase from the organization sponsoring the publication cited.

Single copies of NRC draft reports are available free, to the extent of supply, upon written request to the Division of Technical Information and Document Control, U.S. Nuclear Regulatory Commission, Washington, DC 20555.

Copies of industry codes and standards used in a substantive manner in the NRC regulatory process are maintained at the NRC Library, 7920 Norfolk Avenue, Bethesda, Maryland, and are available there for reference use by the public. Codes and standards are usually copyrighted and may be purchased from the originating organization or, if they are American National Standards, from the American National Standards Institute, 1430 Broadway, New York, NY 10018.

GPO Printed copy price: $5.00

NUREG/CR-3295
MEA-2017
Vol. 1
RF, R5

Light Water Reactor Pressure Vessel Surveillance Dosimetry Improvement Program

Notch Ductility and Fracture Toughness Degradation of A 302-B and A 533-B Reference Plates from PSF Simulated Surveillance and Through-Wall Irradiation Capsules

Manuscript Completed: May 1983
Date Published: April 1984

Prepared by
J. R. Hawthorne, B. H. Menke, A. L. Hiser

Materials Engineering Associates, Inc.
9700 B George Palmer Highway
Lanham, MD 20706

Under Contract to:
ENSA, Inc.
3320 Bailey Avenue
Buffalo, NY 14215

Prepared for
Division of Engineering Technology
Office of Nuclear Regulatory Research
U.S. Nuclear Regulatory Commission
Washington, D.C. 20555
NRC FIN B8133

ABSTRACT

The Light Water Reactor-Pressure Vessel Surveillance Dosimetry Improvement Program of the Nuclear Regulatory Commission (NRC) has irradiated Charpy-V, compact tension and tension test specimens of selected steels in a pressure vessel wall/thermal shield mock-up facility. The investigation is part of a broad NRC effort to develop key neutron physics-dosimetry-metallurgy correlations for making highly accurate projections of radiation-induced embrittlement to reactor vessels.

Mechanical properties data have been developed for two of the materials: the ASTM A302-B correlation monitor reference plate and the A533-B plate No. 03 from the NRC's Heavy Section Steel Technology Program. These results are presented together with an overview of specimen irradiation and testing procedures. Data comparisons are used to describe the observed toughness gradient produced by irradiation where fluences were typical of vessel end-of-life conditions. In addition, assessments are made of the relative irradiation effect at surveillance capsule vs. through-wall locations and the correspondence of Charpy-V vs. fracture toughness test methods in their independent descriptions of radiation-induced embrittlement.

Irradiation in the simulated surveillance capsule location was found to reproduce reasonably well the irradiation effect to vessel inner surface and quarter wall thickness positions. As expected, the adjustment of the ASME lower bound (i.e., dynamic) K_{IR} toughness curve by the radiation induced elevation of the Charpy-V 41 J and the compact specimen 100 MPa $\sqrt{m}$ temperatures was conservative when compared against the static toughness data. However, the temperature elevation of the C_v curve (41 J level) with irradiation frequently did not provide a conservative estimate of the temperature elevation defined by fracture toughness tests (100 MPa $\sqrt{m}$ level). On the other hand, correction of the fracture toughness data for lack of test specimen constraint (β_{Ic}-correction) results in transition temperature elevations less than the C_v 41 J elevations, in most cases. Overall, the toughness gradient observed between in-wall locations after irradiation was small for both materials; the difference between transition temperatures for wall surface vs. mid thickness locations was 31°C or less, independent of the test method used.

Candidate areas for future research investigation are discussed.

CONTENTS

CONTENTS

LIST OF FIGURES

Figure		Page

LIST OF TABLES

ACKNOWLEDGEMENTS

The authors express their appreciation to M. Vagins for helpful discussions, especially in the planning of postirradiation test matrices. They also thank C. Z. Serpan for his advice on overall program objectives and encouragement during the conduct of the investigation.

1. INTRODUCTION

One objective of the Light Water Reactor-Pressure Vessel (LWR-PV) Surveillance Dosimetry Program established by the Nuclear Regulatory Commission (NRC), is the development of key information for the accurate projection of radiation-induced mechanical properties changes in reactor vessel walls (Refs. 1,2). The total effort represents a multi-laboratory program with international participation. MEA was given responsibility for the development and analysis of mechanical properties data required for the study.

Because the neutron energy spectrum incident to a vessel is both modified and attenuated as it passes through the vessel wall, the projection of in-depth property changes occurring in service is not a simple, straightforward task. The prediction of mechanical properties changes produced by irradiation normally requires both an understanding of the damaging portion of the neutron energy spectrum and the trend of the property degradation with total neutron exposure, i.e., fluence (n/cm^2). The correlation of property change with fluence is a nonlinear function and is highly influenced by steel metallurgy, especially composition (Refs. 3,4).

Vessel property changes typically are monitored using surveillance specimen irradiations internal to the vessel but outside of the fuel core (Ref. 5). Extrapolation of spectrum conditions at surveillance capsules and the relationship of mechanical property change data obtained from surveillance specimen tests to locations inside the vessel wall are aspects of the present research problem. Neutron flux (n/cm^2-sec) levels at surveillance test positions(s) can be as much as one order of magnitude higher than at the vessel inner wall. Moreover, extensive changes to the neutron spectral shape develop in transit through intermediate steel or water boundaries between the surveillance capsule location(s) and the vessel wall. Typically, the task of mechanical properties prediction reduces to three key components: proper and accurate definition of the neutron field, accurate projection of field attenuation, and proper estimation of steel response to the local field. For new vessels, a demonstrated technology is available for the routine production of highly radiation resistant steels and weld metals (Ref. 6). With such vessels, questions of appropriate neutron field descriptions and projection methods become academic to vessel integrity analyses. Therefore, the primary thrust of the NRC's study is to the older vessels, i.e., those which did not have the benefit of the new techology (pre 1972 vessels) (Ref. 4).

A pressure vessel mock-up facility was specially constructed for the Surveillance Dosimetry Program for through-wall neutron dosimetry investigations and through-wall neutron exposures of metallurgical specimens which jointly were to yield physics-dosimetry-metallurgy correlations. The facility, known as the Pool Side Facility (PSF), is located at the Oak Ridge Research Reactor (ORR) and simulates a relatively large segment of a reactor thermal shield and vessel wall (Ref. 2). Here, specimens can be irradiated in sealed capsules under closely controlled temperature conditions at simulated surveillance and through-wall locations. To date, five capsules have been irradiated at 288°C (Ref. 7). Two capsules (designated SSC-1 and SSC-2) respectively represent surveillance capsules taken from a pressurized water reactor plant after about 15 years and 30 years of operation, i.e., at plant mid-life and at plant end-of-life. The remaining three capsules (Wall 1, 2 and 3) represent vessel surface (OT), quarter wall thickness (1/4T) and half wall thickness (1/2T) positions. The lead factor, i.e., ratio of neutron flux levels, between the surveillance capsule location and the wall surface location is about eight for the particular PSF configuration used. The capsules contained mechanical test specimens of six pressure vessel materials from U.S.A. and overseas sources.

This report presents the results of mechanical properties determinations by MEA for the two reference plates included in the capsules. One plate is of A533-B steel (HSST Plate 03) and represents the primary candidate in recent vessel production. The second plate is of A302-B steel (ASTM Reference Correlation Monitor Plate) and represents early vessel manufacture. Plate properties established by MEA were Charpy-V (C_v) notch ductility, static fracture toughness (K_{Ic} and J-integral methods) and tensile strength properties. A companion report, in preparation, will provide the results for the remaining four materials (forgings, welds) from the same PSF capsules. Capsule space limitations precluded the irradiation of fracture toughness test specimens for these materials; accordingly, their results are being reported separately.

2. THE PSF FACILITY

Figures 2.1 and 2.2 are schematic illustrations of the PSF facility and show its spatial relationship to the ORR fuel core. In brief, the facility consists of a steel thermal shield (5.9 cm thick), a steel pressure vessel wall simulator (22.5 cm thick) and a void box representing the vessel exterior cavity. The components are located adjacent to but outside of the pressure vessel housing the reactor fuel core. The PSF configuration is positioned at an aluminum window in the side of the vessel specially provided by the original design for exterior-to-the vessel irradiations. The thermal shield is separated from the window by approximately 4 cm of water; the separation of the thermal shield and the vessel simulator is 12 cm. From Fig. 2.2, note that the simulated surveillance capsules are positioned at the thermal shield on the side away from the core. The wall capsules, on the other hand, are placed in cavities within the vessel simulator itself. Temperatures are independently controlled in both capsule types by a combination of resistance heaters and a flowing gas mixture. In the present series of capsules, specimen temperatures typically were held within 10°C of the target exposure temperature of 288°C. An exploded view of a typical capsule showing the general features of the units is provided in Fig. 2.3.

Additional details of the PSF facility and the bases for its particular design configuration are given in the various annual reports for the LWR-PV Surveillance Dosimetry Program issued by the program manager (Hanford Engineering Development Laboratory, HEDL) (Refs. 8-10). In addition to the PSF, an equivalent but lower power facility was built for testing neutron spectrum conditions and neutron transport codes for conditions of a "pure" (unperturbed) fuel core. This second facility, called the Poolside Critical Assembly (PCA), was used in combination with the PSF to obtain a high degree of confidence in the neutron flux conditions assigned to the five metallurgical specimen irradiations (Ref. 11).

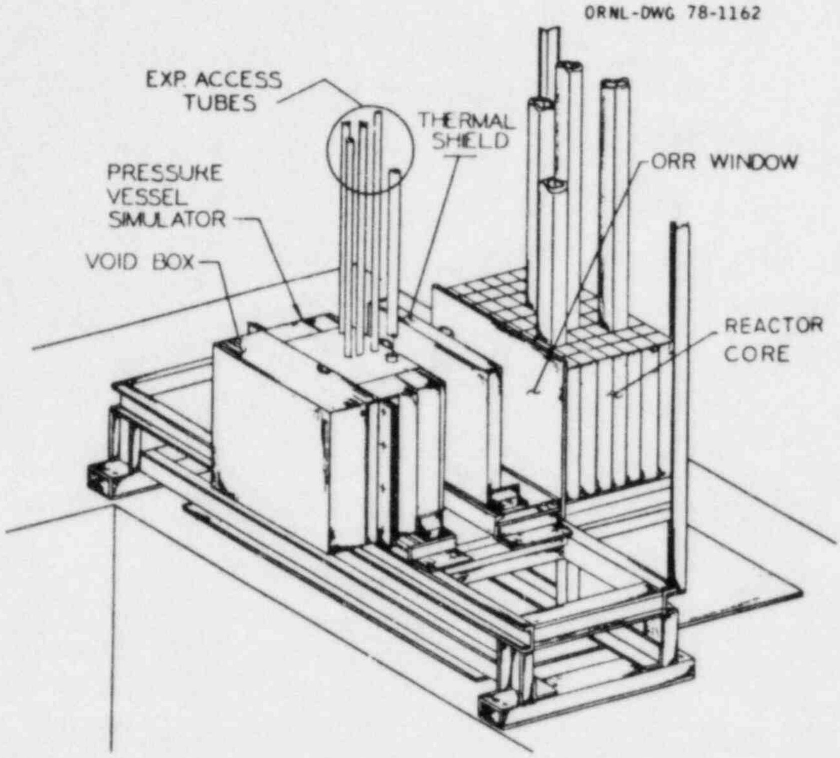

Fig. 2.1 Schematic illustration of PSF Facility. The pressure vessel simulator and the thermal shield are located outside of the aluminum pressure vessel (not shown) housing the reactor core (courtesy ORNL).

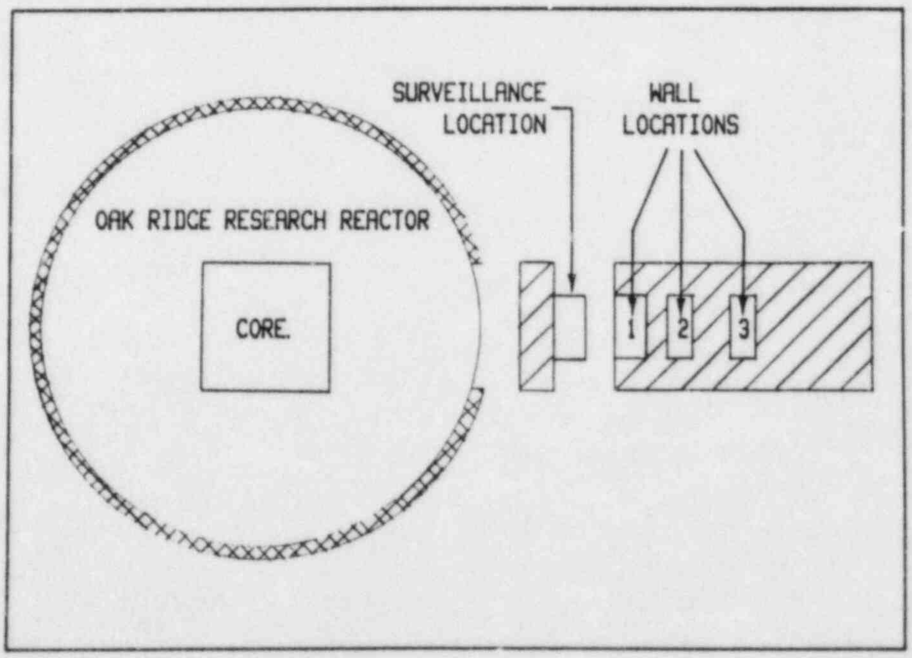

Fig. 2.2 Schematic illustration of the PSF Facility showing the locations of the specimen capsules in simulated surveillance and through-wall irradiation locations.

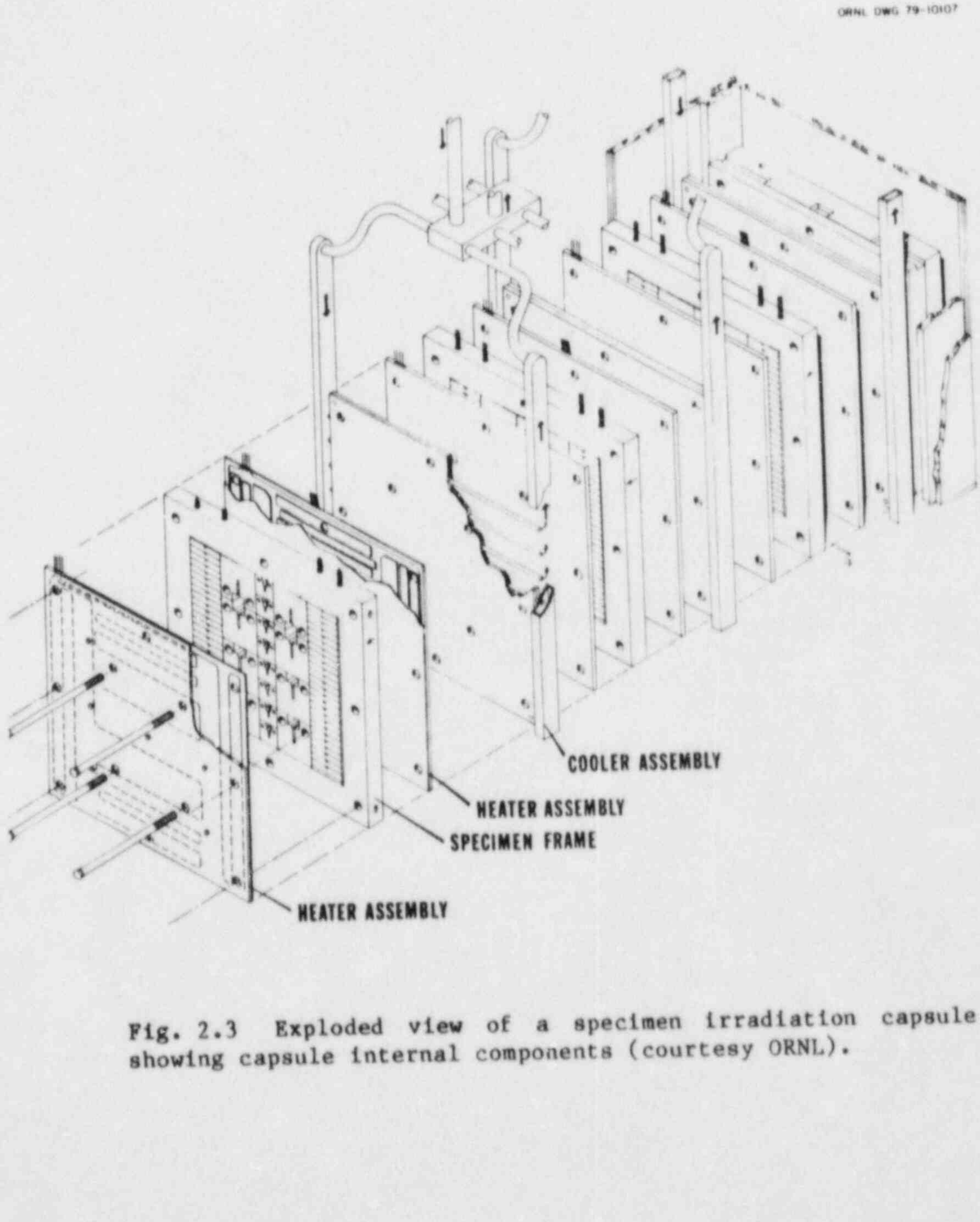

Fig. 2.3 Exploded view of a specimen irradiation capsule showing capsule internal components (courtesy ORNL).

3. MATERIALS

The reference plates are identified by composition, heat treatment and initial strength level in Tables 1 and 2 (Ref. 12, 13). The A302-B plate has seen extensive use in reactor vessel surveillance applications. References 12, 14, 15 and 16 contain extensive data compilations on notch ductility and fracture toughness properties of this plate before and after irradiation. The metallurgical history of the A533-B reference plate is given in detail in Ref. 13. This plate is serving as a reference material in the International Atomic Energy Agency's coordinated program on the behavior of advanced reactor pressure vessel steels under neutron irradiation (Ref. 17). Less extensive irradiation effects data are available in this case and are comprised largely of test reactor experiment findings (Refs. 18, 19).

It should be noted that the materials differ considerably in their content of copper (an impurity) and nickel (an alloying element). (See Tables 1 and 2.) A high copper content in pressure vessel steels is known to be detrimental to radiation embrittlement resistance at 288°C (Ref. 3,4). Nickel alloying in amounts of 0.4% Ni or more reinforces or magnifies the undesirable effect of copper on radiation resistance (Ref. 20). For new reactor vessels, the aim is to employ steels and weld metals having copper contents less than 0.10% Cu (Ref. 4). A low phosphorus content (0.010% max) also is known to be desirable for applications requiring superior radiation resistance (Ref. 3).

Table 1. Chemical Composition, Heat Treatment and Tensile Strength of A302-B Reference Plate (Code F23)

A. Chemical Composition (wt-%)

C	Mn	Si	P	S	Ni	Cr	Mo	Cu	Ti	Sn	V
0.24	1.34	0.23	0.011	0.023	0.18	0.11	0.51	0.20	0.015	0.037	0.001

B. Heat Treatment

899°C-6 h, water quenched;
649°C-6 h, air cooled

C. Tensile Strength (24°C)

Yield Strength* 481.9 MPa
Yield Strength Range 455 to 495 MPa (Ref. 12)
Ultimate Strength 659.8 MPa
Ultimate Strength Range 611 to 650 MPa (Ref. 12)

*Single determination

Table 2. Chemical Composition, Heat Treatment and Tensile Strength of A533-B Reference Plate (Codes 3PS,3PT, 3PU; HSST Plate 03)

A. Chemical Composition (wt-%)

C	Mn	Si	P	S	Ni	Cr	Mo	Cu
0.20	1.26	0.25	0.011	0.018	0.56	0.10	0.45	0.12

B. Heat Treatment

843 to 899°C-4 h, water quenched;
649 to 677°C-4 h, air cooled;
607 to 636°C-20 h, furnace cooled

C. Tensile Strength (24°C)*

Yield Strength 447.5, 458.5 MPa
Yield Strength 457, 460 MPa (Ref. 13)
Ultimate Strength 641.2, 641.2 MPa
Ultimate Strength 624, 626 MPa (Ref. 13)

* Duplicate tests

4. SPECIMEN DESIGNS

Standard Charpy-V (ASTM Type A) specimens, 12.7 mm and 25.4 mm thick compact tension specimens (0.5T-CT and 1T-CT) and 4.52 mm diameter tension specimens were selected for making notch ductility, fracture toughness and strength determinations, respectively. Specimen designs are shown in Figs. 4.1-4.4. The compact tension specimens were fatigue precracked in accordance with ASTM Standard E 399 specifications (Ref. 21) before irradiation. Here the 12.32 and 24.13 mm deep machined notches were extended by fatigue precracking to total notch depths (aim) of 13.59 and 26.57 mm, respectively, providing a final nominal crack depth-to-specimen width ratio (a/W) of 0.53. The stress intensity factor range, ΔK_f, for the last 0.76 mm of fatigue precracking was required to be less than 24 MPa $\sqrt{m}$. Side grooving of the CT specimens when used, was performed after irradiation.

The C_v and tensile specimens were removed from the 152 mm (6 in.) thick A302-B plate in two layers spanning the quarter thickness plane and from the 304 mm (12 in.) thick A533-B plate in four layers spanning the quarter thickness plane. The 0.5T-CT specimens were removed from both plates in two layers while the 1T-CT specimens were taken in one layer centered over the quarter thickness plane. For the A302-B plate, the specimens represent the longitudinal (LT, strong) test orientation. The decision to use the LT orientation and not the transverse (TL, weak) test orientation was to avoid a potential problem in postirradiation analysis stemming from the relatively low preirradiation C_v upper shelf level (~68 J) in the TL orientation. The upper shelf level of the A533-B plate in the TL direction in contrast, was sufficently high for specimens

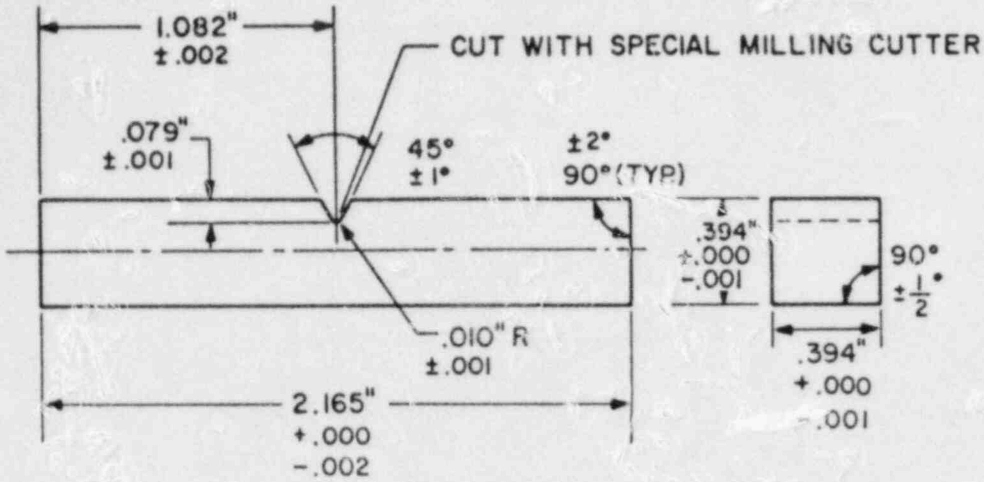

NOTE:

1. It is imperative that the identification number of each individual specimen be retained and that the orientation of the number be retained. The designator on the ends of each specimen serve also to locate the surface to be notched. With the identification number in an upright position, the top surface shall be the notched surface.
2. No irregularities in contour of apex of notch.
3. No. 8 Polish Micro-Inch Finish.

Fig. 4.1 Charpy V-notch specimen design. (Dimensions in inches, 1" = 2.54 cm.)

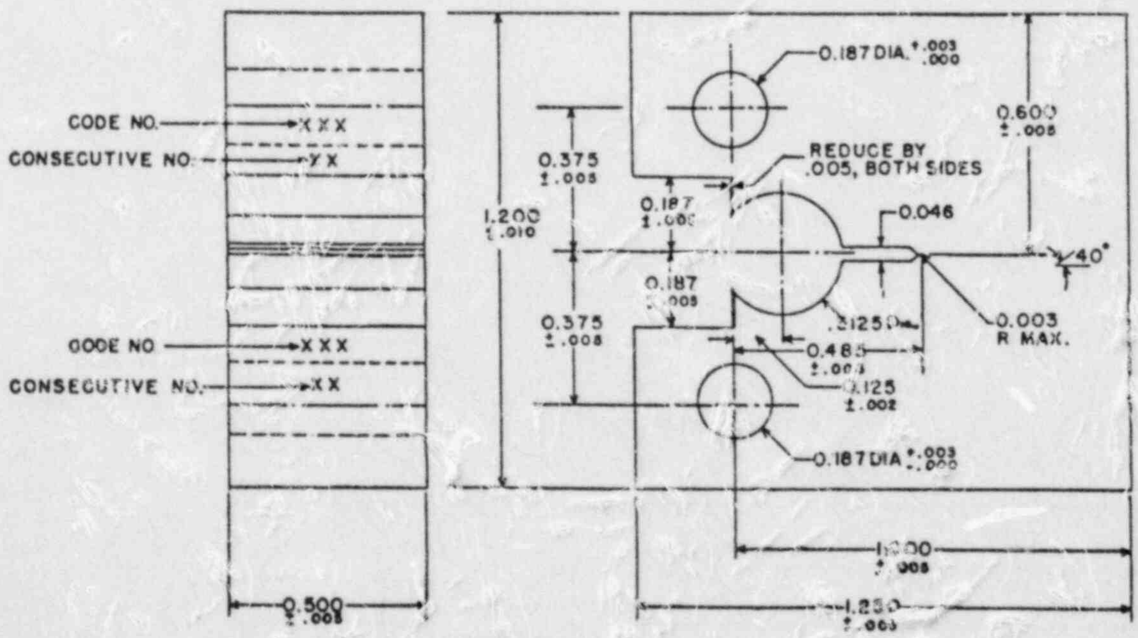

Fig. 4.2 0.5T-CT compact tension specimen design. (Dimensions in inches, 1 in. = 2.54 cm.)

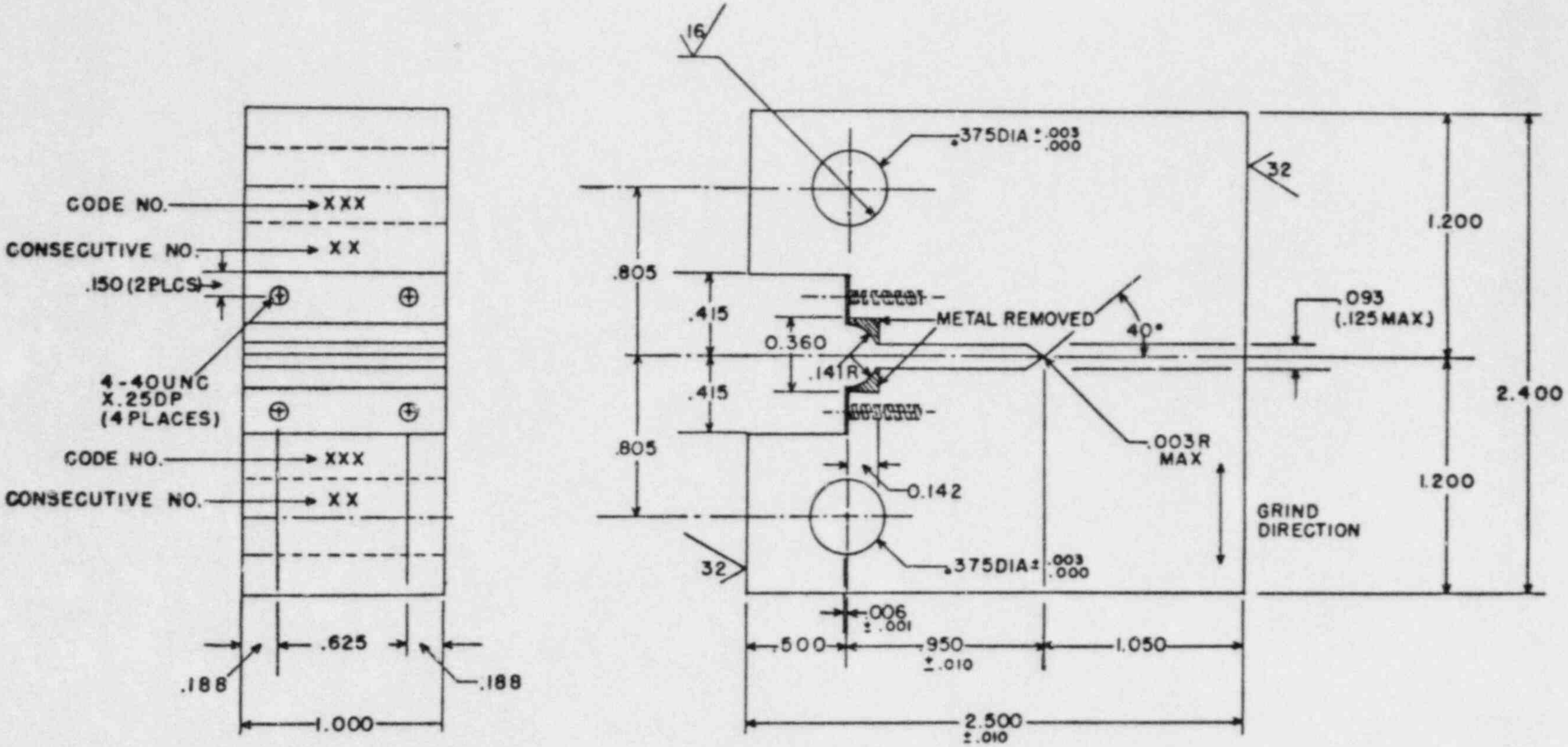

Fig. 4.3 1T-CT compact tension specimen design. (Dimensions in inches, 1 in. = 2.54 cm.)

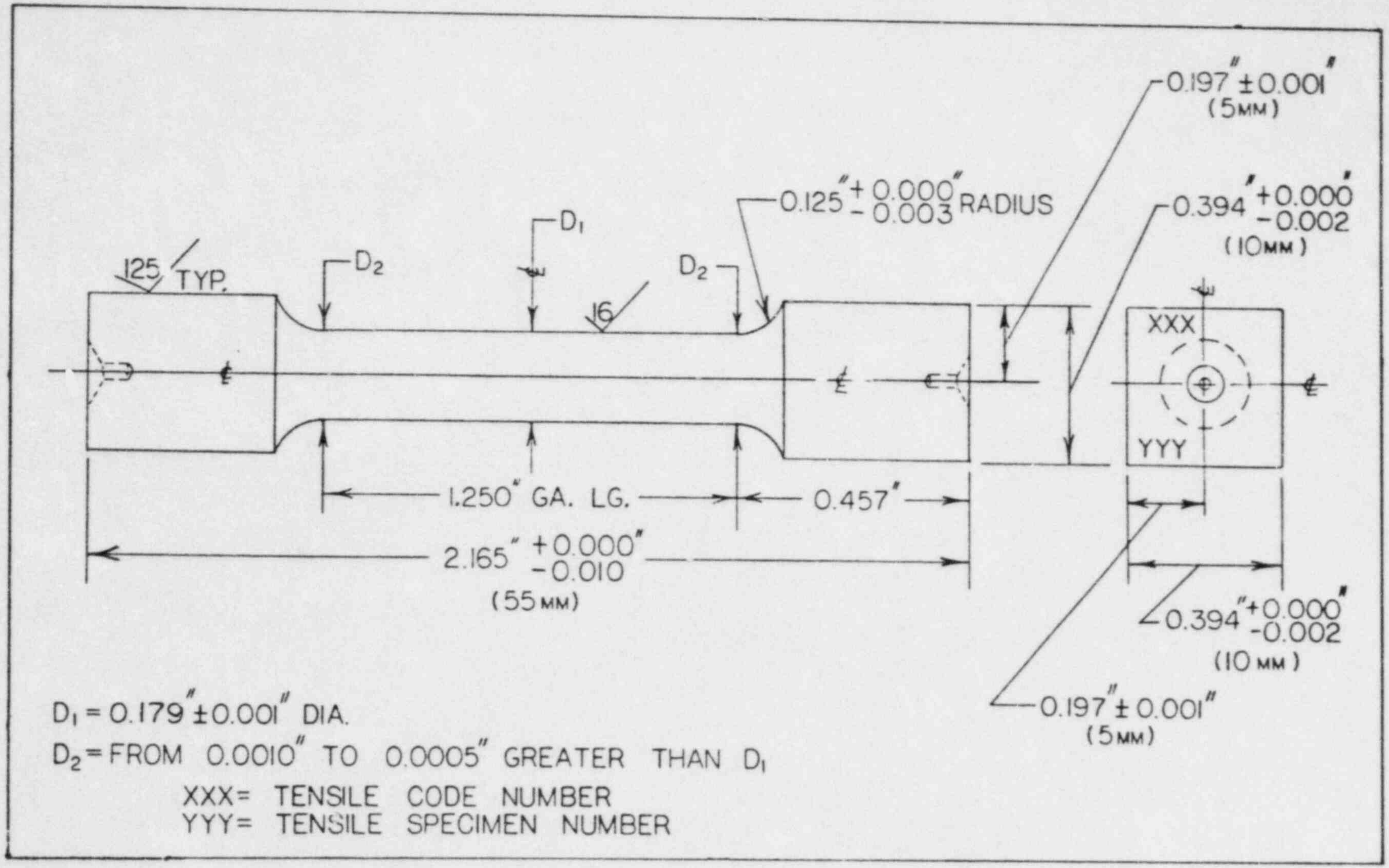

Fig. 4.4 Tension test specimen design. (Dimensions in inches, 1 in. = 2.54 cm.)

to be taken in this orientation. Currently, the TL orientation is that orientation selected for reactor vessel surveillance (Ref. 5).

For the irradiation of tensile specimens, close fitting steel shrouds were placed over the gage sections to aid heat transfer and to aid the uniformity of neutron flux conditions throughout the irradiation capsule. Likewise, filler plugs were placed in the notches and pin holes of the CT specimens.

5. MATERIAL IRRADIATION

Capsule construction, irradiation and disassembly operations were conducted by the Oak Ridge National Laboratory (ORNL) for the NRC. Primary responsibility for neutron dosimetry and fluence determinations is shared by ORNL and HEDL.

The irradiation histories and target fluence conditions of the five capsules are summarized in Table 3. The exposure time of capsule SSC-1 was adjusted to provide a fluence matching that of the Wall-2 capsule located in the quarter wall thickness position. The exposure time of capsule SSC-2 was similarly adjusted to match its fluence against that of the Wall-1 capsule located at the wall inner surface. The Wall-1, Wall-2 and Wall-3 capsules were irradiated simultaneously and were exposed for the same time period. In turn, the spread in fluences between these capsules reflect normal flux attenuation conditions through a vessel wall.

Table 3. Capsule Irradiation Conditions

Capsule No.	PSF Location	Irradiation Time (Hours at Power)	MW Hours Exposure	Target Neutron Fluence (n/cm^2, E > 1 MeV)
SSC-1	Thermal Shield	1,291	32,000	3×10^{19}
SSC-2	Thermal Shield	2,845	64,700	6×10^{19}
Wall-1	Simulator (Surface, OT)	18,748	430,000*	$\sim 6 \times 10^{19}$
Wall-2	Simulator (Quarter T)	18,748	430,000	3×10^{19}
Wall-3	Simulator (Half T)	18,748	430,000	$\sim 1.5 \times 10^{19}$

*Approximate

Specimen and material contents of the individual capsules are shown schematically in Figs. 5.1-5.5. Individual materials are identified by a code number. Code F23 was assigned to the A302-B plate. Code numbers 3PS, 3PT and 3PU designate the A533-B reference plate and, in fact, are code identifications carried over from the sectioning of the original plate (Ref. 13). Irradiation temperatures for all specimens are assumed to be 288°C for the data analyses presented in this report.

6. CHARPY-V ASSESSMENTS

6.1 Procedure

Tests were performed on two impact test machines verified for accuracy against calibration standards supplied by the Army Materials and Mechanics Research Center (AMMRC). One machine, located at the Naval Research Laboratory, was used for preirradiation condition (reference) tests and for tests of the capsule SSC-1 specimens. A second tester, located at the Nuclear Science and Technology Facility of the State University of New York (SUNY) at Buffalo, was used for the balance of the C_V specimens. The SSC-2, Wall-1, Wall-2 and Wall-3 specimens were tested concurrently.

Specimen energy absorption and lateral expansion were determined in each test; in addition, applied load vs. time-of-fracture records were made using a Dynatup system, for future NRC studies. Data listings for the two materials by capsule number are given in Appendix A. Preirradiation test results are illustrated in Figs. 6.1 and 6.2. Postirradiation energy absorption vs. temperature trends are compared against preirradiation results in Fig. 6.3-6.12. Figures showing lateral expansion vs. temperature trends are provided in Appendix B. The C_V 41 J temperature was used as the primary index of the brittle/ductile transition for making radiation-effects comparisons. Radiation-induced elevations of the C_V 68 J and C_V 0.89 mm transition temperatures were also determined. Observations for the materials are summarized in Tables 4 and 5.

6.2 Unirradiated Condition

Referring to Fig. 6.1, good agreement in properties between layer 1 and layer 2 is observed for the A302-B plate. This will be seen to have special importance to the postirradiation data analyses. The 41 J temperature is -4°C (25°F); the upper shelf energy level, taken at 260°C, is 108 J (80 ft-lb). Full shear fracture behavior developed at about 60°C at an average energy level of 103 J.

Tests of the A533-B plate (Fig. 6.2) showed a comparable transition temperature, -1°C (30°F), but a much higher upper shelf energy level, 150 J (111 ft-lb). Good agreement of properties between specimen layers is also found here. In the upper graph, the data suggest a slight increase in the lateral expansion value with temperature; however, the dashed line may be more descriptive of actual behavior in view of the "flat" upper shelf energy trend curve (lower graph).

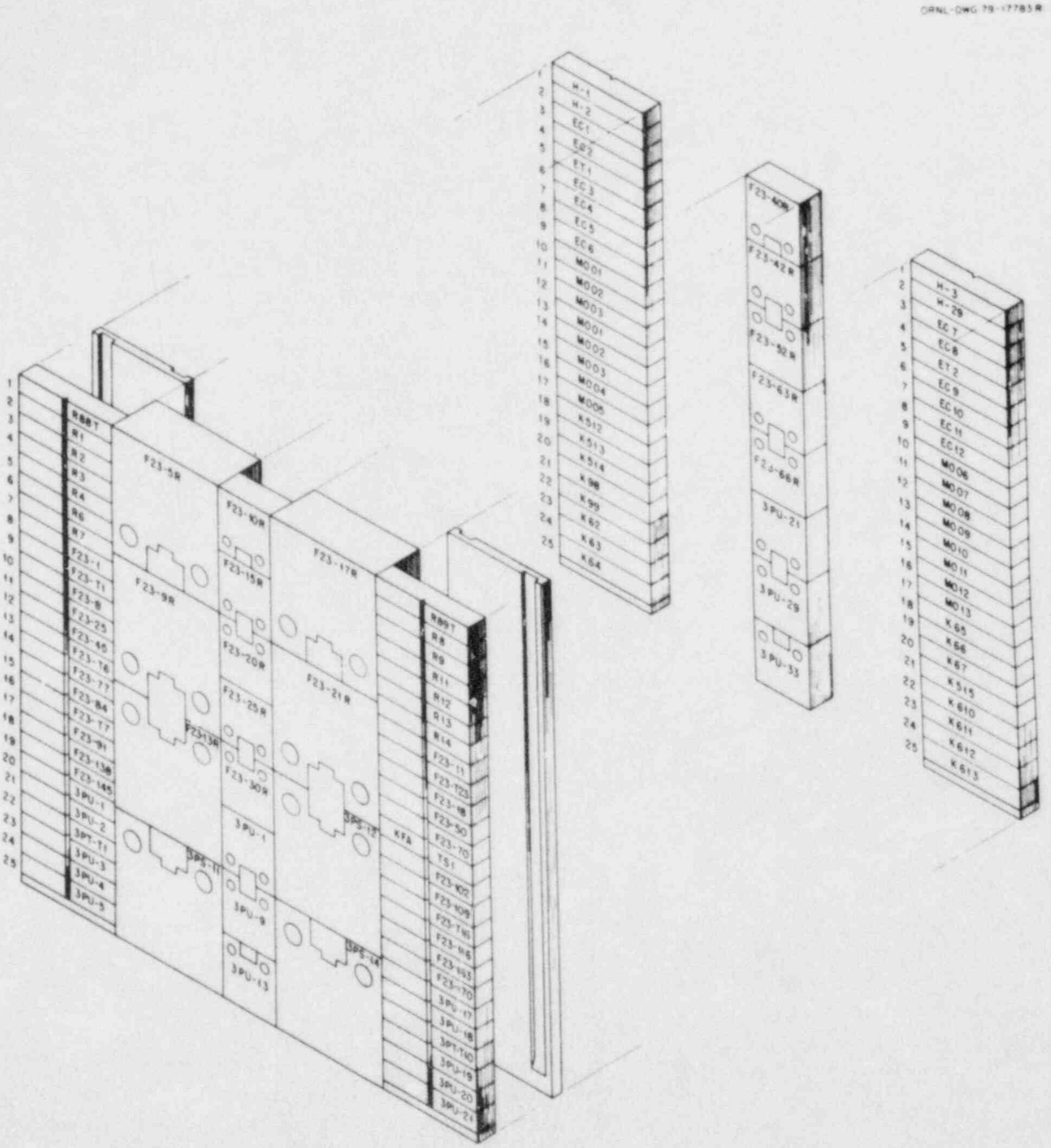

Fig. 5.1 C_V, CT and tension test specimen locations in the simulated surveillance capsule SSC-1 (courtesy ORNL). Tension test specimens are identified by the letter, T, in the specimen number.

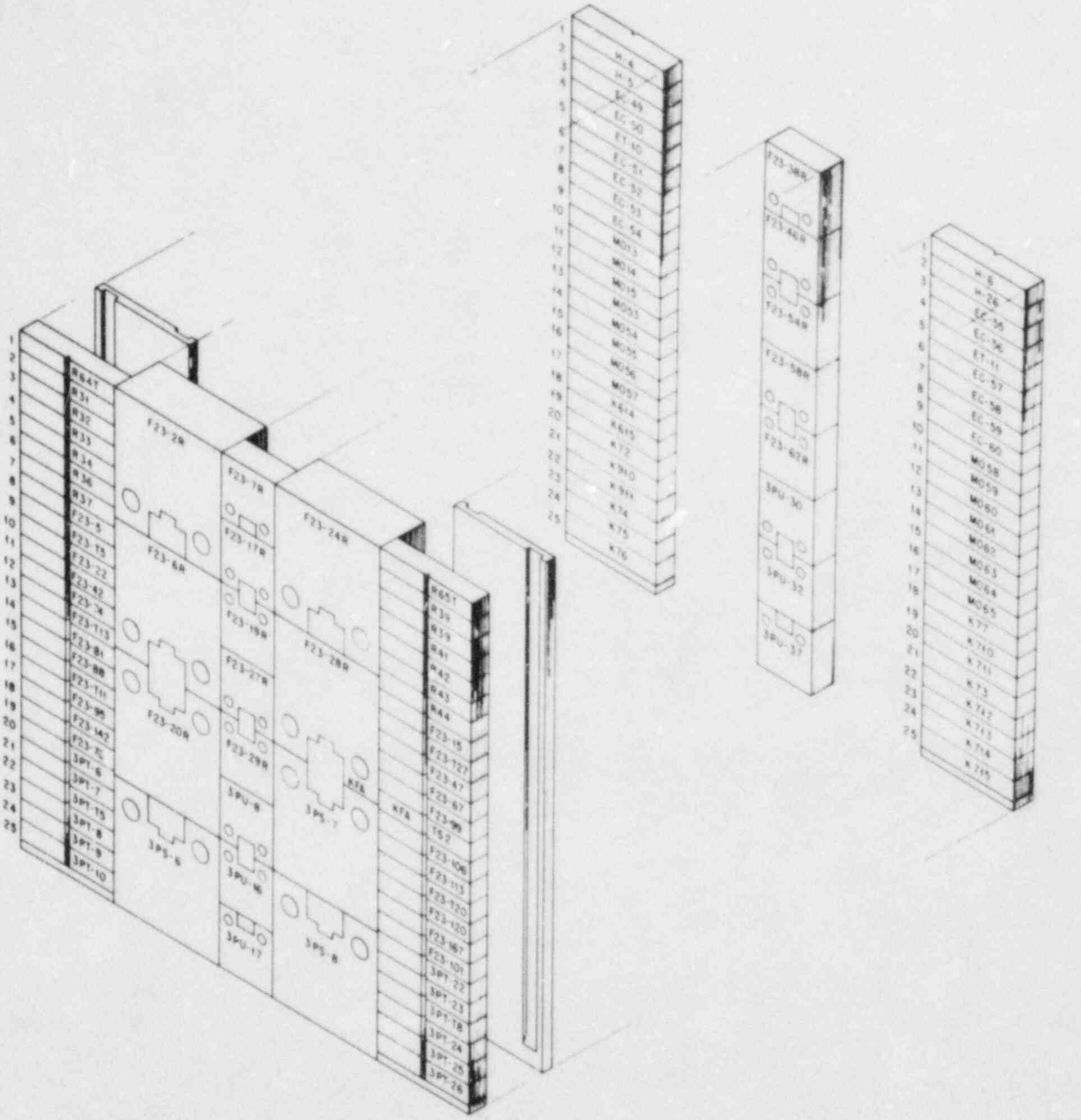

Fig. 5.2 C_V, CT and tension test specimen locations in the simulated surveillance capsule SSC-2 (Courtesy ORNL).

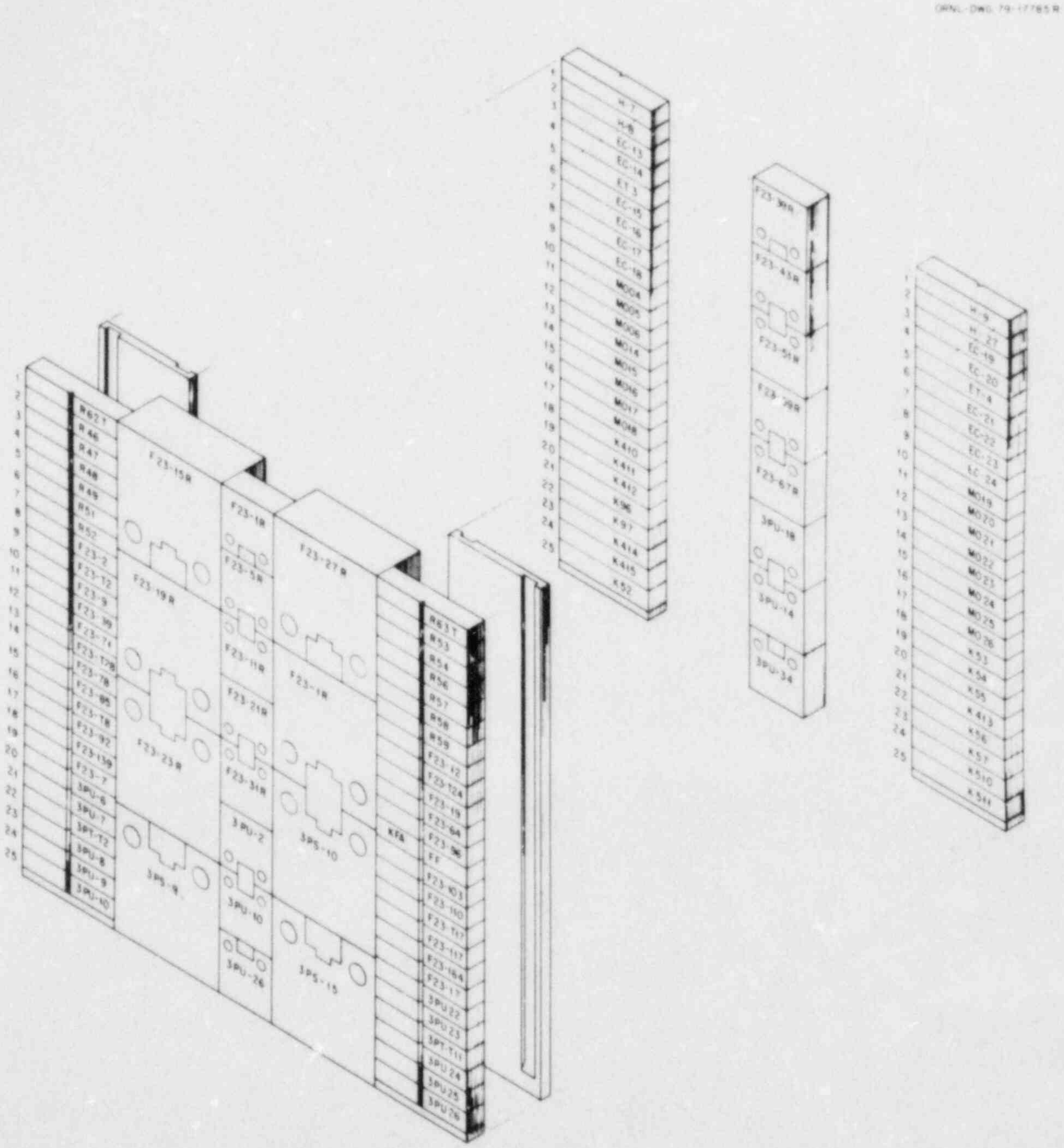

Fig. 5.3 C_v, CT and tension test specimen locations in the pressure vessel wall capsule W-1 (courtesy ORNL).

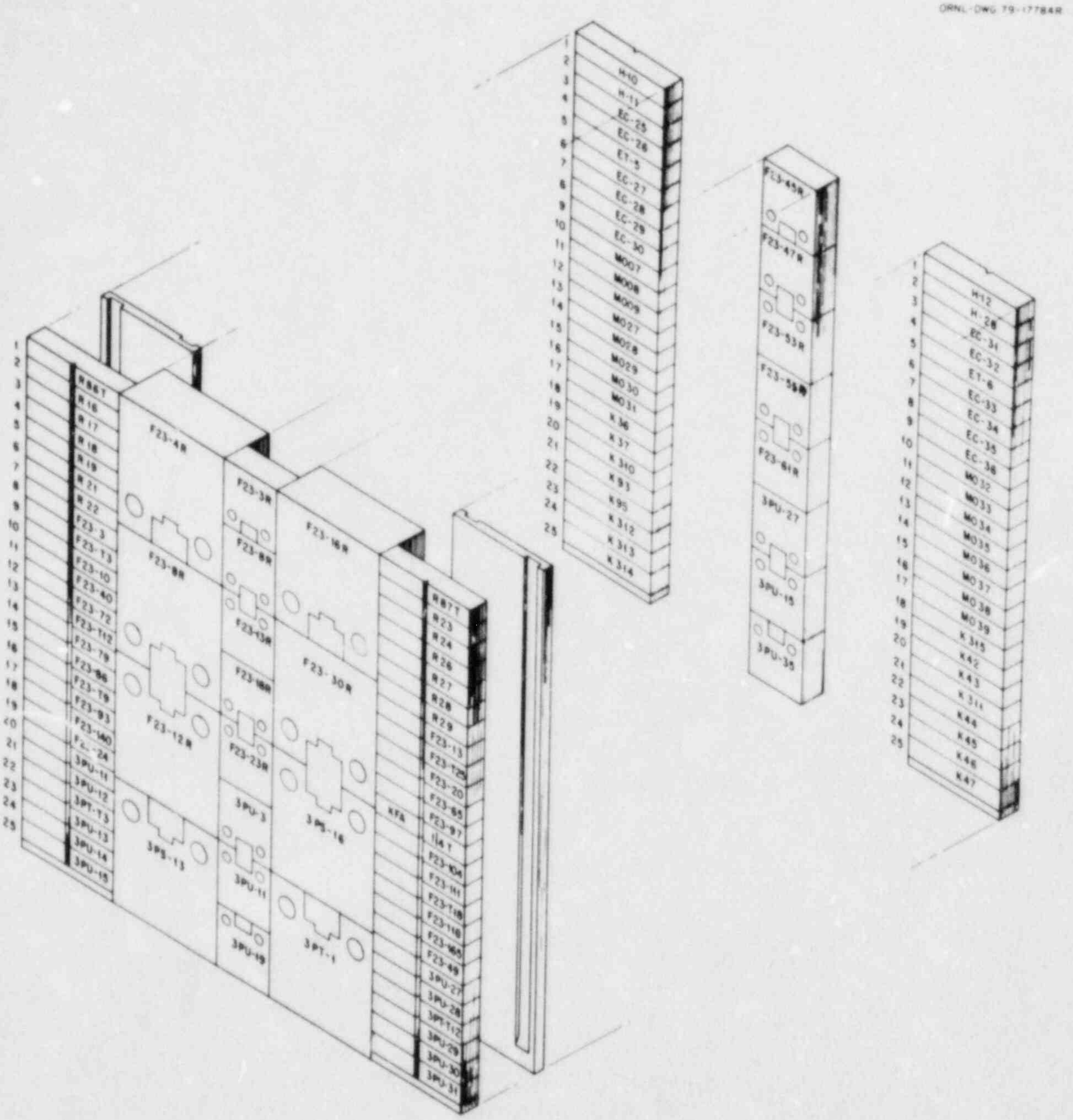

Fig. 5.4 C_v, CT and tension test specimen locations in the pressure vessel wall capsule W-2 (courtesy ORNL).

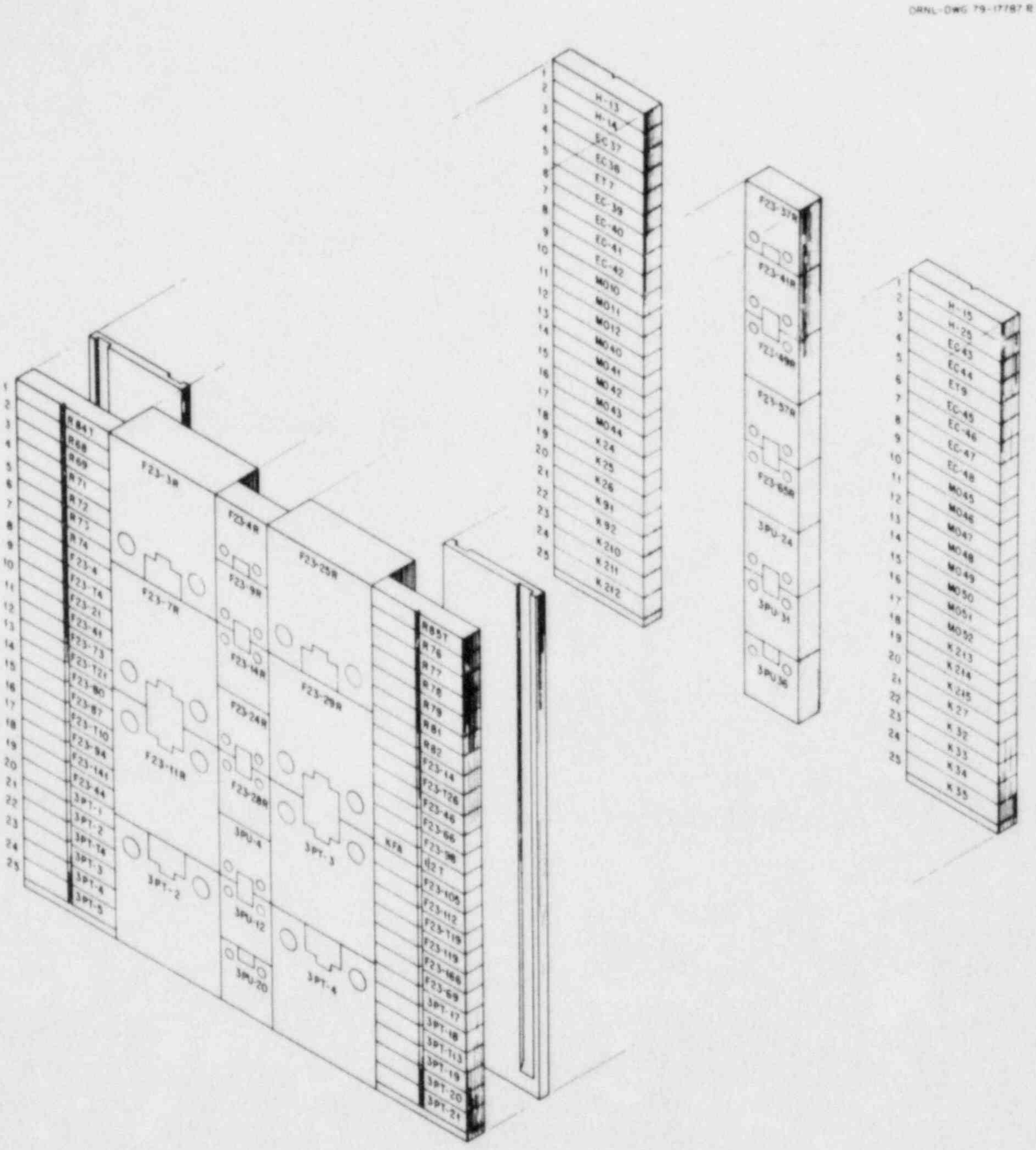

Fig. 5.5 C_V, CT and tension test specimen locations in the pressure vessel wall capsule W-3 (courtesy ORNL).

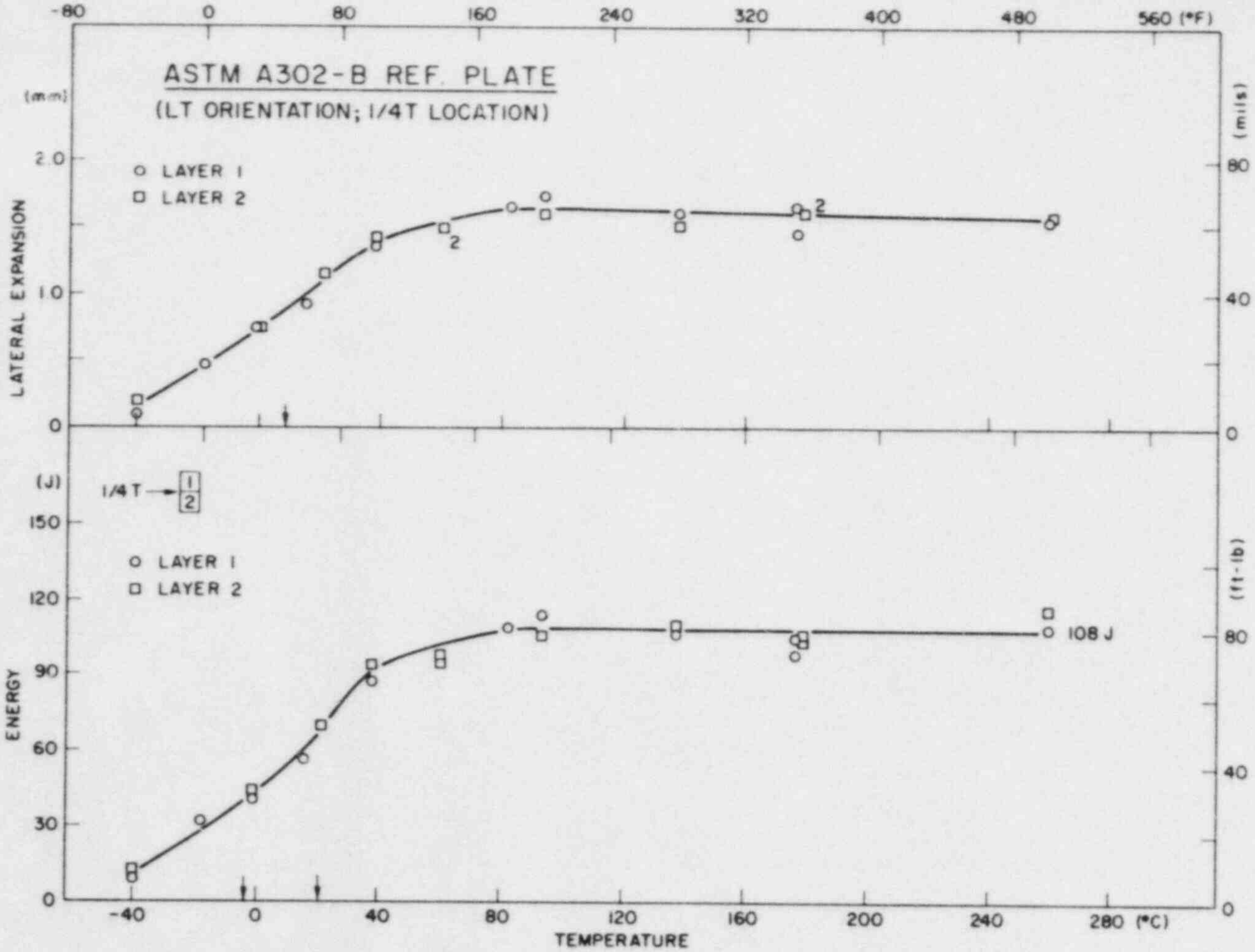

Fig. 6.1 Charpy-V notch ductility of the A302-B reference plate before irradiation. Specimens were selected at random from the total specimen complement fabricated for the study. The vertical arrows on the abscissa show the 41 J, 68 J or 0.89 mm transition temperatures.

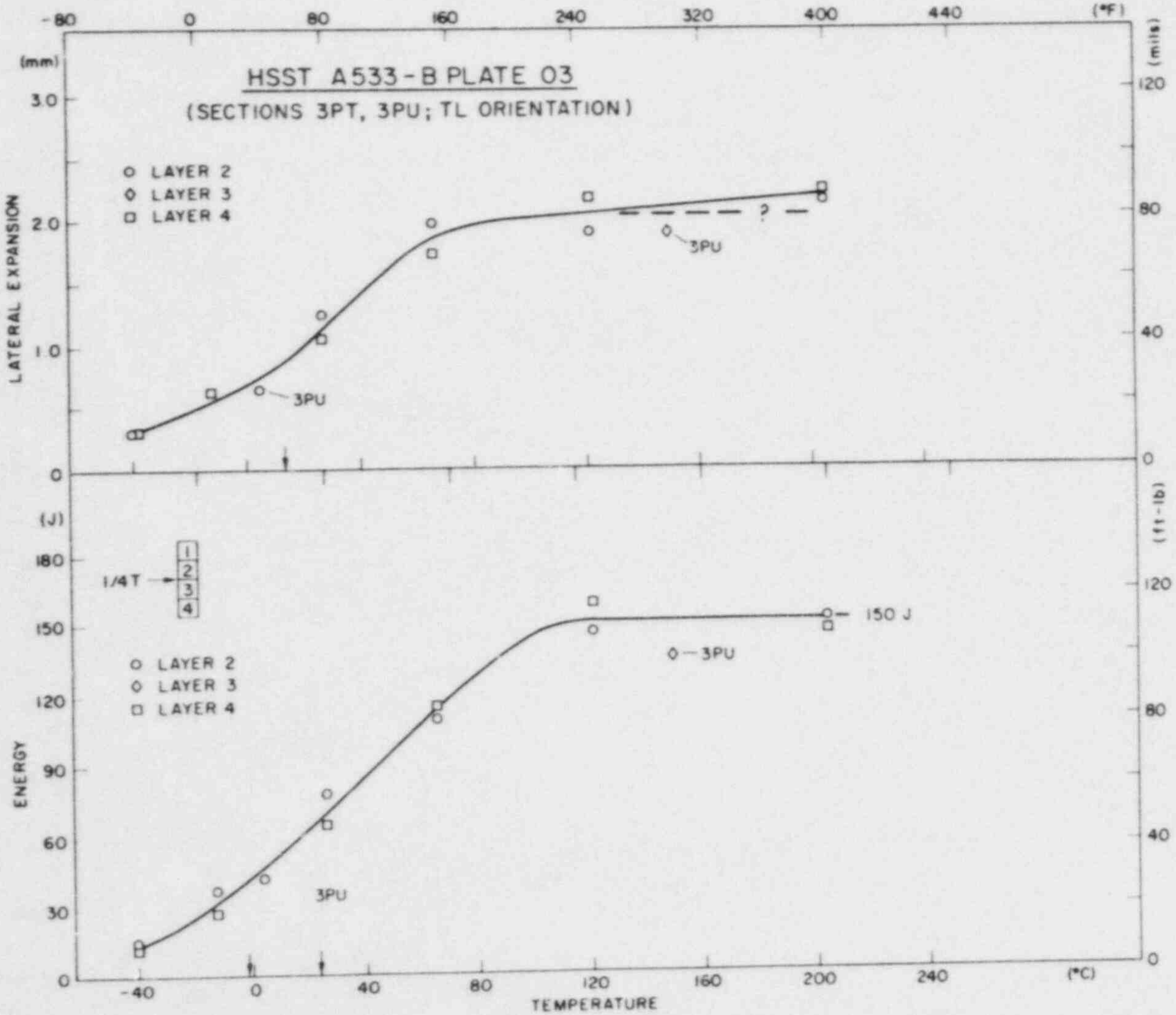

Fig. 6.2 Charpy-V notch ductility of the A533-B reference plate (HSST Program Plate 03) before irradiation. Sections 3PT and 3PU were adjoining blocks (152 x 152 mm x full thickness, each) in the main plate.

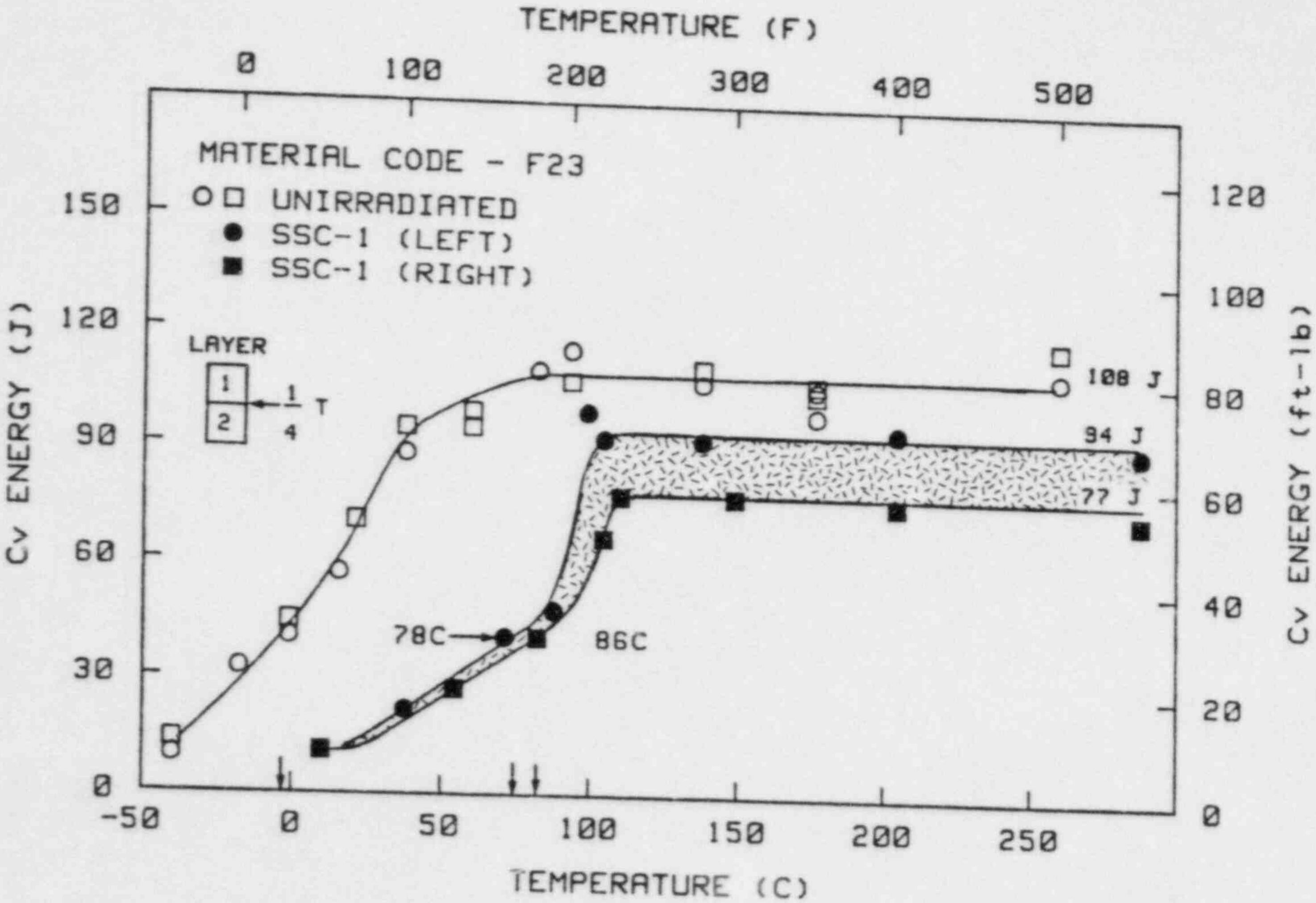

Fig. 6.3 Charpy-V notch ductility of the A302-B plate before and after irradiation in capsule SSC-1. The vertical arrows on the abscissa in this and subsequent figures point to 41 J transition temperatures.

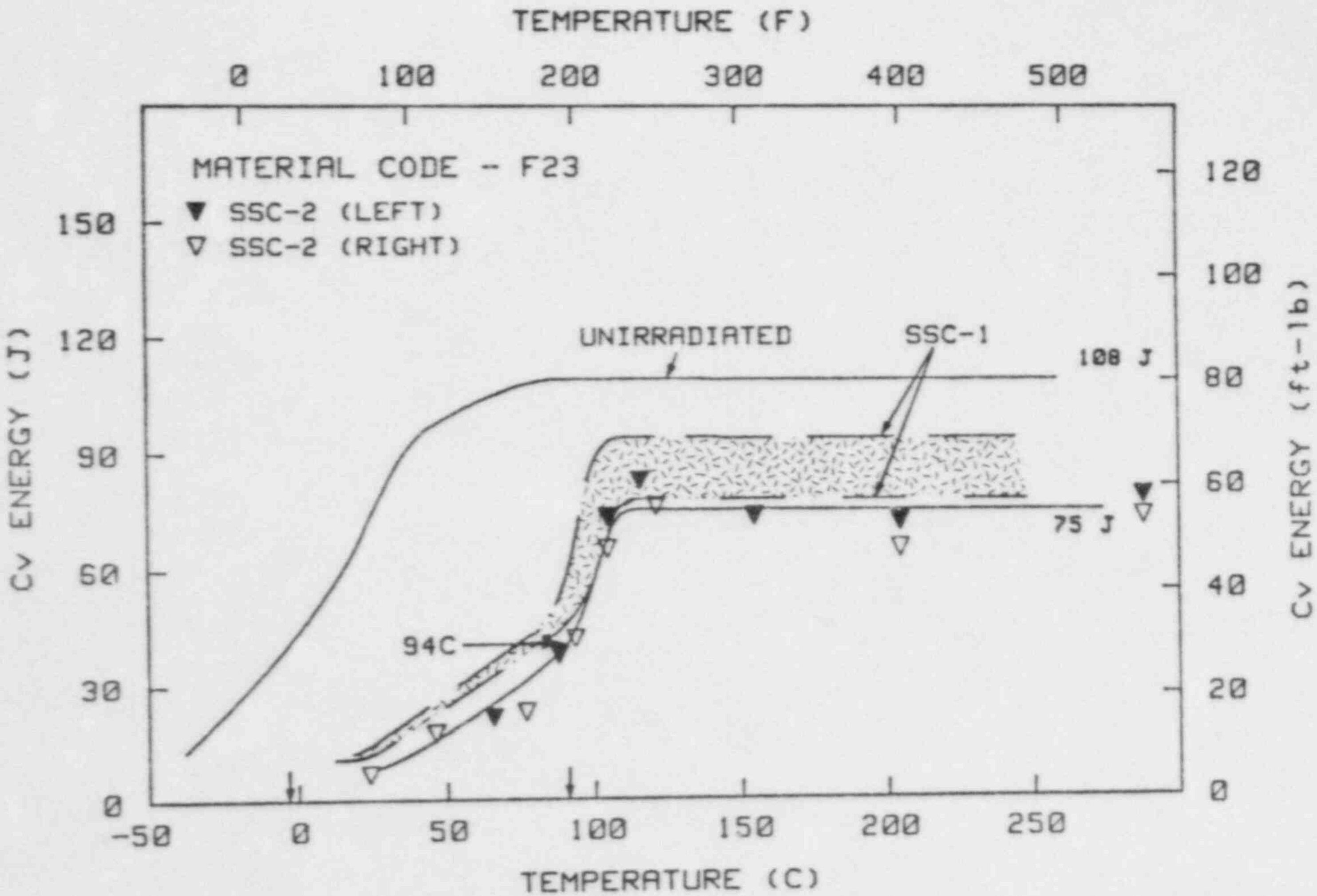

Fig. 6.4 Charpy-V notch ductility of the A302-B plate before and after irradiation in capsule SSC-2.

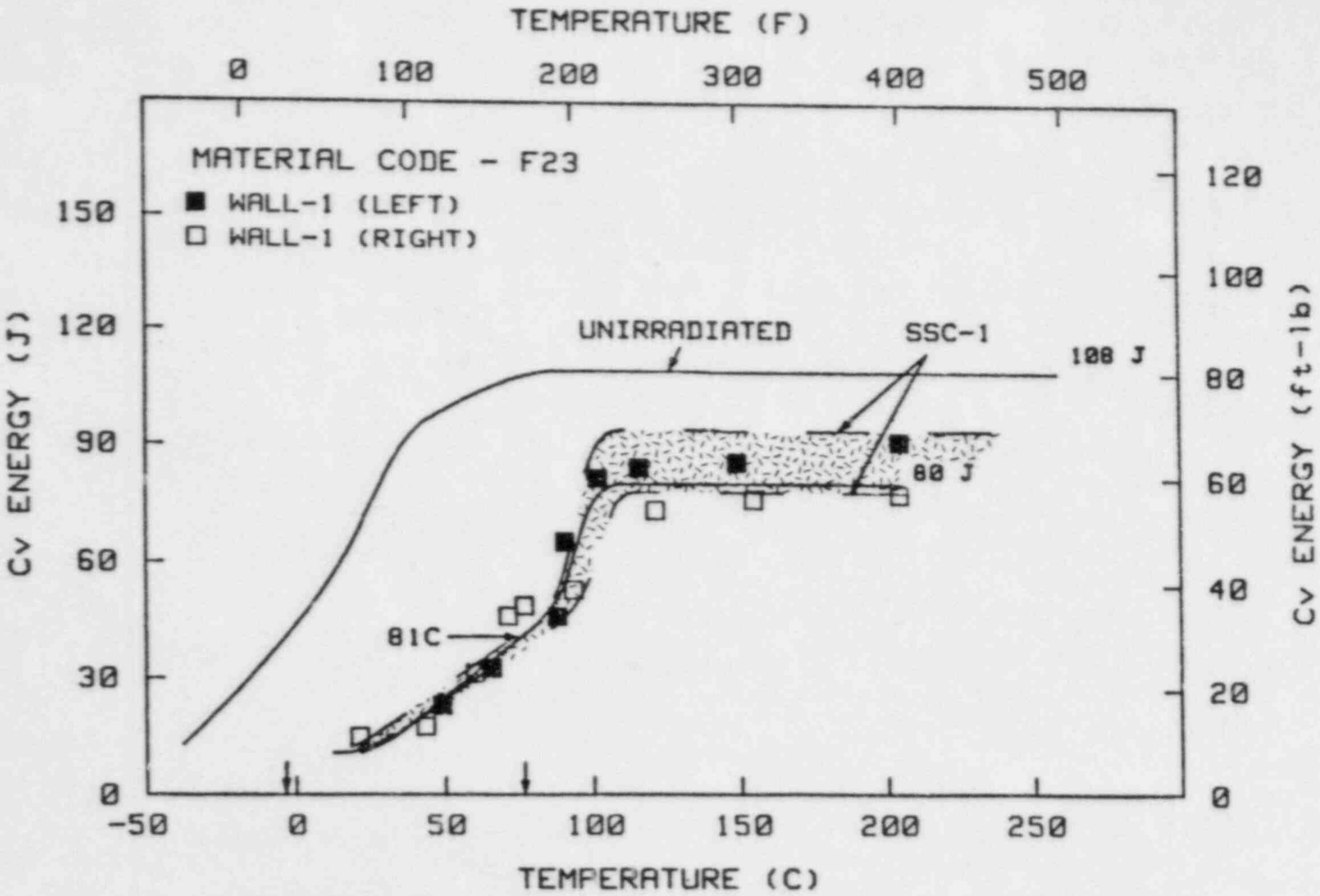

Fig. 6.5 Charpy-V notch ductility of the A302-B plate before and after irradiation in capsule Wall-1.

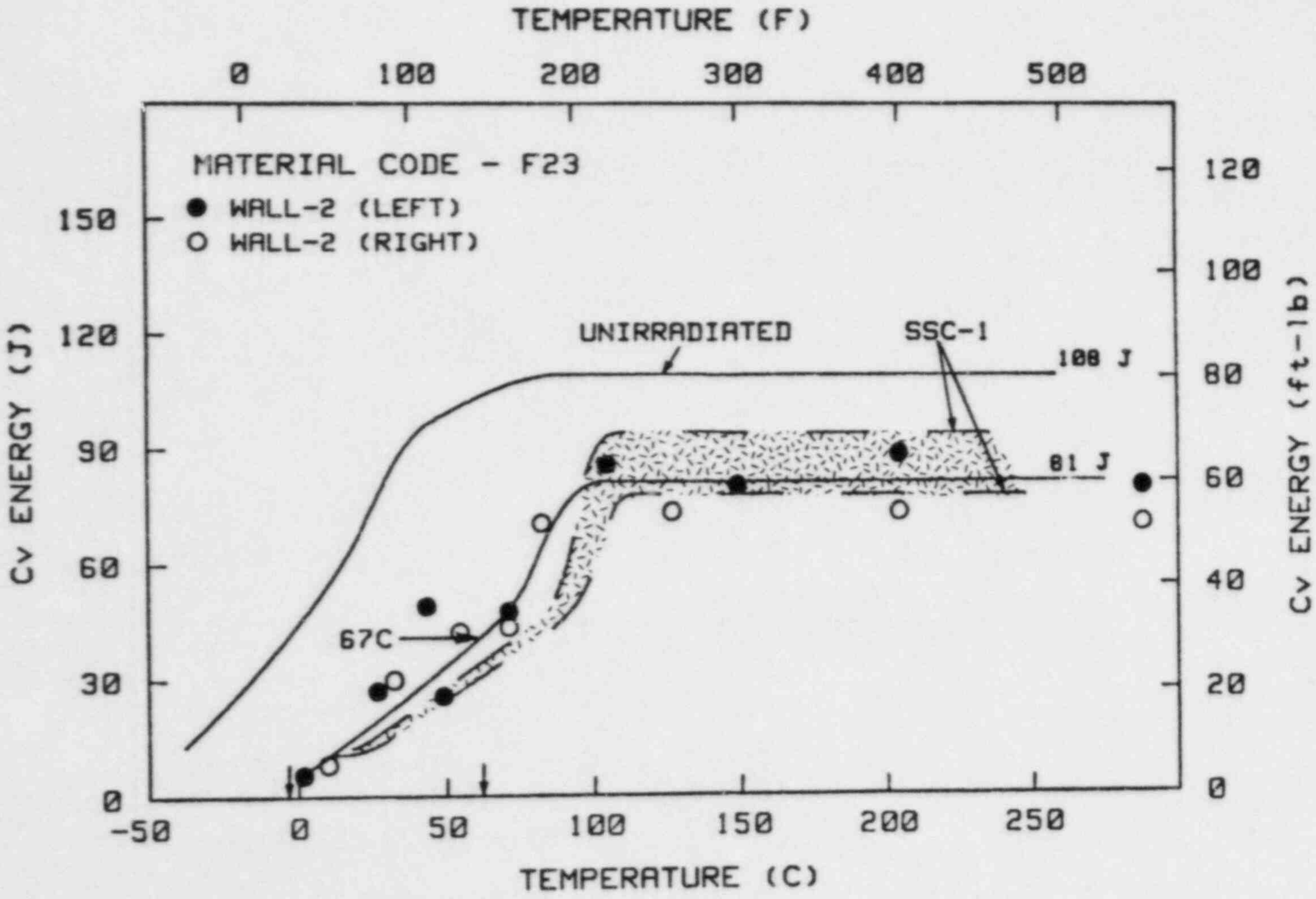

Fig. 6.6 Charpy-V notch ductility of the A302-B plate before and after irradiation in capsule Wall-2.

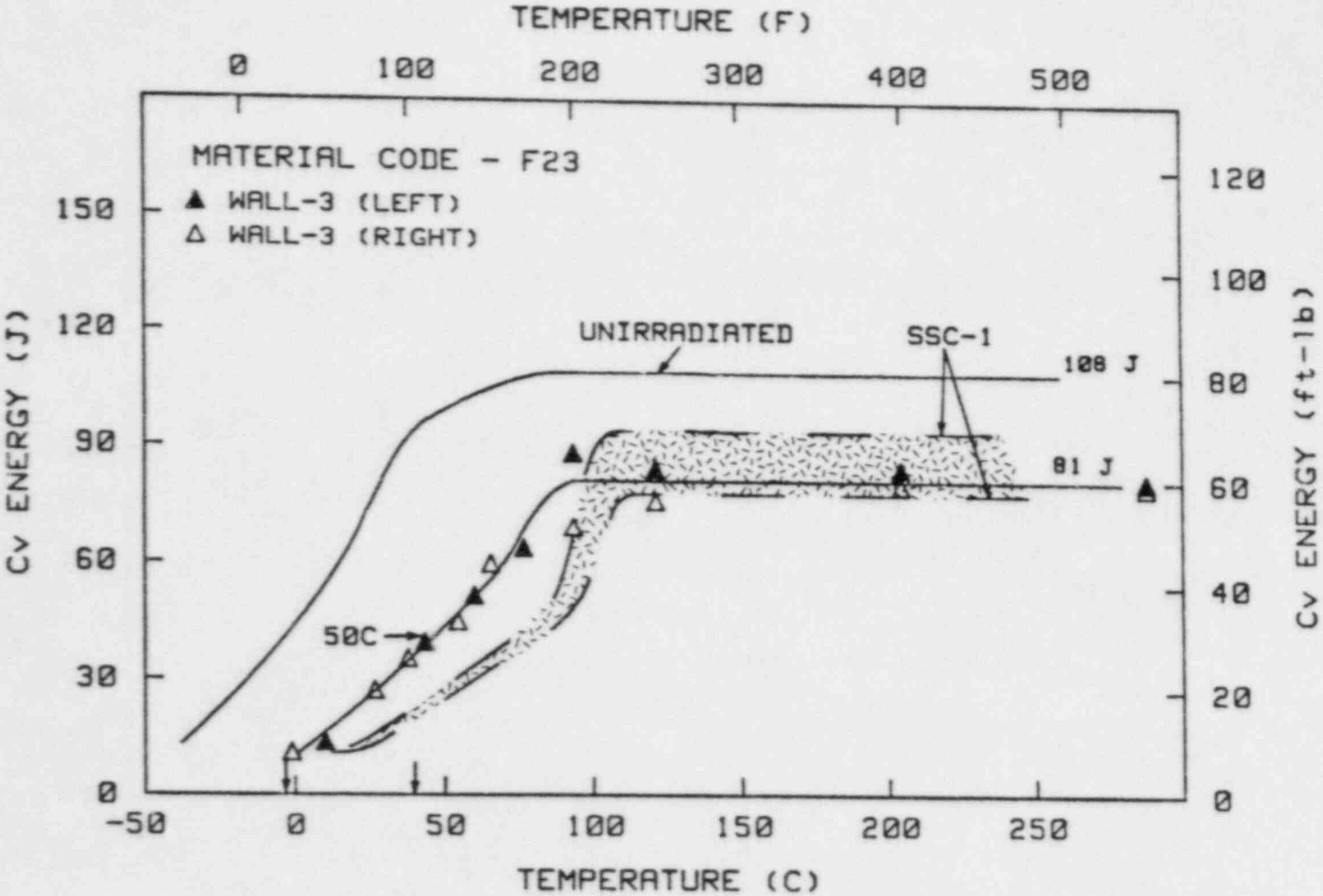

Fig. 6.7 Charpy-V notch ductility of the A302-B plate before and after irradiation in capsule Wall-3.

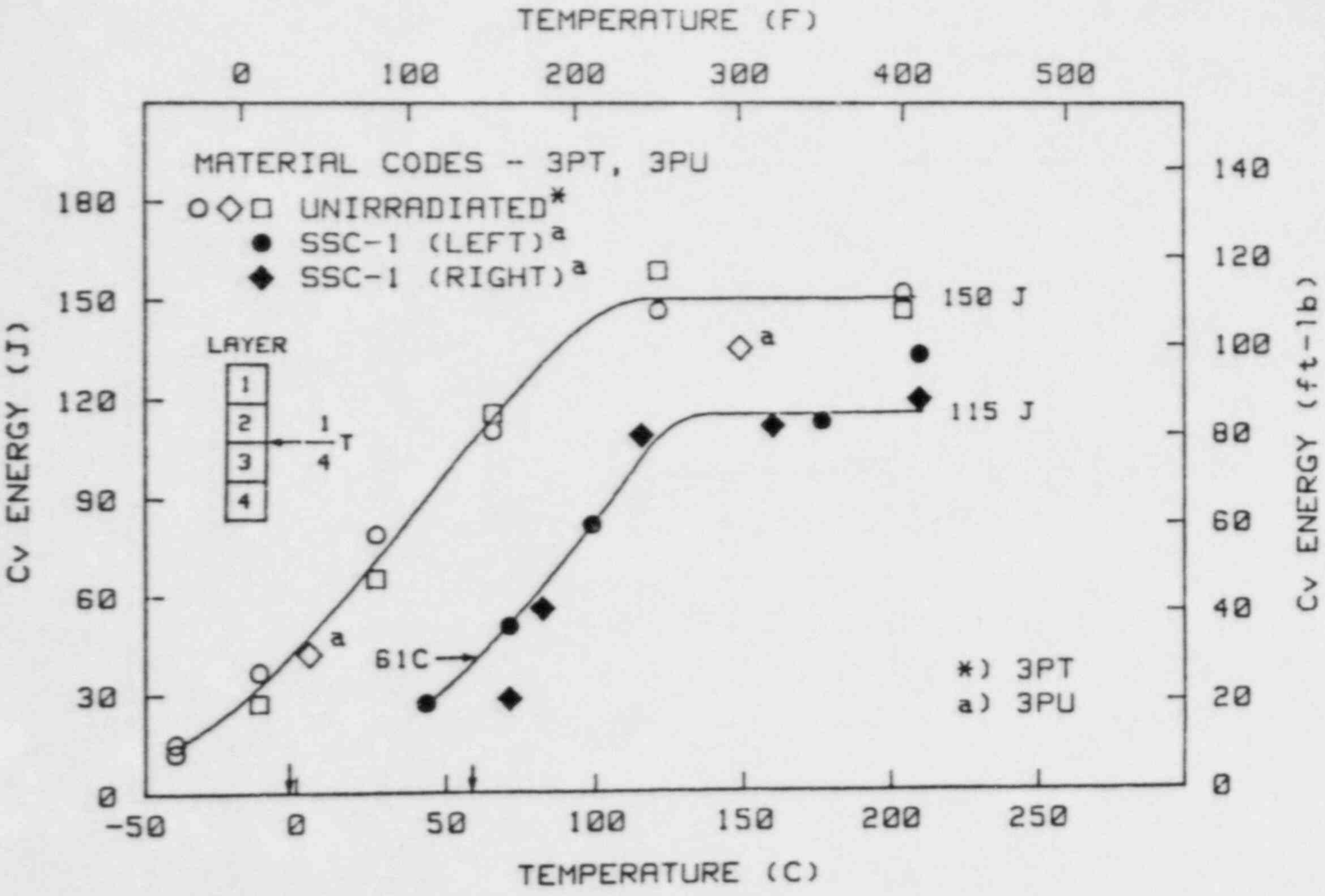

Fig. 6.8 Charpy-V notch ductility of the A533-B plate before and after irradiation in capsule SSC-1.

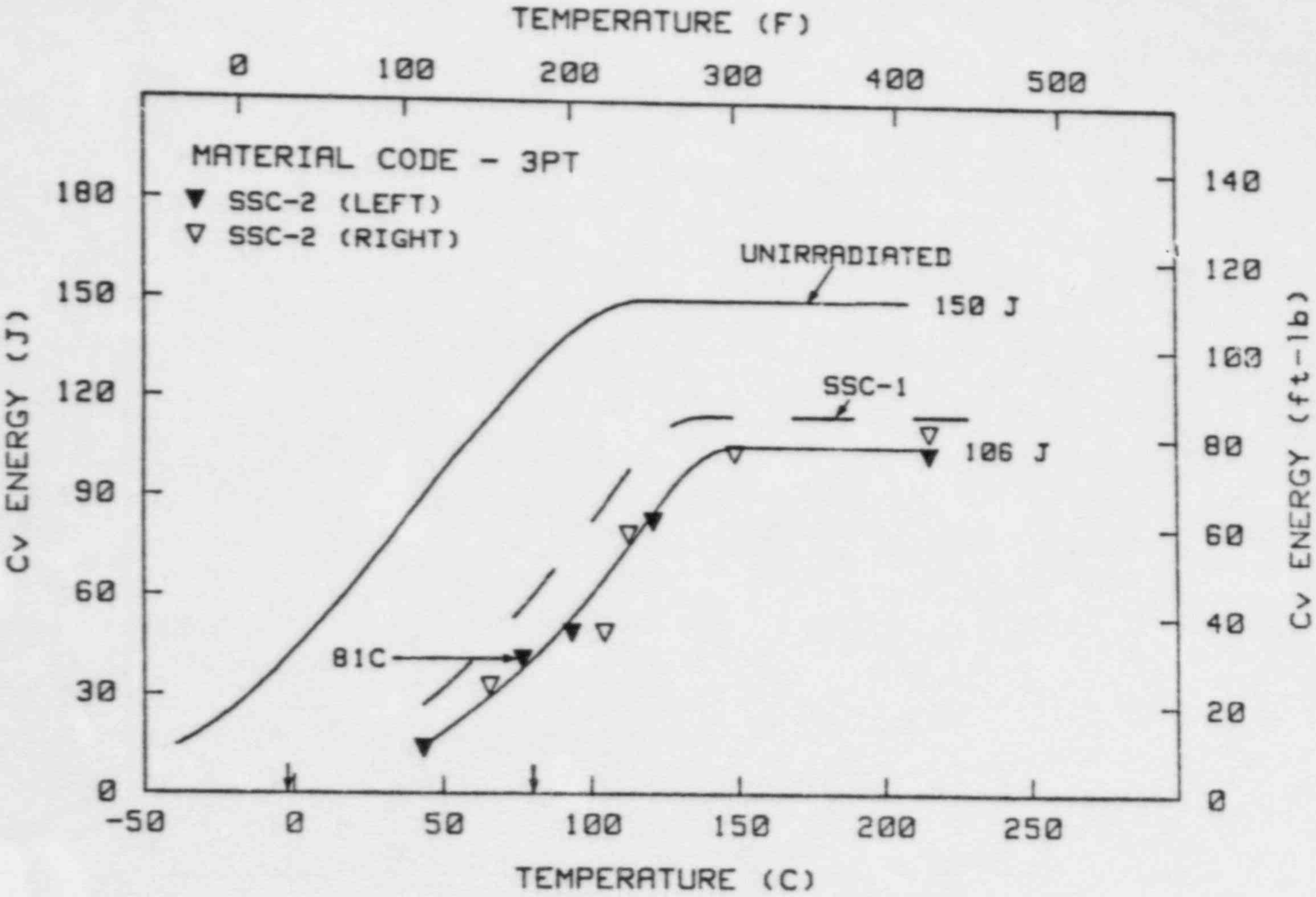

Fig. 6.9 Charpy-V notch ductility of the A533-B plate before and after irradiation in capsule SSC-2.

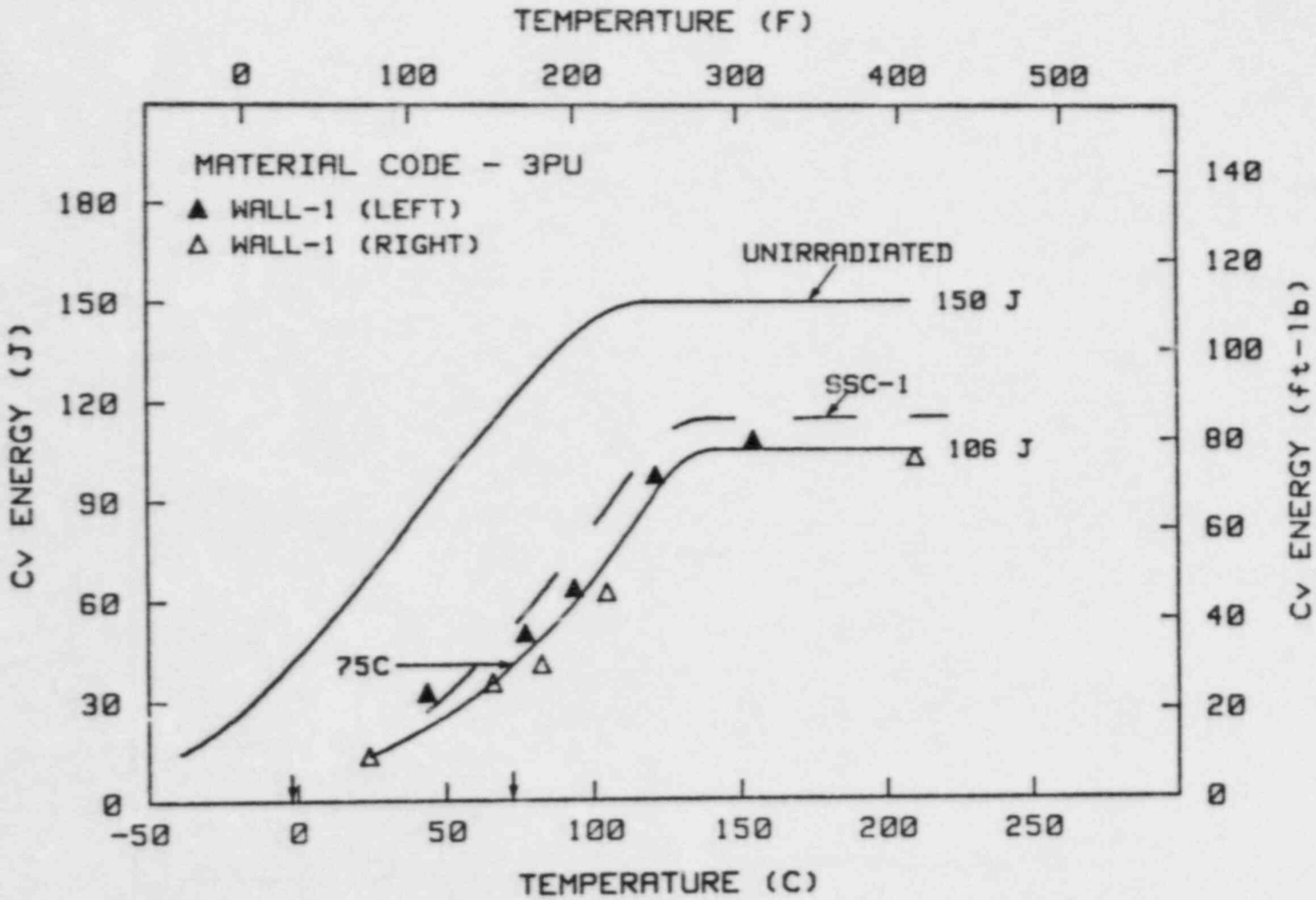

Fig. 6.10 Charpy-V notch ductility of the A533-B plate before and after irradiation in capsule Wall-1.

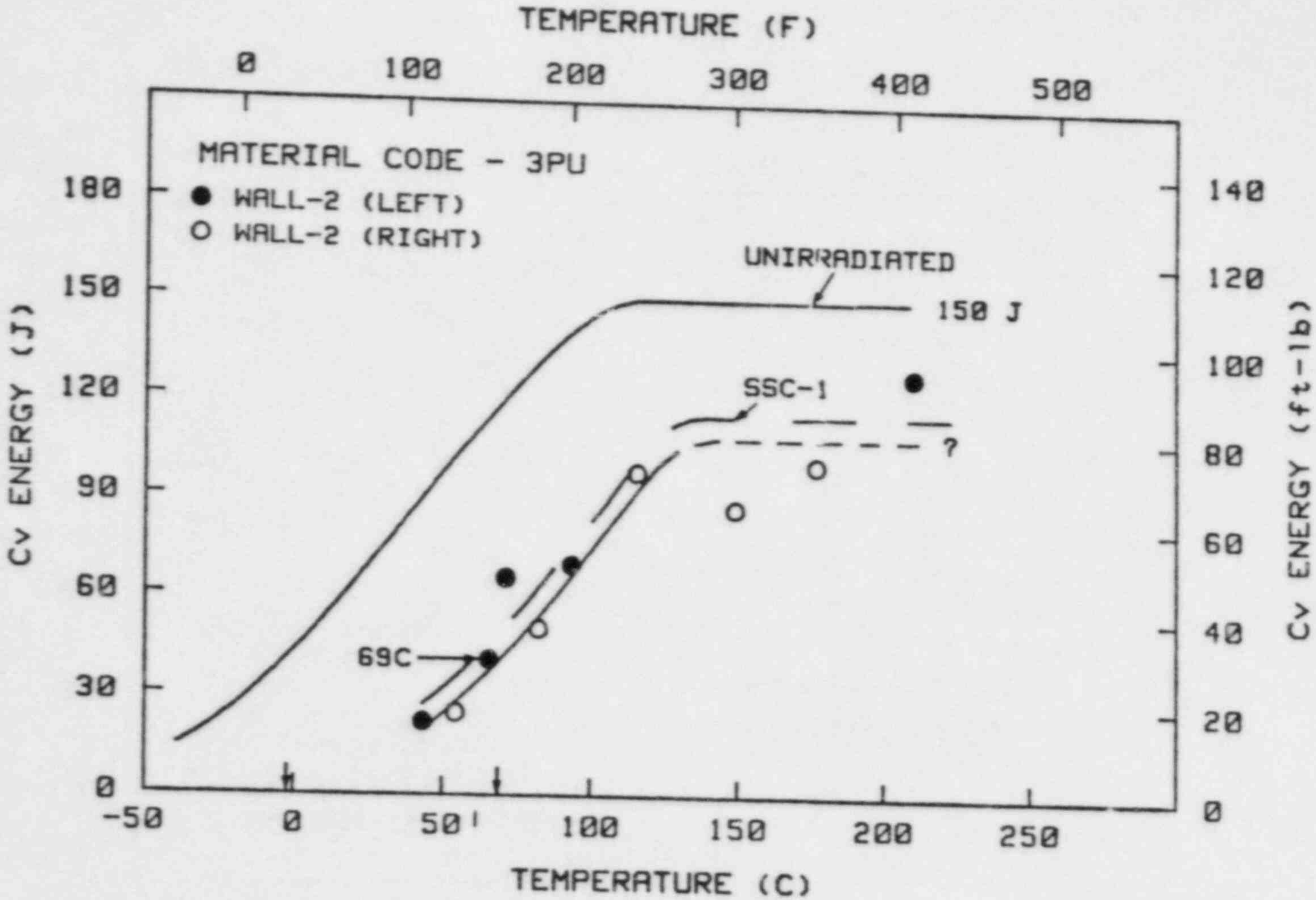

Fig. 6.11 Charpy-V notch ductility of the A533-B plate before and after irradiation in capsule Wall-2.

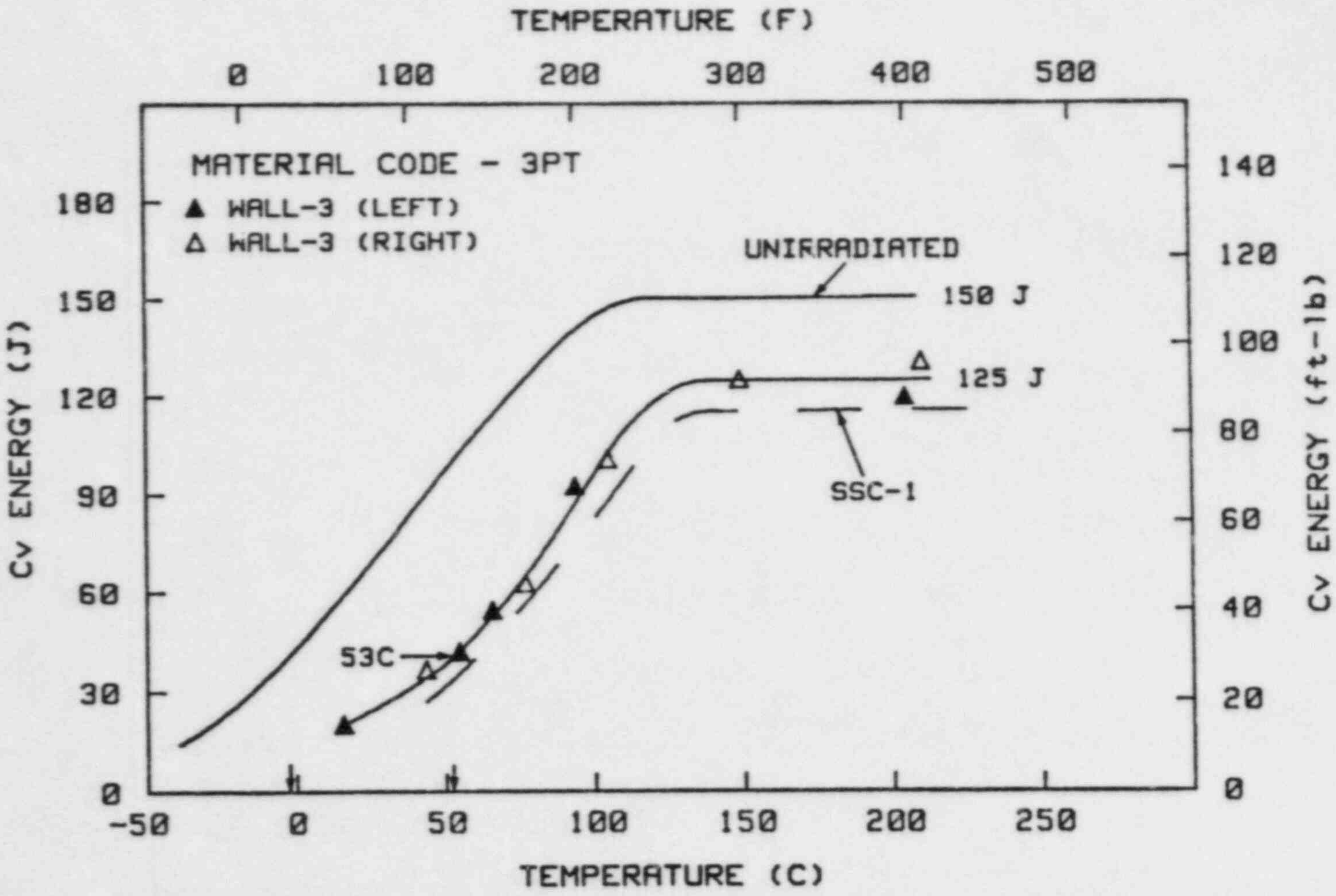

Fig. 6.12 Charpy-V notch ductility of the A533-B plate before and after irradiation in capsule Wall-3.

Table 4. Summary of Observations on Notch Ductility of A302-B Plate

Irradiation Capsule	Transition Temp (°C)			Irradiation Increase (Δ°C)			Upper Shelf Level		Irradiation Decrease	
	41 J	68 J	0.89 mm	41 J	68 J	0.89 mm	J	mm	ΔJ	Δmm
Unirradiated	-4	21	7	---	---	---	108	1.60	--	--
SSC-1 (Left)	74	93	91	78	72	83	94	1.37	14	0.23
(Right)	82	104	102	86	83	94	77	1.17	31	0.43
(Avg.)	78	99	97	82	78	89	86	1.27	23	0.33
SSC-2	90	104	99	94	83	92	75	1.19	33	0.41
Wall-1	77	96	90	81	75	83	80	1.30	28	0.30
Wall-2	63	85	74	67	64	67	81	1.32	27	0.28
Wall-3	46	77	63	50	56	56	81	1.42	27	0.18

Table 5. Summary of Observations on Notch Ductility of A533-B Plate

Irradiation Capsule	Transition Temp (°C)			Irradiation Increase (Δ°C)			Upper Shelf Level		Irradiation Decrease	
	41 J	68 J	0.89 mm	41 J	68 J	0.89 mm	J	mm	ΔJ	Δmm
Unirradiated	-1	24	13	---	---	---	150	2.18	---	---
SSC-1	60	88	82	61	64	69	115	1.68	35	0.50
SSC-2	80	107	99	81	83	86	106	1.73	44	0.45
Wall-1	74	102	93	75	78	80	106	1.60	44	0.58
Wall-2	68	93	85	69	69	72	__[a]	1.68	__[a]	0.50
Wall-3	52	79	66	53	55	53	125	1.93	25	0.25

[a]Not established because of data scatter

6.3 Simulated Surveillance Capsules

Data for capsules SSC-1 and SSC-2 are given in Figs. 6.3, 6.4, 6.8 and 6.9. The fluences received by the A302-B and A533-B specimens in capsule SSC-1 (C_v and tensile specimens) were, respectively, 2.87×10^{19} and 2.66×10^{19} n/cm^2, $E > 1$ MeV based on present calculations. Fluence estimates for the materials in capsule SSC-2 are 5.6×10^{19} and 5.2×10^{19} n/cm^2, respectively. As expected, the A302-B plate showed a greater embrittlement in terms of the 41 J transition temperature elevation than the A533-B plate. The greater radiation effect to the former is consistent with its higher copper content (0.21% vs. 0.12% Cu) and its somewhat higher fluence.

In each figure, data from specimens contained in the left hand compartment of the capsules are separately identified from data for specimens in the right hand compartment. Referring to Fig. 6.3, specimens of the A302-B plate contained in the left compartment (group 1) indicate a different postirradiation notch ductility compared to specimens contained in the right compartment (group 2). The low data scatter suggests that the difference is real. The occurrence of the two separate data patterns cannot be attributed to neutron fluence dissimilarities but may be some unknown reflection of the specimen locations in the parent plate. Specimens forming group 1 were from plate thickness layer 1 only; specimens forming group 2 were from plate thickness 2 only. In Fig. 6.1, unirradiated condition tests of these two adjacent thickness layers indicate identical properties making the postirradiation difference in notch ductility anomalous. The anomaly is compounded by the fact that the specimens for individual capsules were intentionally randomized within the total specimen complement to avoid introducing any across-plate bias. Overall, the difference in transition behaviors is small and average behavior was used for capsule-to-capsule comparisons. In the case of upper shelf behavior, the difference was largest for capsule SSC-1, intermediate with capsule Wall-2 and small for capsules SSC-2, Wall-1 and Wall-3. In the following discussion of data, average properties are assumed for the A302-B material unless noted otherwise.

Three important observations result from the data of capsules SSC-1 and SSC-2. First, the irradiation effect to the A302-B plate, as stated, was greater than the irradiation effect to the A533-B plate. For example, (capsule SSC-1), the former shows an average 41 J temperature elevation of 82°C compared to 61°C for the latter. Secondly, the doubling of the fluence exposure of the materials (capsule SSC-2) produced only a small (almost negligible) additional 41 J temperature elevation. That of the A302-B plate was increased further by only 12°C; that of the A533-B plate was increased by only 20°C. Lastly, findings for both capsules are in general agreement with observations made previously for these materials when irradiated in test reactor experiments, in-core. Figure 6.13 shows the SSC-1 and SSC-2 results entered on data trends developed from in-core irradiations. At both fluence levels, the 41 J temperature elevations of the A302-B plate agree well with the embrittlement trend for this plate established earlier. The small difference in embrittlement between the SSC-1 and SSC-2 exposures also is predicted well by the in-core results.

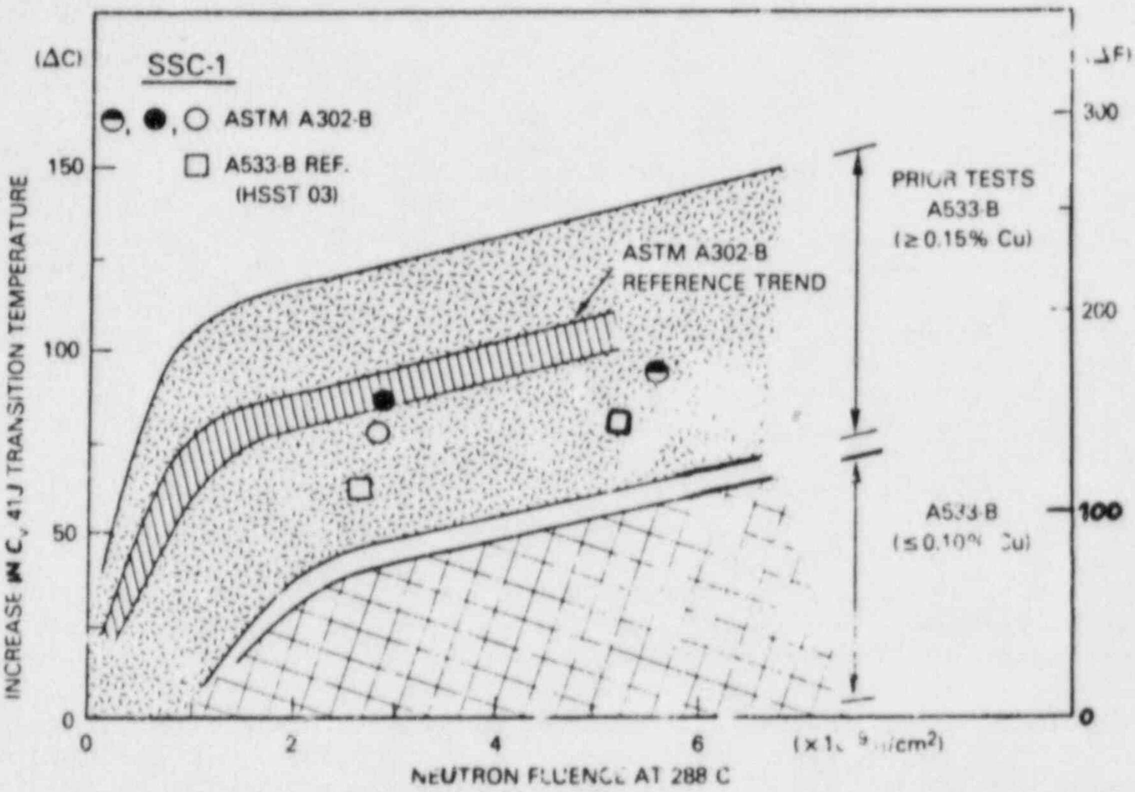

Fig. 6.13 Data from capsules SSC-1 and SSC-2 compared against trends of C_v 41 J transition temperature change with irradiation observed with in-core, test reactor experiments. The trend band, marked ASTM A302-B Reference Trend was established with several independent experiments using code F23 material. Good agreement at both fluence levels is indicated. Data for the A533-B plate with 0.12% Cu fall in the lower portion of the data trend for A533-B plates with >0.15% Cu and agree with projections.

Not shown, a test reactor irradiation of the A533-B plate to ~1.5×10^{19} n/cm^2 at 288°C produced a 41 J temperature increase of 56°C (Ref. 6). The SSC-1 result is consistent with this earlier finding when the fluence difference is considered.

Discussions of the relative effects of irradiation on the upper shelf level and on the 68 J and 0.89 mm transition temperatures are presented in later sections (see Intercapsule Comparisons and Embrittlement Assessments by Alternative Indices).

6.4 Wall Capsules

Figures 6.5-6.7 and 6.10-6.12 depict data obtained from the three wall capsules. The 41 J transition temperature elevations for the A302-B and A533-B specimens contained in capsule Wall-1 were 81°C and 75°C, respectively. Corresponding determinations for specimens irradiated in capsule Wall-3 were only 31°C and 22°C lower, revealing that the gradient in fracture resistance with wall depth (surface to the mid-wall) is neither sharp nor dramatic. Percentage-wise, however, the differences with wall depth are much higher, i.e, 38% (A302-B) and 29% (A533-B).

Of additional interest to this investigation, note that the two plates have about the same transition temperature elevation, i.e., apparent radiation sensitivity, at each of the three wall capsule locations. This is in clear contrast to the difference in apparent embrittlement sensitivity found with the simulated surveillance capsule irradiations. Whether or not this change in relative behavior arose from the much longer exposure time of the wall capsules is a key question.

For the A302-B plate, essentially the same upper shelf levels were observed in the Wall-1, Wall-2 and Wall-3 capsule tests. From lateral expansion data, the upper shelf toughness levels of the A533-B plate would appear to be the same only for the Wall-1 and Wall-2 irradiations. The higher upper shelf toughness for the Wall-3 capsule may or may not be a simple manifestation of biased data scatter. On this point, the high (upper shelf) data scatter for the A533-B plate with the Wall-2 tests cannot be explained but illustrates well a problem which can be encountered when too few specimens are provided. Many early reactor vessel surveillance programs likewise had only limited specimen numbers.

6.5 Intercapsule Comparisons

The data from the two sets of capsules (surveillance vs. wall) are in good agreement in showing that the difference in transition temperature elevations between ~3×10^{19} and ~ 6×10^{19} n/cm^2 is not large for these particular materials. In turn, the fluence attenuation with wall depth between surface and quarter thickness positions does not translate to a dramatic gradient in fracture toughness in the general sense.

One primary objective of the five capsule series, both from the standpoint of neutron physics calculations and the standpoint of metallurgical correlations, was to see how well data from capsule SSC-1 predict the irradiation effects to the quarter wall thickness location (capsule Wall-2), and how well data from capsule SSC-2 predict properties at the wall inner surface (capsule Wall-1). Appropriate comparisons are made in Table 6. In the case of the A302-B plate, the surveillance capsule data tend to over-predict the transition temperature elevation for the wall location in both instances. The amount of overprediction however is ~20°C or less regardless of the brittle/ductile transition index used (41 J, 68 J or 0.89 mm). With the A533-B plate, the agreement is even closer, within ~10°C. Upper shelf energy changes also are predicted well, i.e., are within about 7 J or 5 ft-lb for both steels.

The results permit a conclusion that surveillance capsule results indicate reasonably well the radiation effects to surface and quarter wall thickness locations for A302-B and A533-B materials of the types represented here. Where significant differences are observed, i.e., >10°C, the SSC data appear to be on the conservative side, i.e., show a greater embrittlement than that experienced in the wall itself.

6.6 Embrittlement Assessment by Alternative C_v Indices

Table 7 is a summary comparison of absolute transition temperatures and transition temperature elevations (ΔT's) indexed to the C_v 68 J temperature and the C_v 0.89 mm temperature as alternatives to the C_v 41 J temperature. Typically, the 0.89 mm temperature is higher than the 41 J temperature but is lower than the 68 J temperature. Of greater interest here, the 68 J temperature elevations are found about equal to the corresponding 41 J temperature elevations. The differences are no greater than 11°C and are 6°C or less in most cases. Likewise, the 0.89 mm temperature elevation by irradiation was nearly equal to the 41 J temperature elevation, i.e., within 8°C. Accordingly, the ranking of the irradiation effect by capsule location for the two plates is quite independent of the C_v indexing procedure selected (41 J, 68 J or 0.89 mm temperature). The close agreement of the 41 J and 68 J transition temperature elevations noted is consistent with observations for several other steels (Ref. 15). On the other hand, this same study found a bias toward a greater 0.89 mm transition temperature elevation compared to the 41 J temperature elevation on the order of 15° to 20°C.

7. TENSILE PROPERTIES DETERMINATIONS

7.1 Procedure

Tensile properties were established using button-head specimens machined from selected C_v specimen blanks (Fig. 4.4). All tests were conducted at a loading rate less than 690 MPa/min. based on the slope of the load-extension curve in the elastic region. Specimen strain was not monitored using an extensometer; instead, elongation of the gage section was monitored from test machine actuator displacement. In Fig. 4.4, the uniform gage length is shown to be 31.75 mm. For determinations of the 0.2% offset yield strength, however, an effective gage length of 38.1 mm was assumed in order to account fully for the specimen's reduced section and for a portion of the radius blends.

All tests were performed on a 55 metric ton MTS servohydraulic test machine. Load cell calibration was performed within one year of the present tests. A calibration recheck using shunt resistors was made

Table 6. Comparison of Simulated Surveillance and Wall Capsule Observations (Matching Fluence Conditions)

Capsule	Fluence[a]	41J Temperature (Δ°C)	68J Temperature (Δ°C)	0.89 mm Temperature (Δ°C)	Upper Shelf Energy (ΔJ)
		A302-B Plate (Code F23)			
SSC-1	2.87	82	78	89	23
Wall-2	~2.9	67	64	67	27
Difference	---	15	14	22	(-)4
SSC-2	5.6	94	83	92	33
Wall 1	5.6	81	75	83	28
Difference	---	13	8	9	5
		A533-B Plate (Codes 3PT, 3PU)			
SSC-1	2.66	61	64	69	35
Wall-2	2.7	69	69	72	35[b]
Difference	---	(-)8	(-)5	(-)3	0[b]
SSC-2	5.2	81	83	86	44
Wall-1	5.2	75	78	80	44
Difference		6	5	6	0

[a] x 10^{19} n/cm^2, E > 1 MeV (approximate)
[b] Estimated based on lateral expansion data

Table 7. Comparison of Irradiation Effect Assessments by Alternative C_V Indices

Comparison	A302-B Plate (Code F23)	A533-B Plate (Codes 3PT, 3PU)
ΔT_{68J} vs. ΔT_{41J}	$\Delta T_{41J} > \Delta T_{68J}$ (by 11°C max.)	$\Delta T_{41J} \sim \Delta T_{68J}$ (within 3°C)
$\Delta T_{0.89mm}$ vs. ΔT_{41J}	$\Delta T_{41J} <> \Delta T_{0.89mm}$ (by 8°C max.)	$\Delta T_{41J} < \Delta T_{0.89}$ (within 8°C)
$\Delta T_{0.89mm}$ vs. ΔT_{68J}	$\Delta T_{68J} < \Delta T_{0.89mm}$ (by 11°C Max)	$\Delta T_{68J} \sim \Delta T_{0.89}$ (within 6°C)
$T_{0.89mm}$ vs. T_{68J}	$T_{0.89mm} < T_{68J}$	$T_{0.89mm} < T_{68J}$
$T_{0.89mm}$ vs. T_{41J}	$T_{0.89mm} > T_{41J}$	$T_{0.89mm} > T_{41J}$

immediately before each test. Likewise, a calibration recheck of actuator deflection was performed before the test series commenced and was verified again after the tests were completed. Specimen load vs. actuator deflection was recorded simultaneously on two X-Y plotters. One plotter recorded the entire applied load vs. deflection history through to specimen failure. The second plotter provided an expanded load vs. deflection record which was stored digitally via a computer-controlled data acquisition system.

7.2 Observations

Tensile property determinations are listed in Tables 8 and 9 and are shown graphically in Fig. 7.1. The results represent computer analyses of the stored digital data, and were verified through comparisons with the analog X-Y recorder plots. At this time, percent elongation and percent reduction in area measurements are not available. These measurements will be included in a follow-on report to be issued by MEA.

Referring to Fig. 7.1, the data show the expected increase in yield and tensile strengths with increasing fluence. The strength changes and strength differences overall are small. Tensile strength change was least with capsule Wall-3 and greatest with capsule SSC-2. The changes with capsule Wall-2 were somewhat greater than those of Wall-3 but were less than those observed with capsule Wall-1 or capsule SSC-1. The reason for the somewhat high degree of scatter has not been ascertained but is not due to plate sampling location or testing procedure, i.e., specimens were from one small volume of material and were tested concurrently.

8. FRACTURE TOUGHNESS ASSESSMENTS

8.1 Procedure

Initiation fracture toughness in the brittle-to-ductile transition regime was determined from the J integral-R curve; the R curve was determined by the single specimen compliance (SSC) technique for crack extension evaluation. The SSC technique is described in detail in Ref. 22 and 23. In brief, this technique determines specimen crack extension by means of small specimen unloadings (~10 to 15 percent) at regular intervals during testing. Because these unload and reload segments are conducted under elastic conditions (even though the specimen may have undergone extensive plastic deformation), the change in crack length from one unloading to the next can be inferred through a change in specimen compliance ($EB\delta/P$) where E is Young's modulus, B the specimen thickness, and P and δ the load and loadline deflection respectively. J values were computed using the modified version of the J integral known as J_M (Ref. 24) where J_M is given by:

$$J_M = J_D - \int_{a_o}^{a} \left. \frac{\partial(J_D - G)}{\partial a} \right|_{\delta_{pl}} da \qquad (1)$$

Table 8. Tensile Properties of A302-B ASTM Ref. Plate

SPECIMEN NUMBER	TEST TEMP (°C)	UPPER YIELD STRESS (MPa)	LOWER YIELD STRES (MPa)	0.2% YIELD STRESS (MPa)	ULTIMATE STRESS (MPa)	TEST RATE MPa/Min
Unirradiated Specimens						
F23-T22[a]	24	---	---	482	660	---
SSC-1 Specimens						
F23-T6[a]	24	---	---	581	710	---
F23-T23[a]	24	---	---	611	756	---
F23-T1	163	511	500	507	643	627
F23-T7	288	---	---	499	646	645
F23-T16	288	---	---	538	705	543
SSC-2 Specimens						
F23-T11	26	614	610	610	726	632
F23-T27	26	626	621	620	755	611
F23-T13	163	552	548	549	682	660
F23-T5	288	---	---	518	671	686
F23-T20	288	---	---	559	727	669
Wall-1 Specimens						
F23-T2	24	587	584	584	711	250
F23-T17	24	---	---	605	762	503
F23-T28	163	556	553	556	703	648
F23-T8	288	---	---	516	675	643
F23-T24	288	---	---	538	712	661
Wall-2 Specimens						
F23-T3	26	572	570	571	704	589
F23-T25	26	593	588	588	736	584
F23-T12	163	519	517	519	658	632
F23-T9	288	---	---	506	665	611
F23-T18	288	---	---	527	697	621
Wall-3 Specimens						
F23-T4	27	557	552	553	697	548
F23-T26	27	---	---	580	730	508
F23-T21	163	526	522	523	677	646
F23-T10	288	---	---	496	655	599
F23-T19	288	---	---	517	697	646

[a]Tested at the U. S. Naval Research Laboratory

Table 9. Tensile Properties of A533-B HSST Plate 03

SPECIMEN NUMBER	TEST TEMP (°C)	UPPER YIELD STRESS (MPa)	LOWER YIELD STRESS (MPa)	0.2% YIELD STRESS (MPa)	ULTIMATE STRESS (MPa)	TEST RATE MPa/Min
Unirradiated Specimens						
3PT-14A	24	---	---	448	641	---
3PT-14B	24	---	---	459	641	---
SSC-1 Specimens						
3PT-1[a]	24	---	---	567	715	---
3PT-10	24	577	568	573	710	599
SSC-2 Specimens						
3PT-T5	26	609	606	606	744	610
3PT-8	26	601	591	595	720	606
Wall-1 Specimens						
3PT-T2	27	601	585	585	734	250
3PT-T11	27	582	576	577	725	627
Wall-2 Specimens						
3PT-T3	26	562	552	552	707	568
3PT-T12	27	---	---	565	712	618
Wall-3 Specimens						
3PT-T4	27	---	---	534	687	598
3PT-T13	27	548	536	543	690	610

[a]Tested at the U. S. Naval Research Laboratory.

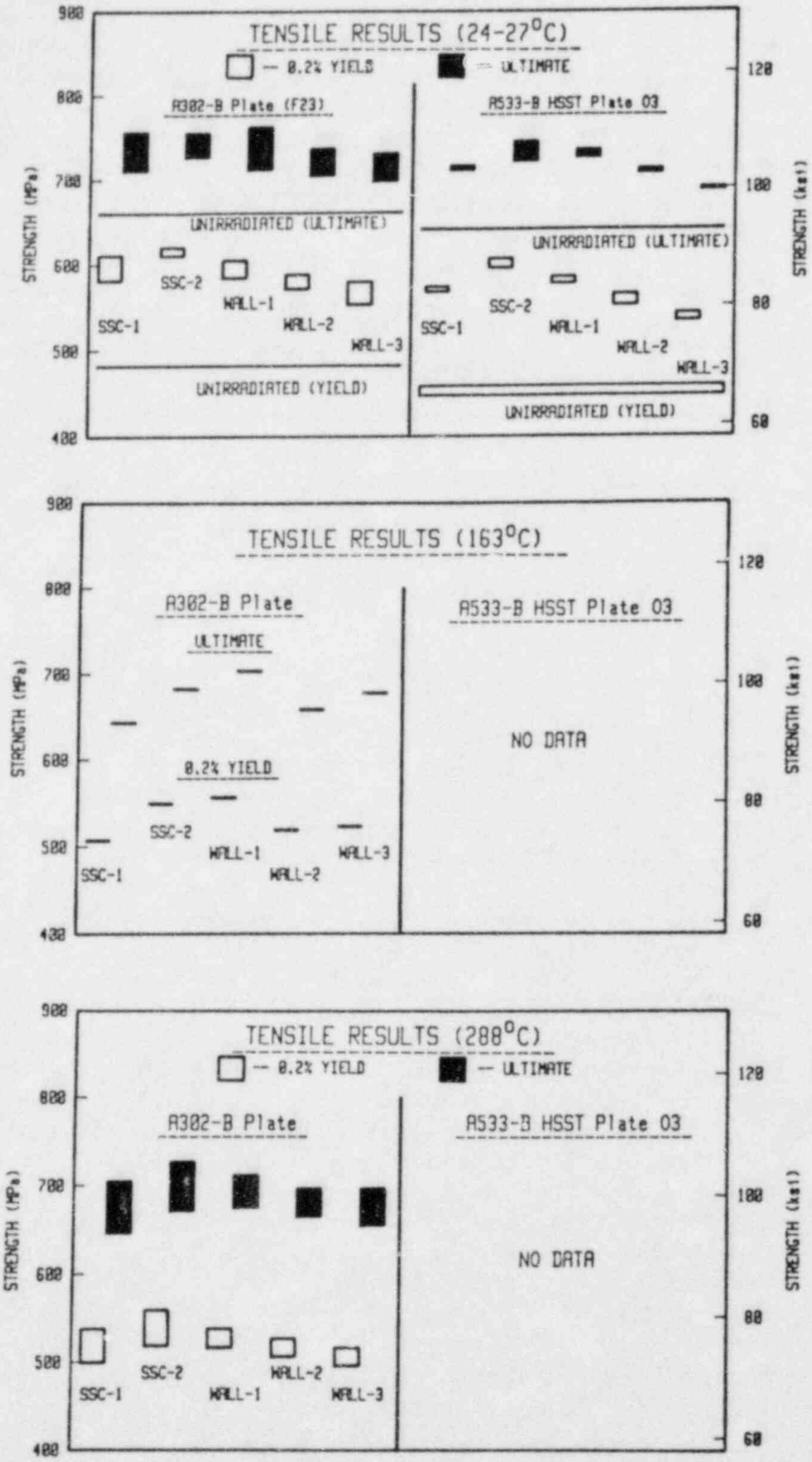

Fig. 7.1 Variation in tensile properties between irradiation capsules at 24°C (upper), 163°C (middle) and 288°C (lower) test temperatures.

where J_D = deformation theory J, G = Griffith linear elastic energy release rate, a_o and a = the initial and current crack lengths, respectively, $\delta - \delta_{el} = \delta_{pl}$ = plastic part of the displacement. The equation incorporates corrections for crack extension and the tension component of specimen loading. A separate correction for specimen rotation was applied to adjust crack length predictions (Ref. 22).

The crack extension resistance curve (R curve) is obtained by plotting J_M vs. crack extension, Δa, as shown in Fig. 8.1. The initiation fracture toughness, J_{Ic}, (as defined by MEA) is determined in two ways. If the R curve data do not extend beyond the 0.15 mm exclusion line due to a cleavage failure interrupting the test, the value of J_M at cleavage is taken as J_{Ic} (R curve, Type A). If the data cross the 0.15 mm exclusion line, J_{Ic} is defined as the intersection of the R curve data with the exclusion line. For cases where the R curve continues past the J_{Ic} point, the test may be terminated by cleavage prior to crossing the 1.5 mm exclusion line (R curve, Type B), or ductile crack extension may continue past the 1.5 mm exclusion line (R curve, Type C). Crossing the 1.5 mm exclusion line, however, does not preclude cleavage. Fractures in a cleavage mode have been observed in other studies at crack extensions well beyond the 1.5 mm exclusion line but only in tests conducted at temperatures below the upper shelf as determined from tests conducted under dynamic loading.

R curves of Type C are the only ones for which the J_{Ic} determination is covered by an ASTM standard test procedure; i.e., by Standard Method E 813 (Ref. 25). For those few cases where a Type C curve occurred in this study both the analysis described above and the E 813 procedure were used to establish J_{Ic}. Very little difference between the two values was observed; however, the focus of the present study is on the brittle-to-ductile transition, i.e., the regime not covered by the ASTM standard. Here, J_{Ic} values were obtained by the MEA method described above and used for subsequent analysis of initiation toughness trends. Thus, analysis of initiation toughness is based on data that were obtained in a consistent manner throughout the transition region.

One of the program objectives was to obtain E 399 valid K_{Ic} data where possible. Due to the relatively small specimen sizes, i.e., 0.5T-CT and 1T-CT, valid data were obtainable only at the very low toughness end of the transition region as illustrated in Fig. 8.2. The normal SSC test procedure was modified to meet E 399 requirements for tests in the transition temperature region. The modified procedure precluded any unloading of the specimen until the load-deflection record violated E 399 requirements, i.e., exceeded the five-percent secant line by a factor of 1.1. After reaching this point, the test was completed using the SSC technique. The test records first were analyzed for K_{Ic} validity according to E 399 procedures. Then an analysis by the MEA procedure for J_{Ic} was performed.

Only a few tests produced valid K_{Ic} results. For the remainder, an initiation toughness, termed K_{Jc}, was computed from J_{Ic} as follows:

$$K_{Jc} = [EJ_{Ic}/(1-\gamma^2)]^{1/2} \quad (2)$$

where γ is Poisson's ratio, taken to be 0.3. While all J_{Ic} values were valid by ASTM E 813, K_{Jc} computed from Eq. 2 should not be interpreted as K_{Ic}. Instead, an estimate of K_{Ic} was obtained from K_{Jc} by means of the "β_{Ic} correction" described below.

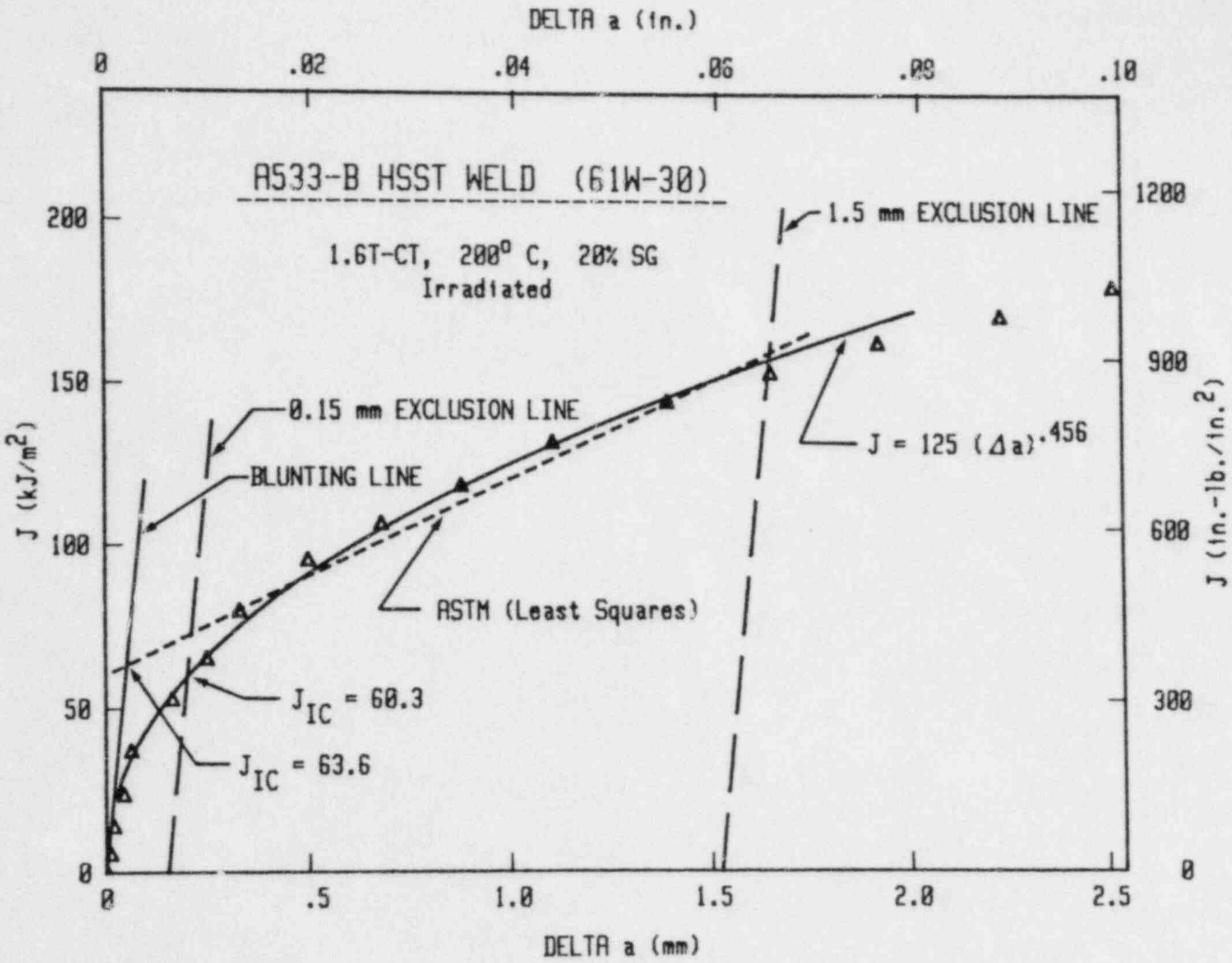

Fig 8.1 Expanded R curve illustrating the power-law behavior exhibited at small crack extension. With the MEA procedure, J_{Ic} is taken as that value where the R curve intersects the 0.15 mm exclusion line. Conversely, J_{Ic} is defined by ASTM Standard E 813 as the intersection of the blunting line and the least squares fit to the data between exclusion lines.

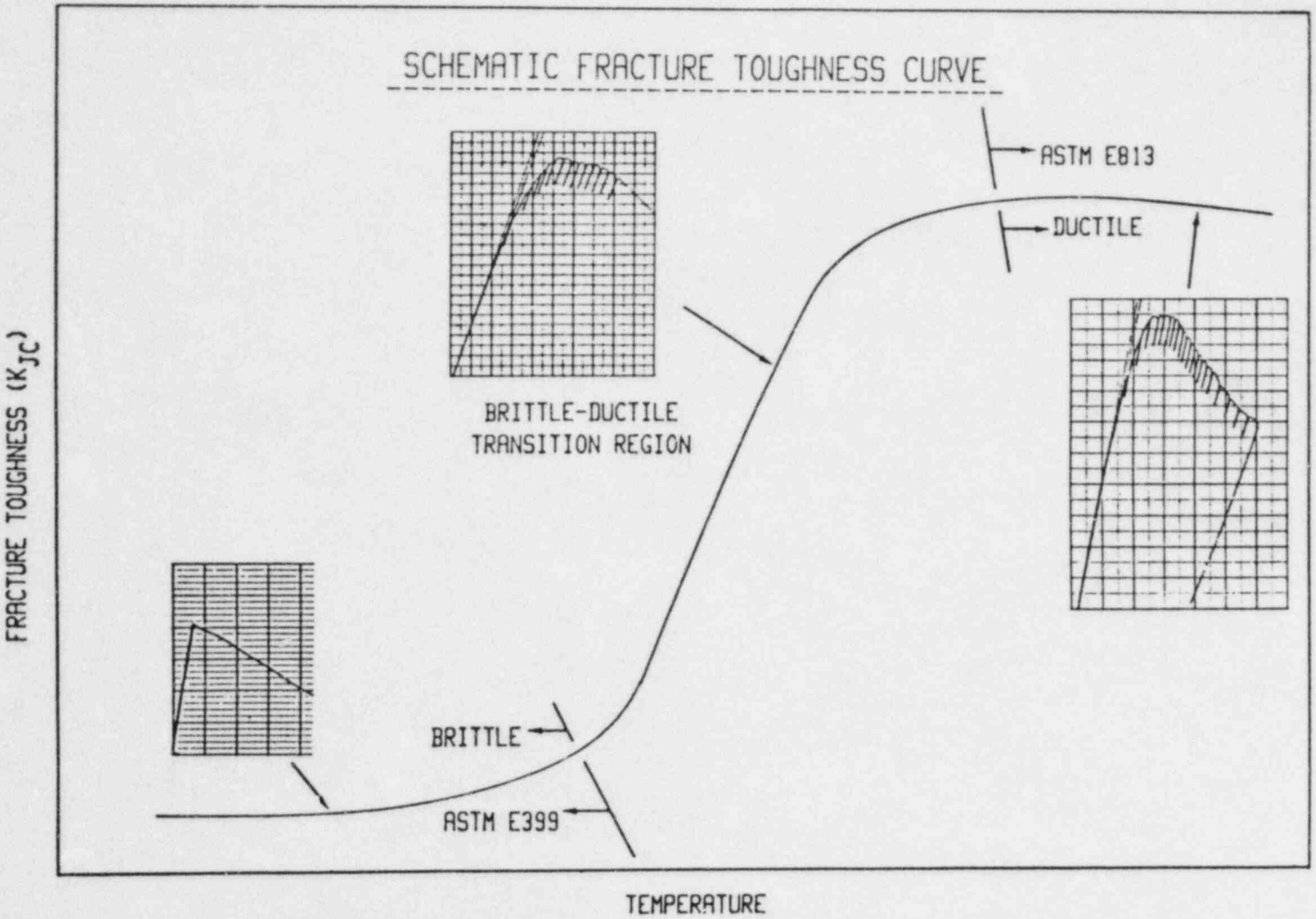

Fig. 8.2 Typical initiation fracture toughness transition behavior with temperature for steels showing the regions covered by ASTM standards for the materials and specimens included in this program. The inserts illustrate specimen load vs. deflection behavior.

8.1.1 Side Grooving

Side-grooving of the CT specimen is necessary to obtain a straight crack-front extension for tests in the upper shelf regime. A few tests in the transition temperature regime were also conducted with side-grooved specimens to compare results against the smooth specimen data. The 1T-CT specimens (only) were side grooved by 10 percent of their thickness on each side (20 percent total). The side grooves were machined to a depth of 2.54 mm using a cutter with a 45° included angle and a 0.25 mm root radius. Each groove was centered on, and parallel to, the plane of the machined notch. For data analysis, the effective specimen thickness, B_e, used to calculate J_M is given by:

$$B_e = B - \frac{(B-B_N)^2}{B} \qquad (3)$$

where B_N is the specimen net thickness remaining after grooving. All fracture mechanics tests were conducted at a stress intensity loading rate ($\dot{K}$) of approximately 44 MPa $\sqrt{m}$/min., with the exception of one 0.5T-CT specimen inadvertently tested at a rate one hundred times faster. The $\dot{K}$ was computed from the loading rate during the initial (elastic) portion of the test and the initial crack length measured after test completion. Irradiated condition tests were conducted with the same testing frame used for the tensile tests; unirradiated condition tests were made with another, identical MTS system. Load cells of both systems were calibrated within one year of the current test series and were checked periodically using shunt calibration resistors during testing. Specimen deflection was measured at the load line with a clip gage. Clip gage calibration was verified periodically between tests. Load and deflection information was obtained with a computer-based data acquisition system, digitized and then stored on disks. Specimen load and deflection data were also recorded with an analog X-Y plotter.

8.1.2 β_{Ic} Correction

With most of the CT tests, the toughness was too high to measure K_{Ic} according to ASTM E 399. Consequently, an initiation toughness (K_{Jc}) was computed from the value of J at crack initiation, i.e., J_{Ic} (Eq. 2). Unfortunately, data in the literature have shown that K_{Jc} generally overestimates K_{Ic}. A similar observation had been made by Irwin in that the plane stress fracture toughness (K_c) also overestimated K_{Ic}. Irwin developed an empirical relationship from which K_{Ic} could be estimated once K_c was known (Ref. 26):

$$\beta_c = \beta_{Ic} + 1.4\,\beta_{Ic}^{3} \qquad (4)$$

where $\beta_{Ic} = \frac{(K_{Ic}/\sigma_f)^2}{B}$ and $\beta_c = \frac{(K_c/\sigma_f)^2}{B}$

and σ_f = 1/2 (yield stress + ultimate stress).

Solving Eq. 4 for β_{Ic} (i.e., K_{Ic}), Merkle recently showed that reasonable estimates of K_{Ic} could be obtained with Eq. 4 for cases in which both K_c and K_{Ic} were known (Ref. 27).

In the present study, it was assumed that K_{Jc} is substantially the same as K_c and can be substituted for the latter in Eq. 4. On this basis, the K_{Jc} values were "β-corrected" to provide estimates of K_{Ic}. The corrected values, provided in Tables 10 and 11, are substantially lower than K_{Jc} in many cases. The "β-corrected" values will be denoted by $K_{\beta c}$ hereafter.

8.2 J-R CURVE RESULTS

The fracture toughness test results for the A302-B and A533-B plates are listed in Tables 10 and 11, respectively. Plots of K_{Jc} vs. temperature for the individual materials and irradiation capsules are also contained in Appendix B. These figures illustrate the observed K_{Jc} data scatter and the elevation in the K_{Jc} transition curve. The K_J 100 MPa $\sqrt{m}$ temperature was used to index the transition for irradiation and preirradiation toughness comparison.

Figure 8.3 is a summary plot for the A302-B plate and illustrates the relative increases in the transition temperature for the surveillance capsules (upper graph) and the wall capsules (lower graph). Figure 8.4 combines the data from the upper and the lower graphs. The transition temperature elevations are 118°C, 102°C, 105°C, 92°C and 78°C respectively for the SSC-2, Wall-1, SSC-1, Wall-2 and Wall-3 capsules, (see Table 12). The ranking in general is commensurate with projections, based on the target fluences.

Figure 8.5 is the summary plot for the A533-B plate. Figure 8.6 combines the data in the format of Fig. 8.4. The ranking of SSC-2, Wall-1, Wall-2 and Wall-3 data (Table 13) is the same as that for the A302-B material. However, note that the A533-B data from capsule SSC-1 deviates somewhat from the trend described by the A302-B findings. In the lower transition region, the SSC-1 data are about equal to the Wall-1 data but in the upper transition region, the SSC-1 data show less of a transition shift than that observed for the Wall-1 capsule but approximately the same shift as the Wall-2 capsule data. This anomaly could be due to temperature or fluence differences among the CT specimens within the SSC-1 capsule. Unfortunately, fluence values (final) are not yet available from HEDL and ORNL for capsule SSC-1.

Side-grooving did not have a significant effect on the location of the brittle-to-ductile transition for either material. For the A302-B plate, Fig. 8.3, data from the side-grooved specimens define the upper temperature bound of the transition thus indicating a slight bias to a higher temperature transition. However, for the A533-B plate, Fig. 8.5 the side-grooved specimen results are intermixed within the data scatter observed with the non-side-grooved (1T and 0.5T-CT) specimen tests.

Two side-grooved specimens of the A533-B plate and three side-grooved specimens of the A302-B plate were used to establish upper shelf toughness levels for the unirradiated condition. The data indicate an inverse temperature dependence which is more pronounced with the A302-B material. While both

Table 10. J-R Curve Initiation Fracture Toughness Data (A302-B ASTM Ref. Plate)

SPECIMEN NUMBER	TEST TEMP	J_{IC}	K_{JC}	$K_{\beta C}$[a]	B	a/W	YIELD[b] STRESS	FLOW[b] STRESS
	(°C)	(kJ/m^2)	(MPa $\sqrt{m}$)	(MPa $\sqrt{m}$)	(mm)		(MPa)	(MPa)
Unirradiated Specimens								
F23-22R[c]	-75	13.7	56.4	52.7	25.4	0.542	546	650
F23-26R[c]	-35	69.6	126.6	84.5	25.4	0.548	508	612
F23-10R[ce]	0	138.4	177.5	---	25.4	0.549	489	586
F23-18R[cf]	95	113.3	158.5	---	25.4	0.545	462	543
F23-14R[cf]	200	71.5	124.1	---	25.4	0.543	444	535
F23-60R	-125	5.6	36.3 (35.5)[d]	35.4	12.7	0.554	611	712
F23-48R	-100	14.8	58.9	51.8	12.7	0.537	577	680
F23-16R	-85	26.3	78.3	61.2	12.7	0.541	558	662
F23-12R	-75	50.8	109.0	71.8	12.7	0.490	546	650
F23-26R	-75	23.4	73.7	58.7	12.7	0.555	546	650
F23-44R	-75	40.4	96.9	67.9	12.7	0.555	546	650
F23-6R	-60	43.7	101.0	68.3	12.7	0.522	531	635
F23-32R	-50	38.9	93.9	65.5	12.7	0.558	521	625
F23-56R	-50	82.9	138.4	78.2	12.7	0.555	521	625
F23-22R	-40	90.6	145.0	78.9	12.7	0.557	512	616
F23-68R	-35	167.3	196.0	88.8	12.7	0.557	508	612
F23-64R[e]	-25	174.8	200.2	---	12.7	0.550	502	604
F23-2R[e]	-15	271.9	249.3	---	12.7	0.555	496	596
SSC-1 Specimens								
F23-5R	0	14.1	56.7 (55.4)[d]	54.3	25.4	0.537	615	679
F23-13R	30	32.1	85.2	73.6	25.4	0.532	593	658
F23-9R	55	52.3	108.0	84.3	25.4	0.533	574	641
F23-17R	60	49.5	105.4	82.8	25.4	0.533	572	638
F23-21R[f,c]	110	82.9	135.3	---	25.4	0.545	538	606
F23-30R	-80	4.5	32.4 (30.8)[d]	31.9	12.7	0.543	681	742
F23-40R	-50	6.2	37.9 (34.5)[d]	36.8	12.7	0.551	656	718
F23-52R	-25	10.3	48.6	45.3	12.7	0.548	635	698
F23-15R	0	18.6	65.2	55.4	12.7	0.546	615	679
F23-10R	30	31.1	83.9	63.4	12.7	0.554	593	658
F23-66R	38	34.2	87.9	64.7	12.7	0.557	587	652
F23-25R	45	23.8	73.2	58.3	12.7	0.535	581	647
F23-63R	55	66.9	122.6	75.2	12.7	0.536	574	640
F23-42R[e]	60	133.0	172.6	---	12.7	0.556	572	638
F23-20R[e]	75	129.2	169.7	---	12.7	0.563	561	627
SSC-2 Specimens								
F23-2R	30	9.9	47.3 (47.0)[d]	46.3	25.4	0.537	618	682
F23-20R	55	25.3	75.4	67.9	25.4	0.537	603	667
F23-6R	60	36.0	89.8	76.4	25.4	0.534	600	664
F23-28R[f]	70	56.6	112.4		25.4	0.539	595	659
F23-54R	-50	7.3	41.2 (39.5)[d]	39.8	12.7	0.554	681	742
F23-62R	0	7.5	41.4 (40.3)[d]	39.7	12.7	0.552	640	702
F23-38R	30	26.0	76.6	61.2	12.7	0.552	618	682
F23-29R	45	23.1	72.2	58.8	12.7	0.558	609	672
F23-19R	55	36.6	90.7	66.5	12.7	0.562	603	667
F23-27R	60	41.8	96.8	68.6	12.7	0.588	600	664
F23-17R[e]	65	68.1	123.4	---	12.7	0.565	597	661
F23-58R[f]	70	97.0	147.1	---	12.7	0.552	595	659
F23-7R[f]	80	123.0	165.5	---	12.7	0.562	589	653

[a] Beta corrected K_{Jc}
[b] Estimated value used for validity/initiation determination
[c] Specimen side grooved 20%
[d] Number in parenthesis is valid E399 K_{Ic} value
[e] Type B R Curve
[f] Type C R Curve

Table 10. Continued

SPECIMEN NUMBER	TEST TEMP	J_{IC}	K_{JC}	$K_{\beta C}$[a]	B	a/W	YIELD[b] STRESS	FLOW[b] STRESS
	(°C)	(kJ/m^2)	(MPa $\sqrt{m}$)	(MPa $\sqrt{m}$)	(mm)		(MPa)	(MPa)
Wall 1 Specimens								
F23-1R	0	14.4	57.3(56.0)[d]	54.8	25.4	0.538	612	680
F23-15R	27	22.3	71.0	65.0	25.4	0.543	600	669
F23-19R	40	37.3	91.7	77.5	25.4	0.539	596	665
F23-27R	50	67.1	122.8	91.5	25.4	0.538	591	661
F23-23R	60	78.9	132.9	95.2	25.4	0.540	587	658
F23-67R	-60	4.5	32.3(31.1)[d]	31.7	12.7	0.550	637	704
F23-1R	-30	17.4	63.2	54.6	12.7	0.544	624	691
F23-5R	0	9.3	46.2	43.2	12.7	0.555	611	679
F23-11R	25	17.2	62.4	53.6	12.7	0.548	601	671
F23-43R	26	46.1	102.2	70.8	12.7	0.549	600	670
F23-39R	40	45.8	101.6	70.3	12.7	0.549	596	665
F23-21R	50	40.5	95.5	68.0	12.7	0.555	591	661
F23-59R[f]	55	109.8	156.9	---	12.7	0.538	589	660
F23-51R	60	68.0	123.4	76.6	12.7	0.548	587	658
F23-31R[f]	70	160.5	189.3	---	12.7	0.550	583	655
Wall 2 Specimens								
F23-16R	-30	8.3	43.7(43.6)[d]	42.9	25.4	0.537	609	675
F23-30R	-1	12.2	52.9(51.5)[d]	50.9	25.4	0.536	594	661
F23-12R	27	38.2	92.9	77.4	25.4	0.536	579	648
F23-4R	42	39.9	94.8	78.0	25.4	0.538	572	642
F23-8R	50	68.6	124.2	90.5	25.4	0.536	569	638
F23-45R	-100	6.5	39.2(36.7)[d]	37.6	12.7	0.548	648	676
F23-61R	-60	13.4	55.7	50.0	12.7	0.551	625	689
F23-53R	-30	16.8	62.1	53.5	12.7	0.548	609	675
F23-8R	0	15.9	60.3	52.1	12.7	0.553	593	660
F23-23R[g]	15	24.3	74.3	59.0	12.7	0.559	586	654
F23-13R	15	27.8	79.4	61.3	12.7	0.543	586	654
F23-3R	24	55.6	112.2	72.9	12.7	0.550	585	651
F23-18R	38	38.0	92.6	66.0	12.7	0.554	574	643
F23-55R	42	70.4	125.9	76.2	12.7	0.544	572	642
F23-47R	50	129.7	170.1	86.2	12.7	0.526	569	638
Wall 3 Specimens								
F23-3R	-50	7.1	40.6(39.7)[d]	40.1	25.4	0.530	612	677
F23-29R	-20	21.7	70.5	64.5	25.4	0.544	596	662
F23-11R	20	37.9	92.6	77.1	25.4	0.534	576	645
F23-7R	40	59.5	115.8	87.2	25.4	0.542	568	637
F23-25R	50	101.7	151.2	99.2	25.4	0.542	563	632
F23-65R	-80	6.3	38.3(36.5)[d]	37.0	12.7	0.554	628	692
F23-41R	-50	16.0	60.8	52.8	12.7	0.551	612	677
F23-4R	-20	14.7	58.0	50.8	12.7	0.546	596	662
F23-9R	0	25.9	76.9	60.2	12.7	0.548	586	653
F23-14R	20	48.4	104.8	70.2	12.7	0.542	576	645
F23-57R	27	111.2	158.6	84.1	12.7	0.546	574	642
F23-37R	34	99.4	149.7	81.8	12.7	0.525	570	638
F23-49R	40	60.9	117.2	73.5	12.7	0.542	568	637
F23-24R	50	166.2	193.2	90.1	12.7	0.548	563	632
F23-28R	60	155.3	186.5	88.6	12.7	0.543	558	628

[a] Beta corrected K_{Jc}
[b] Estimated value used for validity/initiation determination
[c] Specimen side grooved 20%
[d] Number in parenthesis is valid E399 K_{Ic} value
[e] Type B R Curve
[f] Type C R Curve
[g] Specimen tested at high rate, 14.5 mm/min.

Table 11. J-R Curve Initiation Fracture Toughness Data A533-B HSST Plate 03E

SPECIMEN NUMBER	TEST TEMP	J_{IC}	K_{JC}	$K_{\beta C}$[a]	B	a/W	YIELD[b] STRESS	FLOW[b] STRESS
	(°C)	(kJ/m^2)	(MPa $\sqrt{m}$)	(MPa $\sqrt{m}$)	(mm)		(MPa)	(MPa)
Unirradiated Specimens								
3PT-5	-100	10.1	48.7(48.7)[d]	46.9	25.4	0.531	507	603
3PS-2[c]	-75	23.3	73.7	62.0	25.4	0.541	495	591
3PT-7	-50	28.5	81.1	68.2	25.4	0.538	485	580
3PS-5[c]	-30	35.8	90.7	69.0	25.4	0.546	475	571
3PT-6	-25	28.9	81.4	67.8	25.4	0.536	474	569
3PS-1[c]	0	69.2	125.6	80.2	25.4	0.544	463	558
3PT-8	0	115.7	162.4	95.7	25.4	0.534	463	558
3PS-3[c,e]	25	159.7	190.0	---	25.4	0.545	454	548
3PS-4[c,f]	200	137.7	172.1	---	25.4	0.542	405	500
3PU-39	-100	6.8	40.1	37.6	12.7	0.523	507	603
3PU-6	-75	10.3	49.0	43.6	12.7	0.556	495	591
3PU-22	-50	27.1	78.4	57.6	12.7	0.560	485	580
3PU-40	-50	14.2	57.4	48.2	12.7	0.536	485	580
3PU-28	-30	30.7	84.0	59.2	12.7	0.547	475	571
3PU-25	-25	53.9	111.2	67.4	12.7	0.546	474	569
3PU-5	0	81.8	136.5	72.8	12.7	0.550	463	558
3PU-23	5	84.7	138.9	73.1	12.7	0.554	461	556
3PU-7	15	166.1	194.1	83.0	12.7	0.553	457	552
3PU-38	15	311.9	266.0	93.3	12.7	0.549	457	552
SSC-1 Specimens								
3PS-14	10	13.9	56.3(55.1)[d]	53.6	25.4	0.533	576	648
3PS-11	50	26.9	77.8	68.3	25.4	0.537	560	632
3PS-12	60	58.3	114.3	86.1	25.4	0.540	557	629
3PU-9	-50	7.3	41.1(39.3)[d]	39.2	12.7	0.554	601	674
3PU-21	10	12.3	52.9	47.4	12.7	0.567	576	648
3PU-13	50	46.3	102.0	68.6	12.7	0.548	560	632
3PU-33	60	136.4	174.8	86.4	12.7	0.539	557	629
3PU-29[f]	70	185.5	203.5	---	12.7	0.561	554	625
3PU-1[f]	100	179.3	199.3	---	12.7	0.543	544	616
SSC-2 Specimens								
3PU-6	0	14.3	57.2(55.9)[d]	54.7	25.4	0.538	610	677
3PS-8	60	41.3	96.2	79.3	25.4	0.536	588	654
3PU-7	80	29.3	80.8	70.6	25.4	0.537	581	647
3PU-37	0	23.0	72.4	59.0	12.7	0.556	610	677
3PU-17	30	16.6	61.3	52.8	12.7	0.550	599	665
3PU-16	60	35.3	89.0	65.2	12.7	0.551	588	654
3PU-30	70	48.7	104.4	70.4	12.7	0.544	585	650
3PU-8	80	25.3	75.2	59.2	12.7	0.552	581	647
3PU-32[f]	100	181.2	200.3	---	12.7	0.541	575	641

[a]Beta corrected K_{Jc}
[b]Estimated value used for validity/initiation determination
[c]Specimen side grooved 20%
[d]Number in parenthesis is valid E399 K_{Ic} value
[e]Type B R Curve
[f]Type C R Curve

Table 11. Continued

SPECIMEN NUMBER	TEST TEMP	J_{IC}	K_{JC}	$K_{\beta C}$[a]	B	a/W	YIELD[b] STRESS	FLOW[b] STRESS
	(°C)	(kJ/m^2)	(MPa $\sqrt{m}$)	(MPa $\sqrt{m}$)	(mm)		(MPa)	(MPa)
Wall-1 Specimens								
3PS-10	0	9.4	46.4(46.1)[d]	45.4	25.4	0.545	595	668
3PS-9	60	54.9	110.9	85.7	25.4	0.538	573	645
3PS-15	80	185.2	203.1	113.7	25.4	0.543	566	638
3PU-18	-60	5.2	34.8(33.1)[d]	33.9	12.7	0.552	621	695
3PU-10	0	11.2	50.7	46.3	12.7	0.539	595	668
3PU-14	60	42.9	98.1	68.1	12.7	0.544	573	645
3PU-2	80	86.9	139.2	79.3	12.7	0.542	566	638
3PU-26[f]	100	196.2	208.4	---	12.7	0.553	560	632
Wall-2 Specimens								
3PS-13	0	25.3	75.9	67.6	25.4	0.538	567	645
3PT-1	38	28.3	79.9	69.5	25.4	0.542	554	630
3PS-16[e]	65	166.3	192.8	---	25.4	0.539	544	620
3PU-19	-60	7.7	42.3(39.6)[d]	40.1	12.7	0.542	594	671
3PU-11	0	11.2	50.7	45.8	12.7	0.548	567	645
3PU-35	26	44.0	99.8	67.2	12.7	0.553	558	620
3PU-15	38	47.5	103.5	69.0	12.7	0.547	554	630
3PU-27	50	76.1	130.8	76.3	12.7	0.542	549	625
3PU-3	65	117.7	162.3	83.1	12.7	0.534	544	620
Wall-3 Specimens								
3PT-4	-20	13.8	56.3	53.4	25.4	0.540	556	633
3PT-3	25	27.5	79.0	68.4	25.4	0.543	539	615
3PT-2	60	126.3	168.2	101.4	25.4	0.539	526	602
3PU-36	-80	5.9	37.2(34.9)[d]	35.9	12.7	0.550	584	661
3PU-20	-50	12.7	54.3	48.7	12.7	0.548	570	647
3PU-12	0	24.9	75.3	58.4	12.7	0.540	548	625
3PU-31	26	76.4	131.5	75.7	12.7	0.550	538	614
3PU-4	50	73.2	128.2	74.3	12.7	0.543	530	605
3PU-24	60	152.2	184.7	85.9	12.7	0.548	526	602

[a] Beta corrected K_{Jc}
[b] Estimated value used for validity/initiation determination
[c] Specimen side grooved 20%
[d] Number in parenthesis is valid E399 K_{Ic} value
[e] Type B R Curve
[f] Type C R Curve

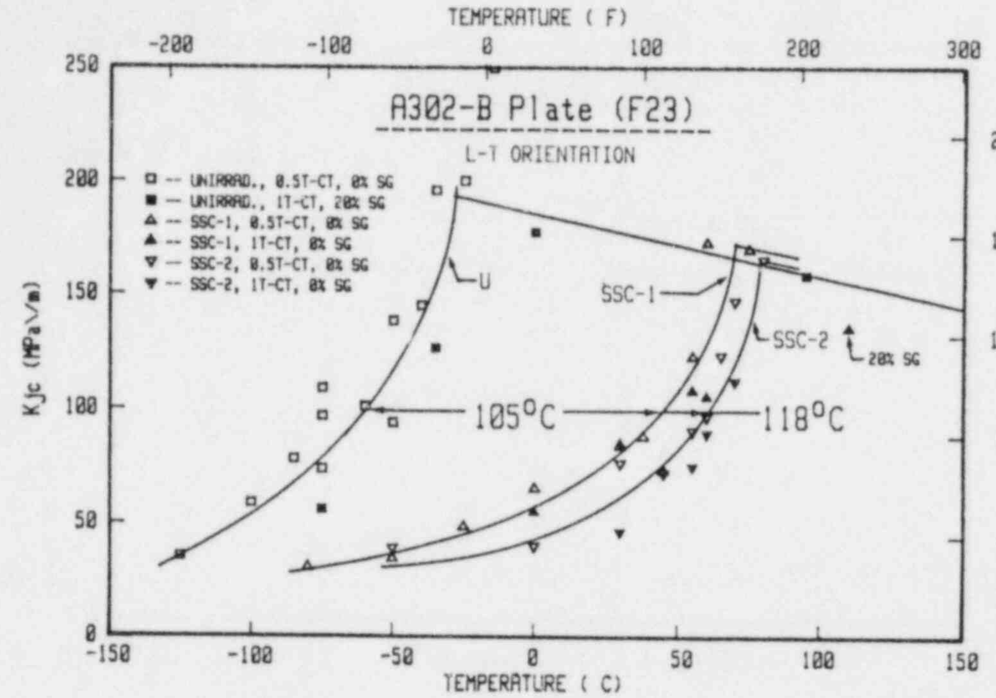

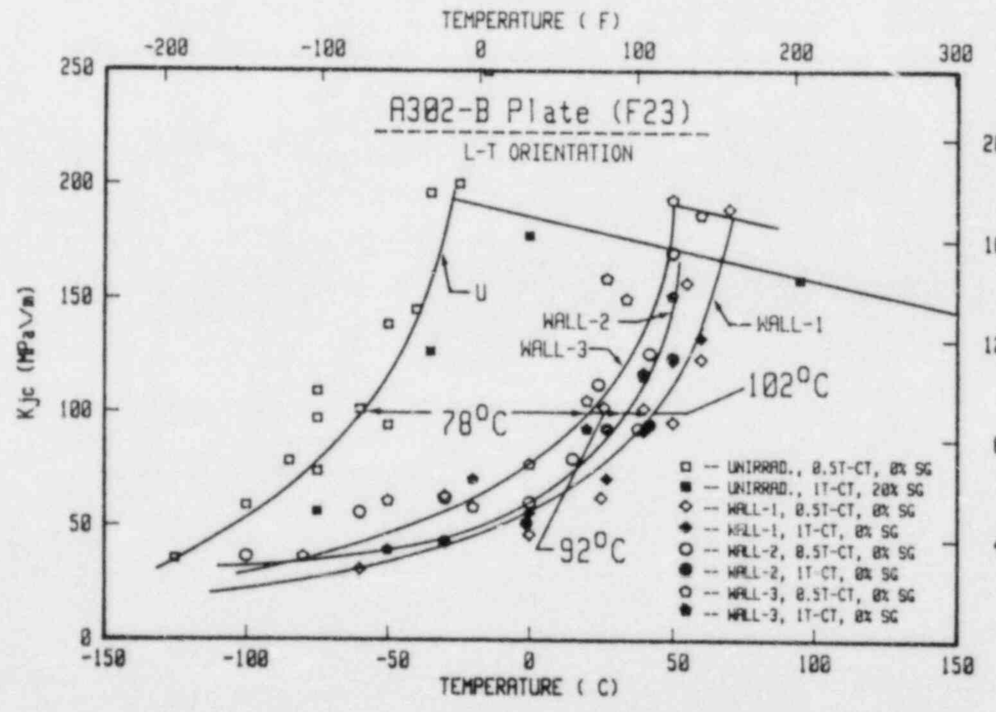

Fig. 8.3 Static initiation fracture toughness data for the A302-B plate illustrating the relative increase in brittle-to-ductile transition temperature for the surveillance capsule material (upper plot) and wall capsule material (lower plot).

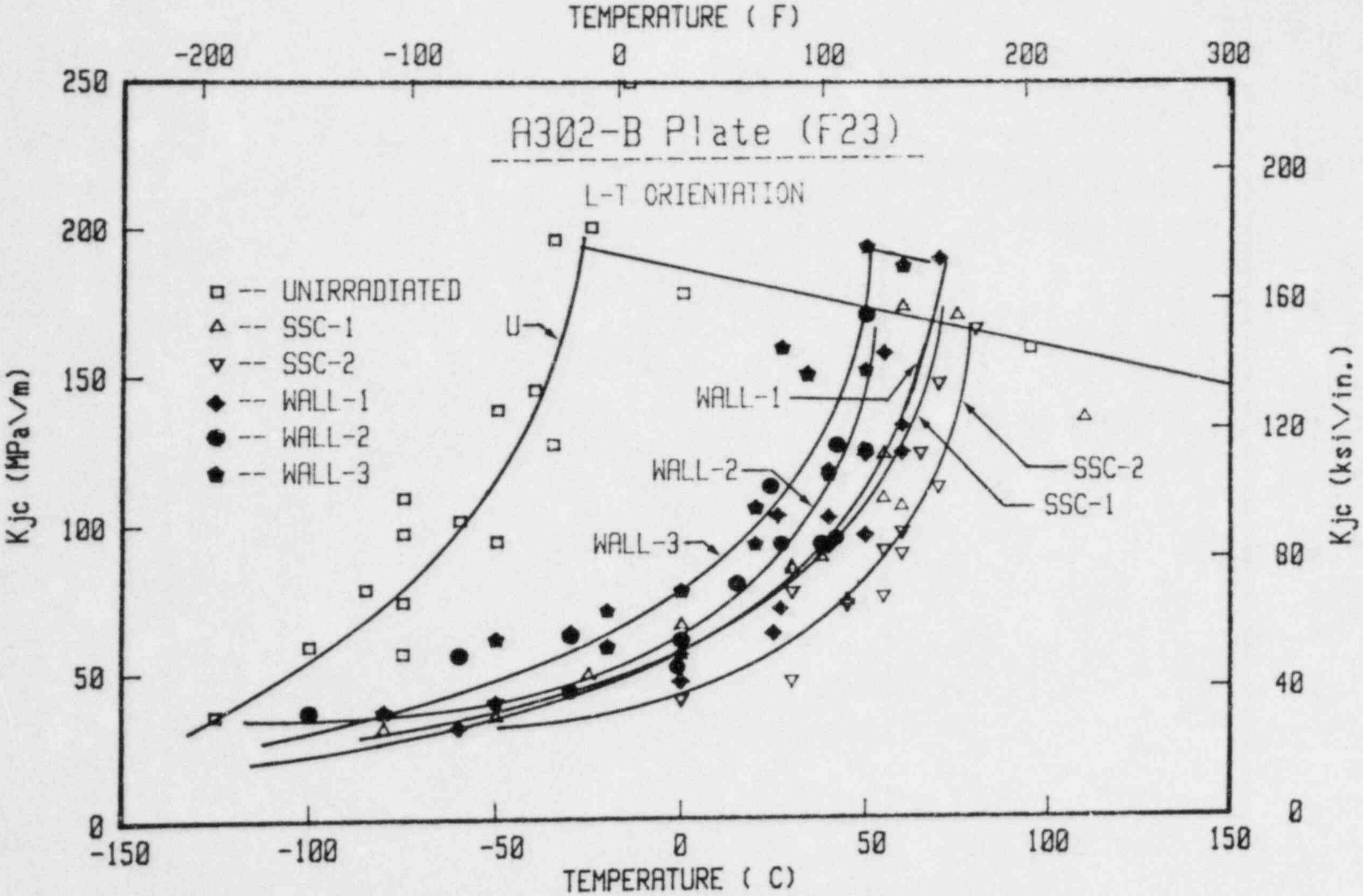

Fig. 8.4 Illustration showing the relative position of the brittle-to-ductile transition for all capsules (A302-B plate).

Table 12. Summary of A302-B Fracture Toughness Brittle-to-Ductile Transition

Irradiation Capsule	Transition Temperature Index (°C)					Transition Temperature Shift (°C)				
	K_{Jc}			$K_{\beta c}$		K_{Jc}			$K_{\beta c}$	
	75[a]	100[a]	150[a]	75[a]	100[a]	75[b]	100[b]	150[b]	75[b]	100[b]
Unirradiated	-77	-56	-35	-48	-6	---	----	----	---	---
SSC-1	25	49	68	50	83	102	105	103	98	89
SSC-2	43	62	76	63	87	120	118	111	111	93
Wall-1	25	46	65	44	64	102	102	100	92	70
Wall-2	17	36	50	36	56	94	92	85	84	62
Wall-3	0	22	45	24	55	77	78	80	72	61

[a] $MPa\sqrt{m}$ level where the transition temperature is indexed.

[b] $MPa\sqrt{m}$ level where the increase in temperature of the transition is determined.

Table 13. Summary of A533-B Fracture Toughness Brittle-to-Ductile Transition

Irradiation Capsule	Transition Temperature Index (°C)					Transition Temperature Shift (°C)				
	K_{Jc}			$K_{\beta c}$		K_{Jc}			$K_{\beta c}$	
	75[a]	100[a]	150[a]	75[a]	100[a]	75[b]	100[b]	150[b]	75[b]	100[b]
Unirradiated	-48	-23	6	-11	27	---	---	---	---	---
SSC-1	32	49	65	52	74	80	72	59	63	47
SSC-2	50	74	95	74	100	98	97	89	85	73
Wall-1	34	57	80	59	79	82	80	74	70	52
Wall-2	13	36	62	45	66	61	59	56	56	39
Wall-3	6	33	57	36	61	54	56	51	47	34

a MPa $\sqrt{m}$ level where the transition temperature is indexed.

b MPa $\sqrt{m}$ level where the increase in temperature of the transition is determined.

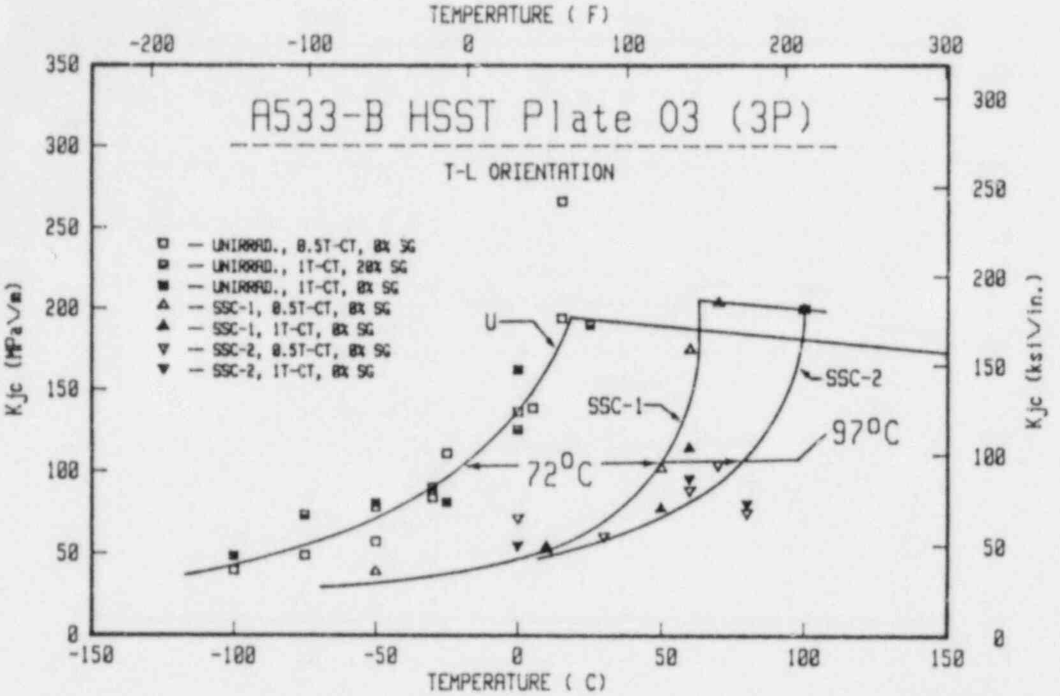

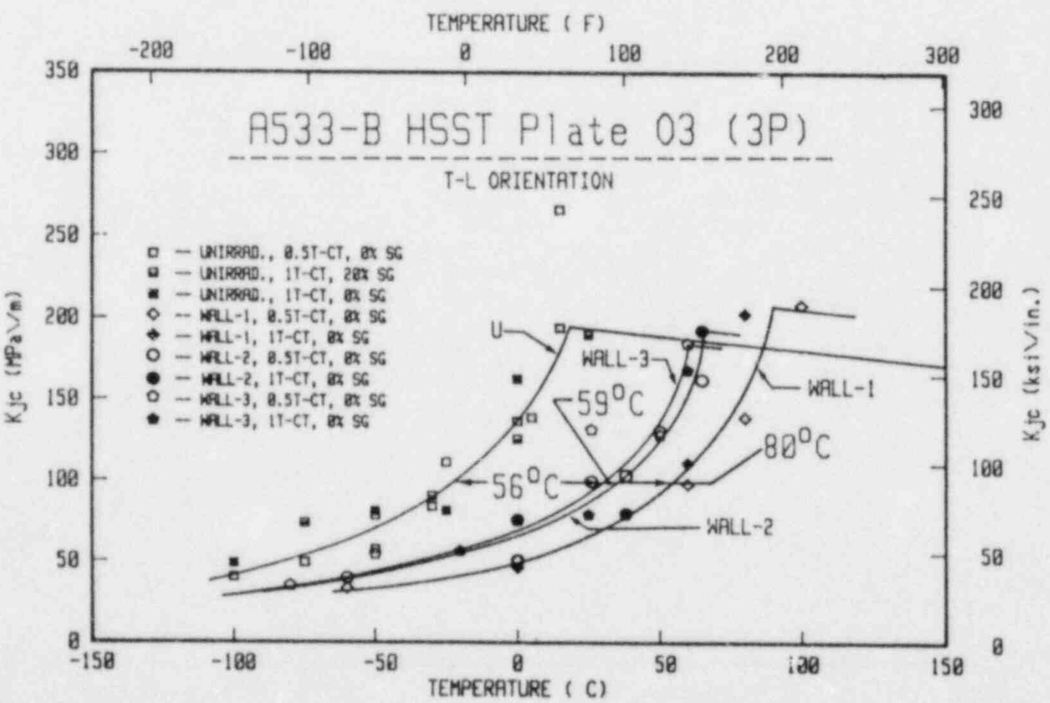

Fig. 8.5 Static initiation fracture toughness data for the A533-B plate illustrating the relative increase in the brittle-to-ductile transition temperature for the surveillance capsule material (upper plot) and wall capsule material (lower plot).

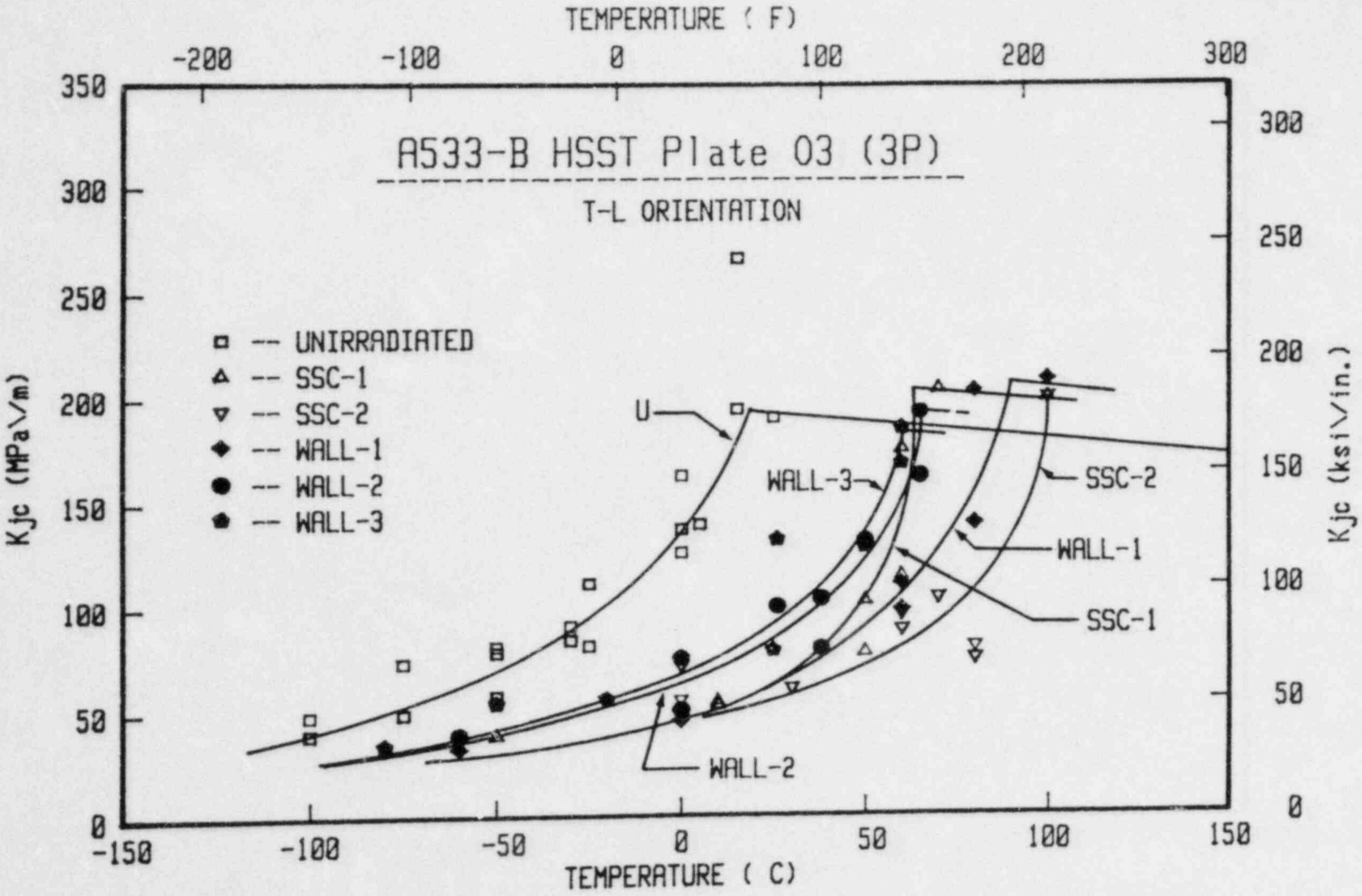

Fig. 8.6 Illustration showing the relative position of the brittle-to-ductile transition for all capsules (A533-B plate).

steels exhibit an upper shelf toughness of ~190 MPa$\sqrt{m}$ at the onset of the upper shelf, the toughness at 200°C is 130 MPa$\sqrt{m}$ and 170 MPa$\sqrt{m}$ for the A302-B and A533-B steels, respectively.

Only one irradiated specimen was side-grooved. This specimen (A302-B material from capsule SSC-1) tested at 110°C or just beyond the onset of the K_{Jc} upper shelf, indicated a shelf drop of 12 percent.

A comparison of the 1T-CT and 0.5T-CT test results (non-side-grooved specimens) for the transition region indicates a possible bias by the larger specimens toward a higher temperature transition (<5°C). The bias, however, is not sufficient to place the data from the larger specimens outside of the bounds of the data scatter for the smaller specimens.

One 0.5T-CT A302-B specimen from wall capsule 2 inadvertently was tested dynamically, due to a test system malfunction. The testing rate was on the order of 4,300 MPa$\sqrt{m}$/min., one hundred times higher than that of the remaining tests. The test temperature corresponded to the low toughness portion of the transition region and the specimen failed by cleavage without any stable ductile crack extension. The load vs. deflection record was linear. J_{Ic}, calculated from this record, did not reveal a significant rate effect. The datum fell within the data scatter band obtained with the slower rate (0.5T-CT and 1T-CT) tests.

8.2.1 β_{Ic} Correction

The application of the β_{Ic}-correction to the fracture toughness results for the A302-B plate is illustrated in Fig. 8.7 and 8.8. The effect of the β_{Ic}-correction is to depress the K_{Jc} values in every case. The magnitude of the correction is directly related to the K_{Jc} magnitude and is inversely related to the flow stress. Both of these quantities have a nonlinear effect on the magnitude of the correction. In other words, a percentage decrease in flow stress yields a greater percentage decrease in K_{Jc}, while a percentage increase in K_{Jc} value would yield a greater percentage decrease in magnitude due to the β_{Ic}-correction. The comparative effect of the β_{Ic}-correction is to decrease K_{Jc}-values in the upper transition region by a greater percentage than values in the lower transition region, and also to decrease unirradiated values by a greater percentage than irradiated values.

As indicated in Fig. 8.7 and 8.8 for the A302-B plate and in Fig. 8.9 and 8.10 for the A533-B plate, many of these $K_{\beta c}$ data do not extend above 100 MPa$\sqrt{m}$. Therefore, indexing the transition temperature at 100 MPa$\sqrt{m}$ may yield inaccurate results due to the necessity to extrapolate the curves to reach that level.

Table 12 (A302-B) and Table 13 (A533-B) list the transition temperatures and the transition temperature shifts for both the K_{Jc} and $K_{\beta c}$ data. Indices of 75 and 100 MPa$\sqrt{m}$ are used for both the K_{Jc} and $K_{\beta c}$ data, while an additional index of 150 MPa$\sqrt{m}$ is referenced for the K_{Jc} data. For both the A302-B and A533-B plates, the $K_{\beta c}$ temperature at an index of 75 MPa$\sqrt{m}$ matches the K_{Jc} temperature at 100 MPa$\sqrt{m}$ very closely. In all cases, the $K_{\beta c}$ temperature at 100 MPa$\sqrt{m}$ is essentially equal to or greater than the temperature at any of the other indices.

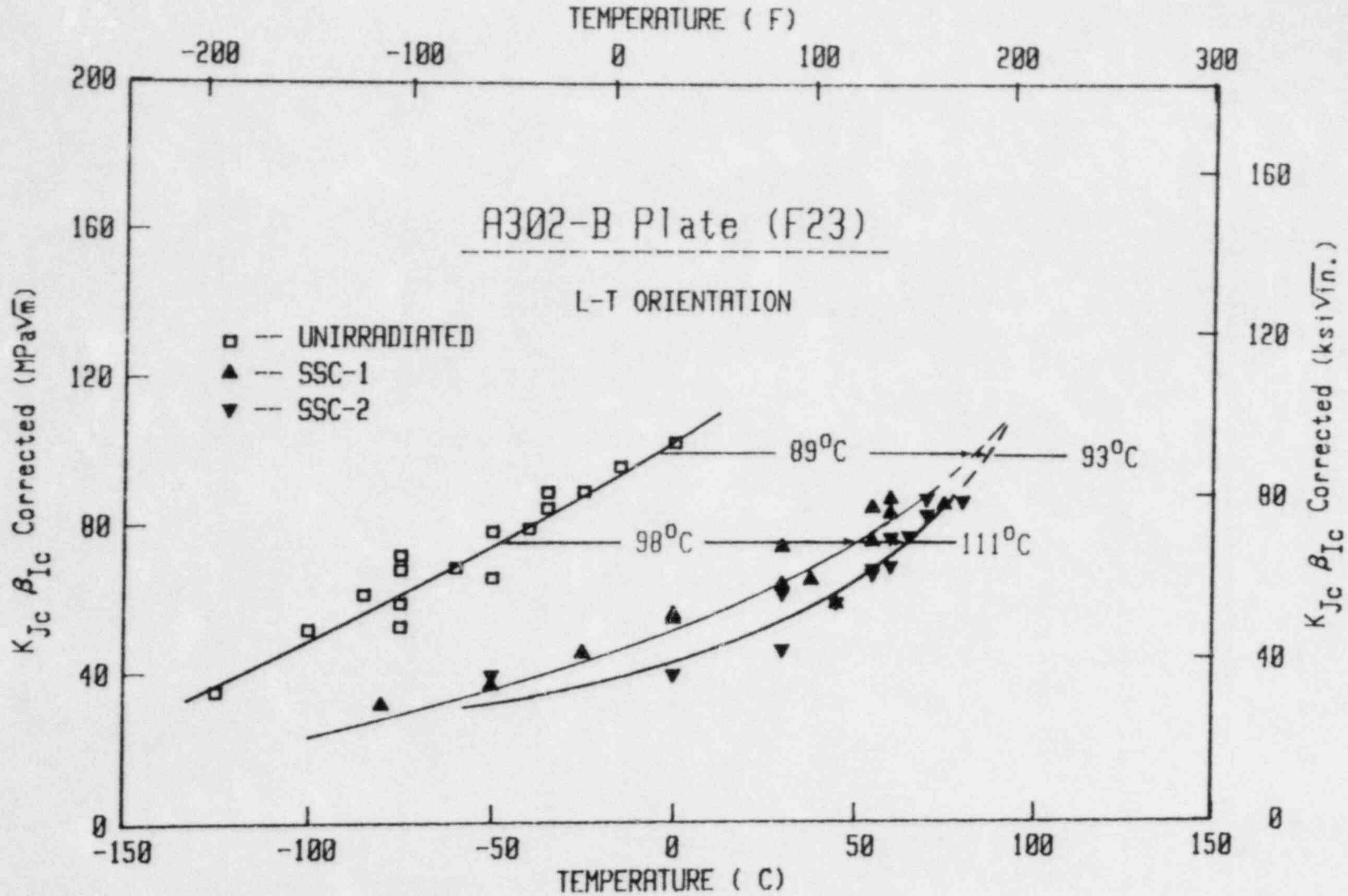

Fig. 8.7. $K_{\beta c}$ fracture toughness data for surveillance capsules (A302-B plate).

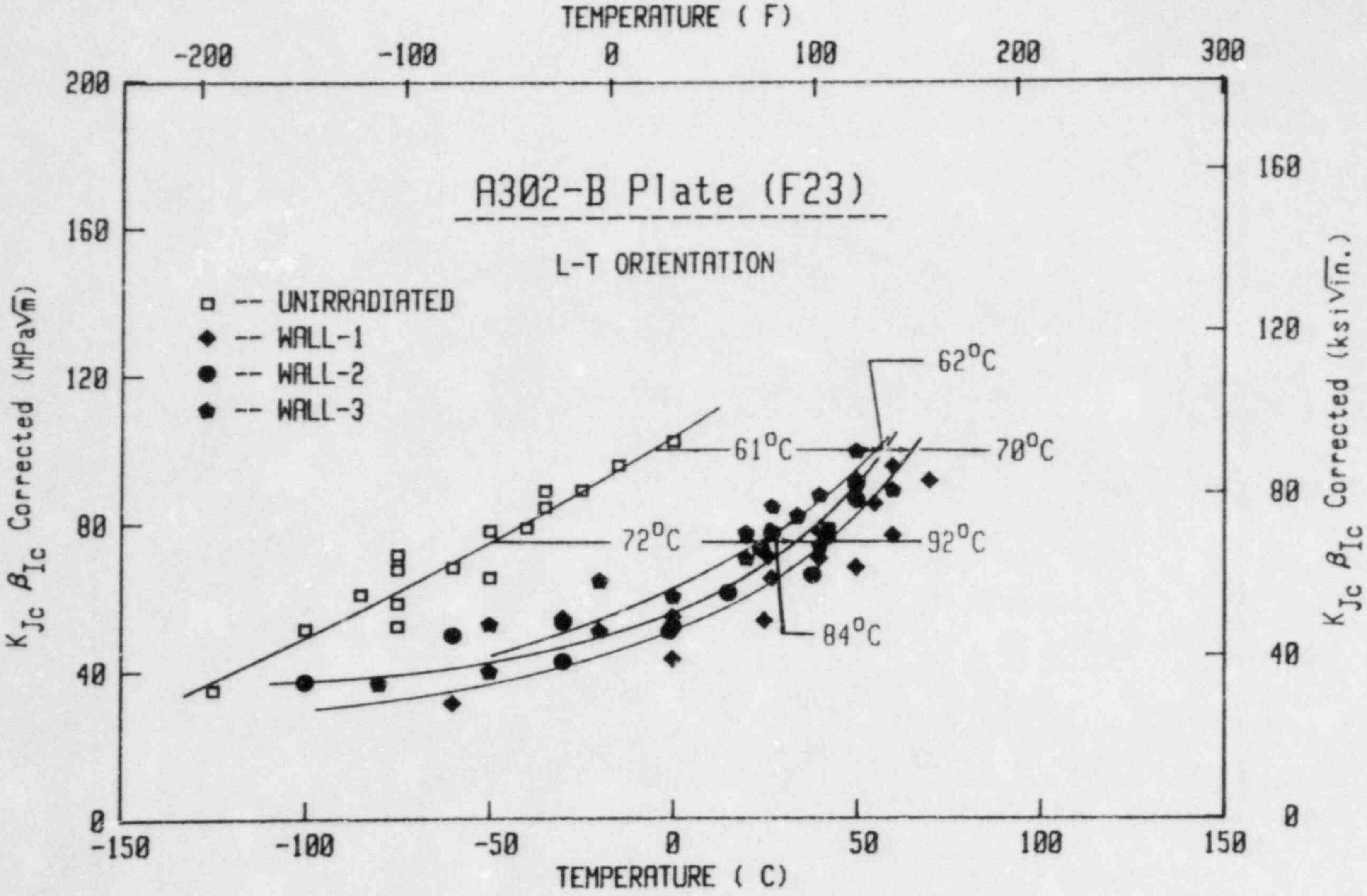

Fig. 8.8. $K_{\beta c}$ fracture toughness data for wall capsules (A302-B plate).

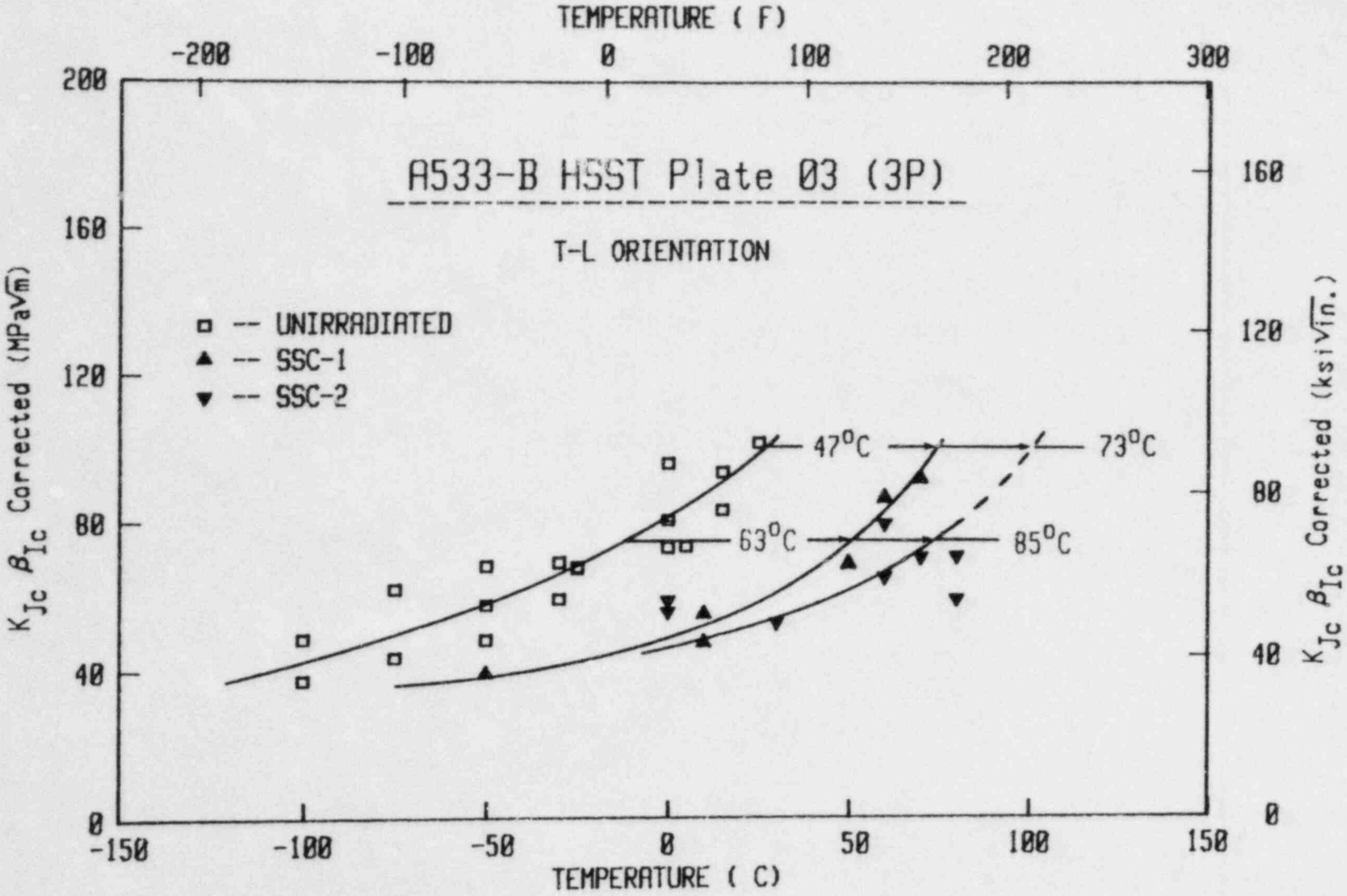

Fig. 8.9. $K_{\beta c}$ fracture toughness data for surveillance capsules (A533-B plate).

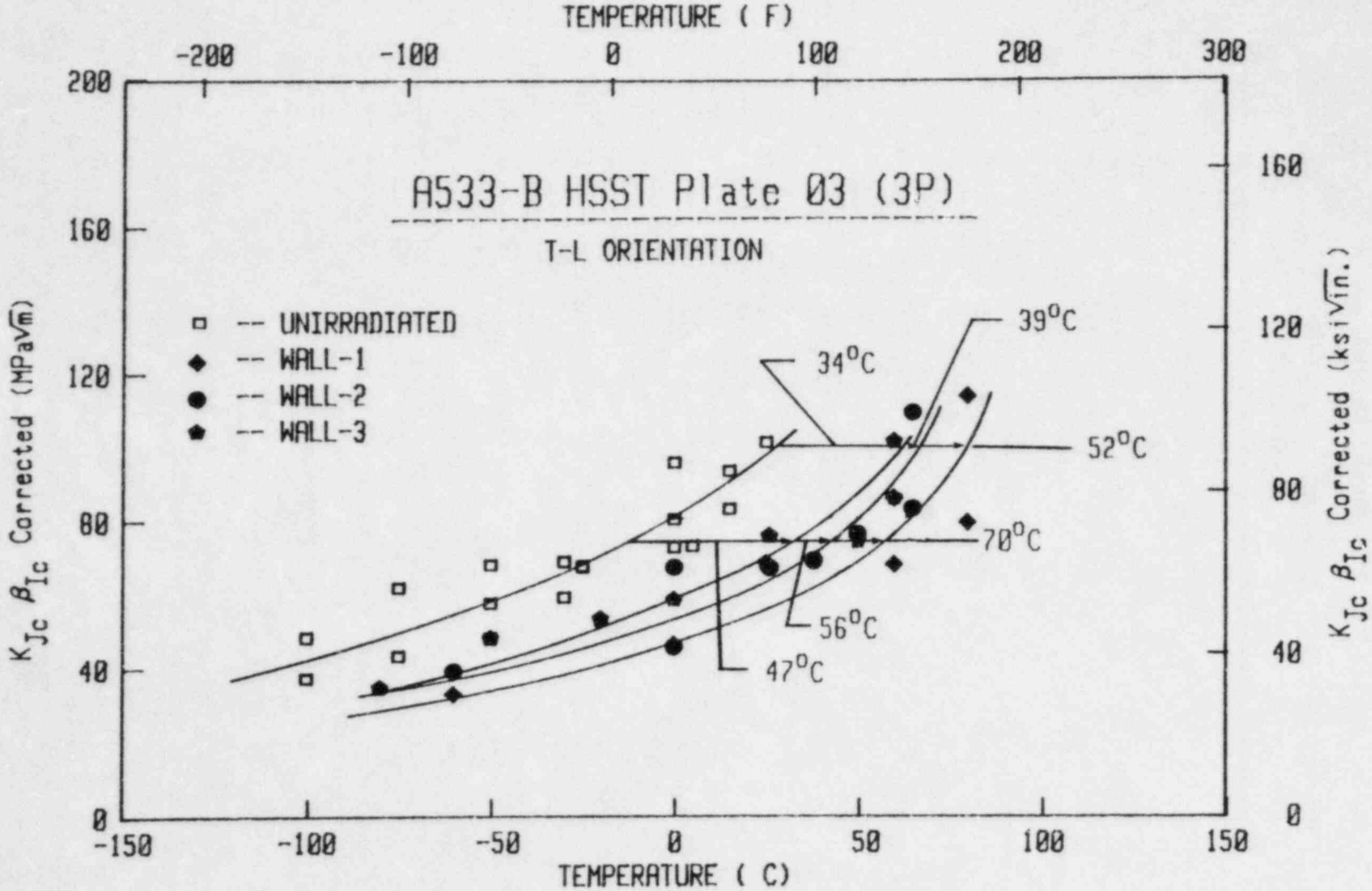

Fig. 8.10. $K_{\beta c}$ fracture toughness data for wall capsules (A533-B plate).

On the other hand, the $K_{\beta c}$ transition temperature shifts are less than virtually all of the K_{Jc} transition temperature shifts. This result confirms that the β_{Ic}-correction decreases unirradiated values more than irradiated values. Further, the $K_{\beta c}$ shift at 100 MPa $\sqrt{m}$ is always less than the 75 MPa $\sqrt{m}$ shift.

8.2.2 Comparisons with ASME Code

Article G-2000 from Section III, Appendix G of the ASME Boiler and Pressure Vessel Code defines a reference or K_{IR} curve in terms of the RT_{NDT} temperature. The latter is indexed in terms of either C_v or drop weight nil ductility transition (NDT) results, whichever produces the higher value for RT_{NDT}. For the subject steels, the NDT temperature governs RT_{NDT}. The K_{IR} curve is based on lower bound static, dynamic and crack arrest K_I data for several steels, including A533-B Class 1, and is used for design and safety analyses.

Figures 8.11 and 8.12 show the K_{IR} curve indexed to the unirradiated condition drop weight NDT temperature, i.e., RT_{NDT}, for the plates and the β_{Ic} corrected fracture toughness data ($K_{\beta c}$) for the unirradiated and irradiated conditions. For the irradiated condition, the K_{IR} curve was shifted to the right by an amount equal to the temperature elevation found in the C_v (41 J) and CT (K_{Jc}, 100 MPa $\sqrt{m}$) tests. It is apparent that the adjusted K_{IR} curve is indeed conservative for the irradiated as well as the unirradiated condition in each case. This observation was expected in that static toughness as obtained in this program, is generally higher than the dynamic toughness (i.e., the toughness values which form the K_{IR} curve).

Article A-4000 from Section XI, Appendix A of the ASME Boiler and Pressure Vessel Code defines an additional reference curve which is founded on lower-bound static K_{Ic} fracture toughness data for several steels including A533-B Class 1. In Fig. 8.13, this curve is shown referenced to the NDT temperature of the A533-B HSST Plate 03 in the unirradiated condition and shifted by an amount equal to the transition temperature elevations found in the C_v (41 J) and the CT (K_{Jc}, 100 MPa $\sqrt{m}$) tests. The reference curve appears to be unconservative in some cases based on the data of Fig. 8.13, i.e., the $K_{\beta c}$ data fall to the right of the appropriate reference curve but only by 15°C at most. Further study of this behavior is anticipated. It is emphasized that the data in the present case are all based on $K_{\beta c}$, as opposed to valid K_{Ic} data.

9. CT vs. C_v ASSESSMENTS OF IRRADIATION EFFECT

The correspondence between the CT and C_v test methods in their independent determinations of the irradiation effect to the brittle-ductile transition is illustrated in Fig. 9.1 for the K_{Jc} data and in Fig. 9.2 for the $K_{\beta c}$ data. In Tables 14 (A302-B) and 15 (A533-B), the K_{Jc} and $K_{\beta c}$ data are both evaluated in terms of the temperature at 100 MPa $\sqrt{m}$. In the figures, the left hand graphs compare the radiation-induced elevations of the C_v and CT test methods for the A302-B plate; the right hand graphs are a similar construction for the A533-B plate. Parallel comparisons for other temperature indices can be readily developed by referring to Tables 4, 5, 12 and 13 for the K_{Jc} data. Initial discussion of these comparisons will concentrate on the K_{Jc} data.

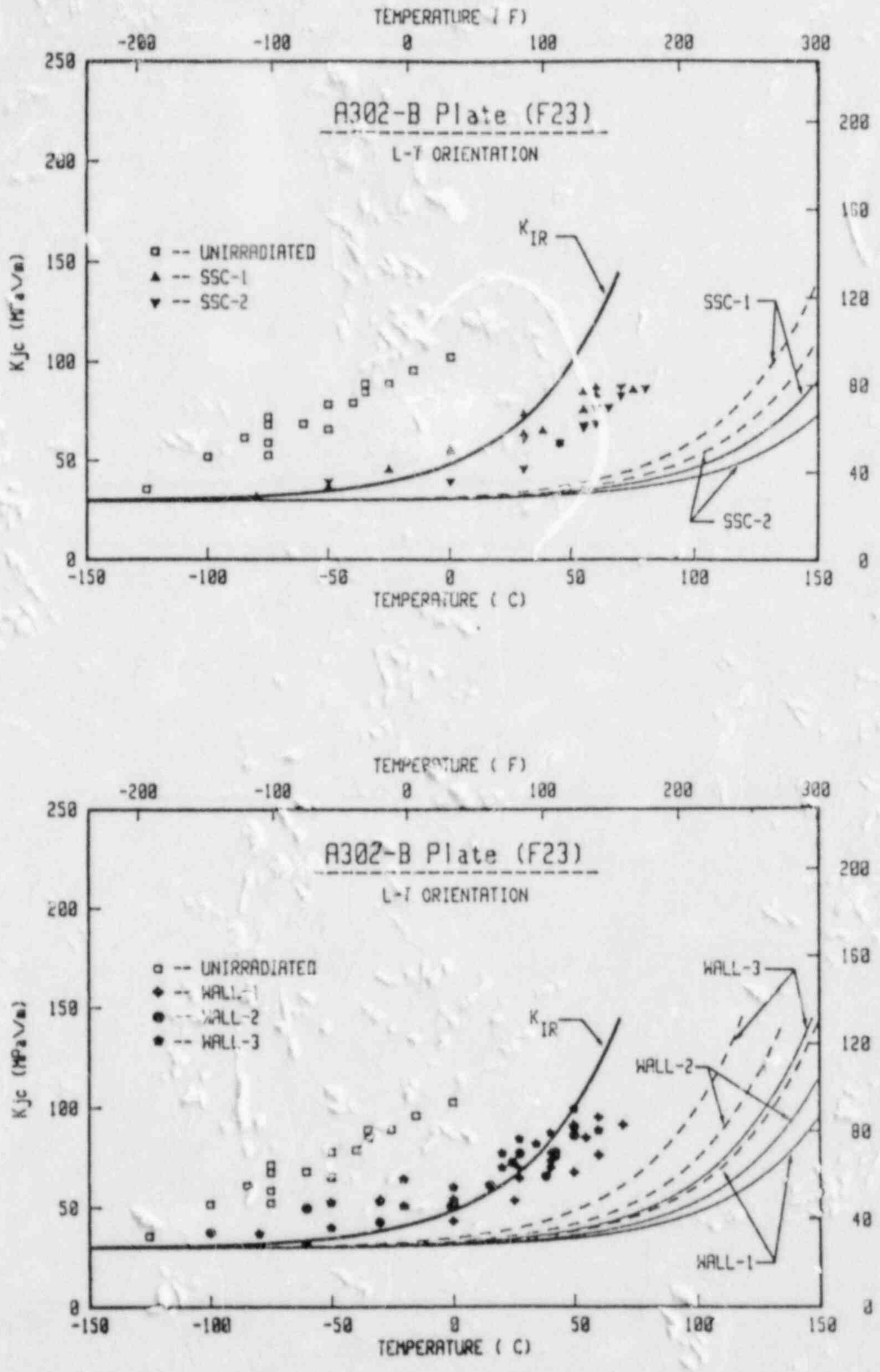

Fig. 8.11. ASME K_{IR} reference curve indexed to the A302-B unirradiated nil ductility transition temperature. The K_{IR} curve has been shifted by an amount equal to that of both Charpy (41 J, dashed lines) and compact (K_{Jc}, 100 MPa $\sqrt{m}$, solid lines) specimen data from the various capsules.

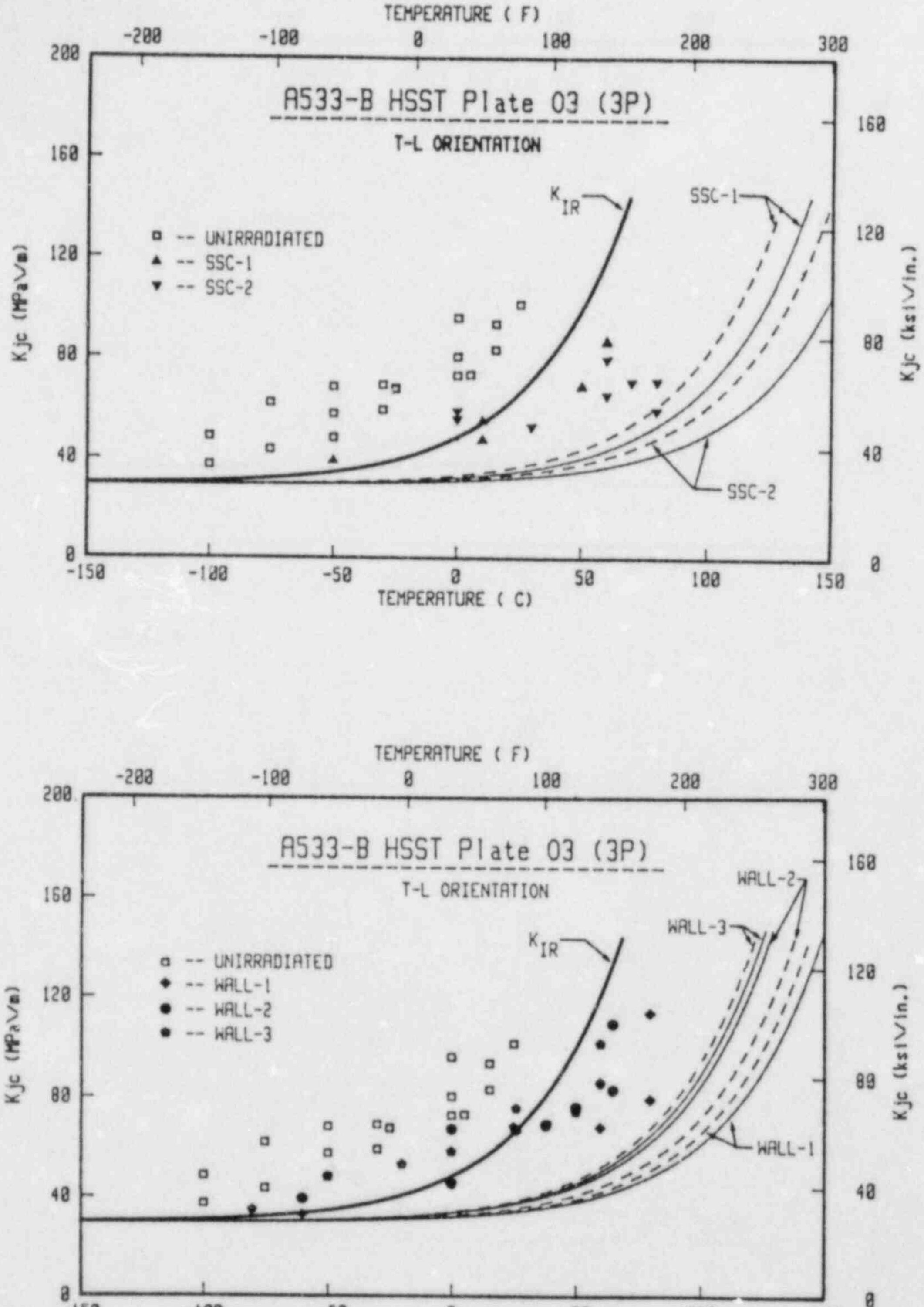

Fig. 8.12. ASME K_{IR} reference curve indexed to the A533-B unirradiated nil ductility transition temperature. The K_{IR} curve has been shifted by an amount equal to that of both Charpy (41 J, dashed lines) and compact (K_{Jc}, 100 MPa $\sqrt{m}$, solid lines) specimen data from the various capsules.

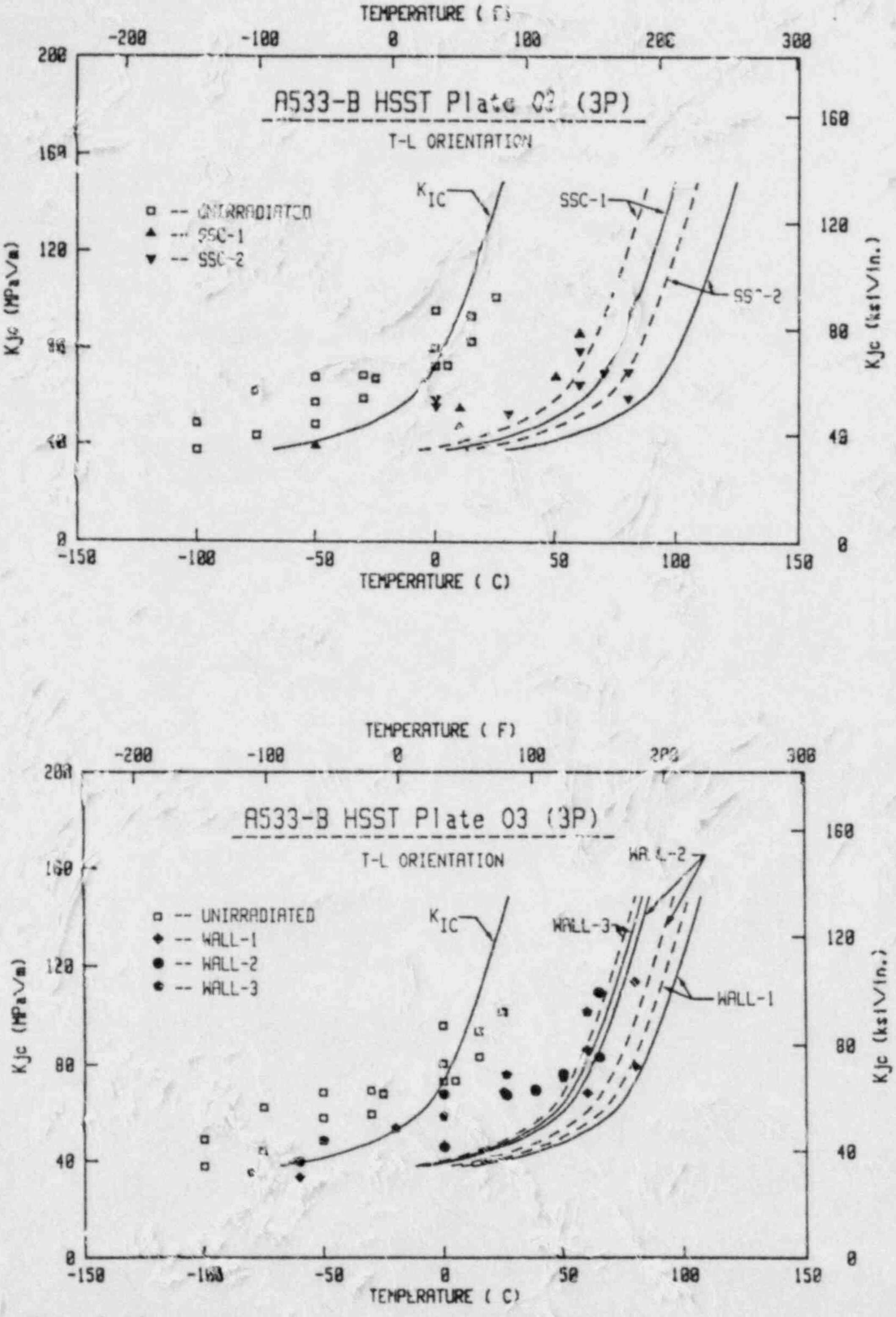

Fig. 8.13. ASME K_{Ic} reference curve indexed to the A533-B reference transition temperature RT_{NDT}. The K_{Ic} curve has been shifted by an amount equal to that of both Charpy (41 J, dashed lines) and compact (K_{Jc}, 100 MPa $\sqrt{m}$, solid lines) specimen data from the various capsules.

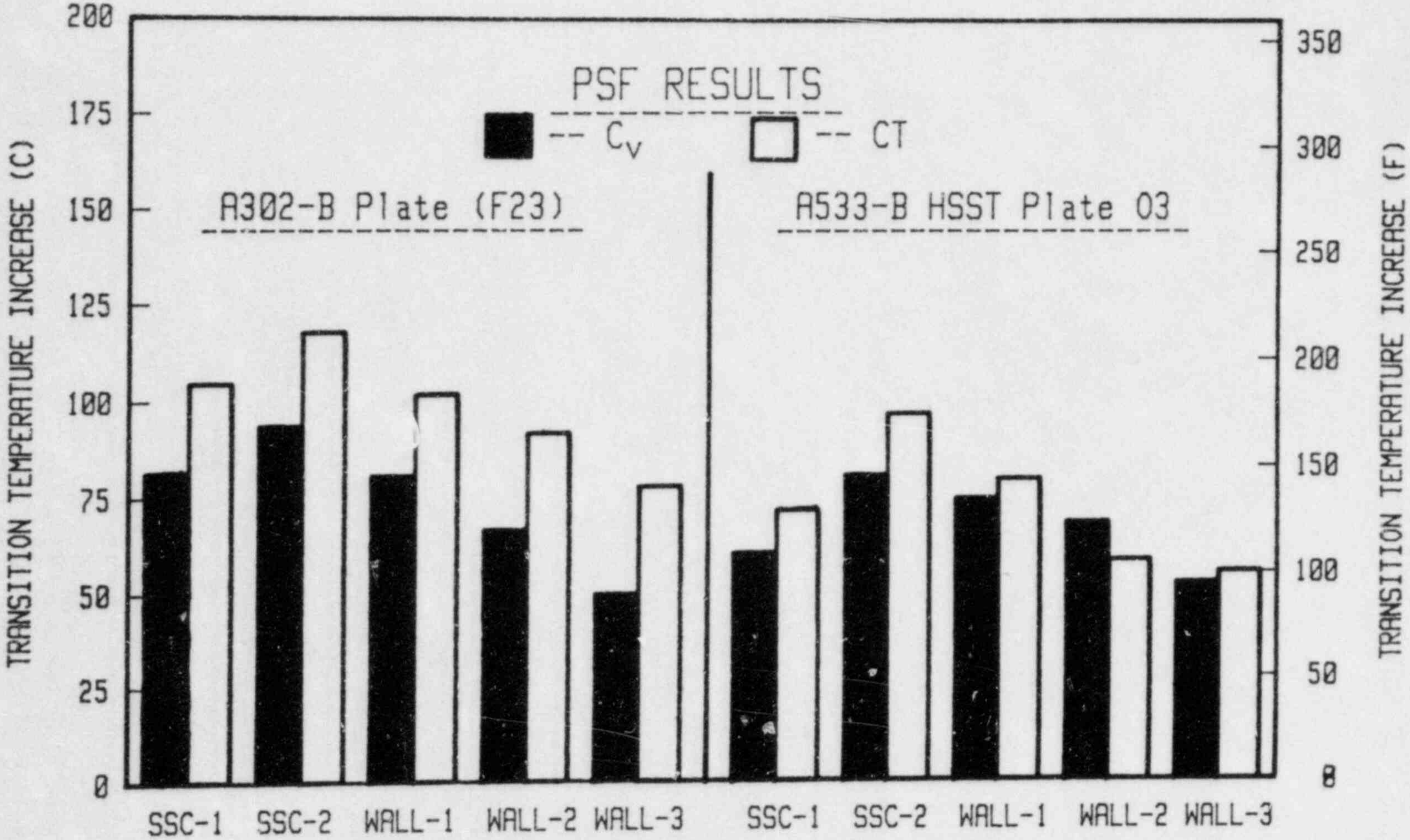

Fig. 9.1 Comparison of 41 J (C_v) and 100 MPa$\sqrt{m}$ (CT) transition temperature elevations.

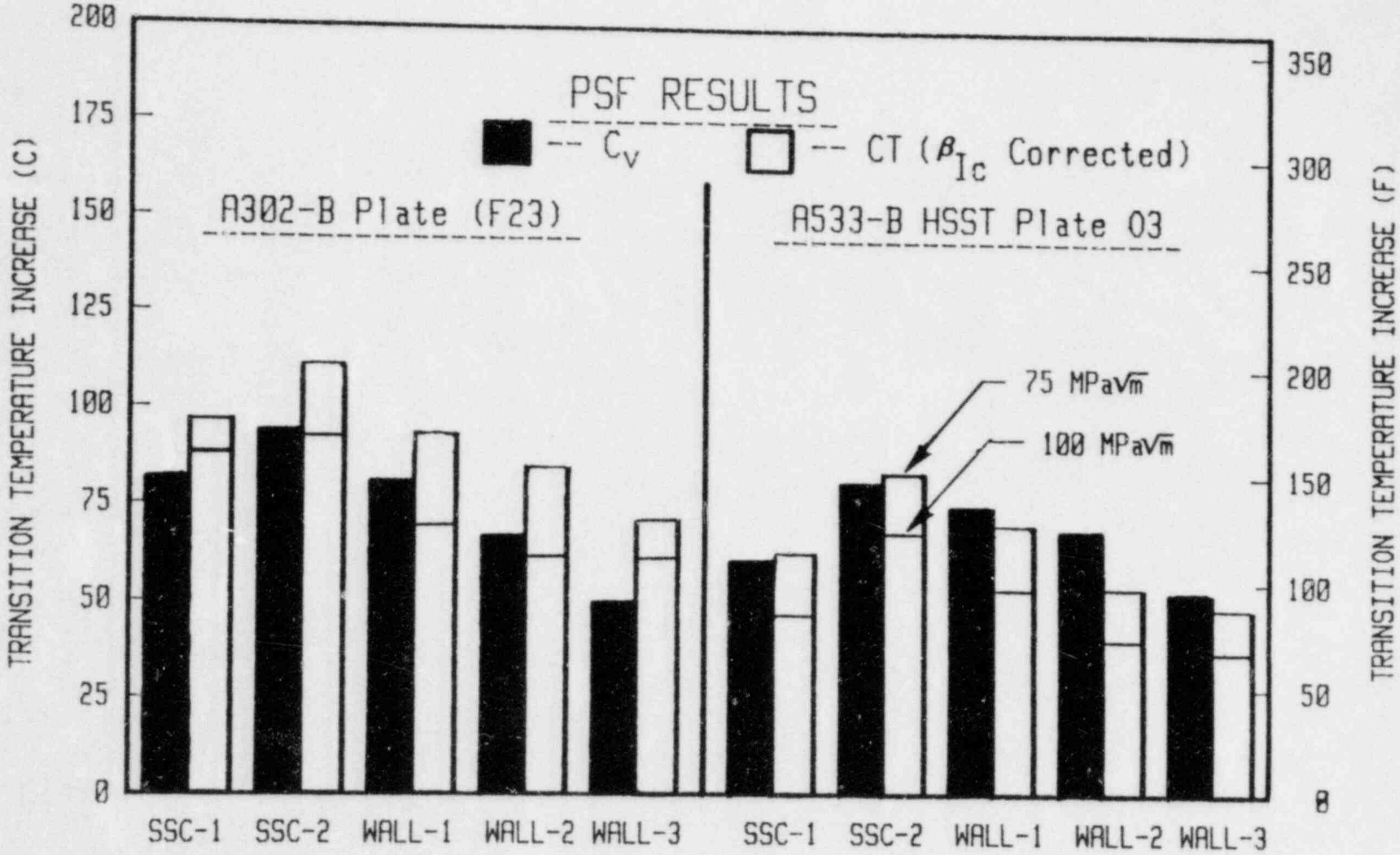

Fig. 9.2. Comparison of 41 J (C_v) and $K_{\beta c}$ (CT) transition temperature elevations.

Table 14. Comparison of CT vs. C_v Test Method Assessments of Irradiation Effect to Transition Temperature for A302-B Plate

Irradiation Capsule	Transition Temp. (°C)					Irradiation Elevation (ΔC)				
	(A) (K_{Jc} 100 MPa $\sqrt{m}$ Index)	(B) ($K_{\beta c}$ 100 MPa $\sqrt{m}$ Index)	(C) 41 J Index	(C−A) Diff.	(C−B) Diff.	(D) (K_{Jc} 100 MPa $\sqrt{m}$ Index)	(E) ($K_{\beta c}$ 100 MPa $\sqrt{m}$ Index)	(F) 41 J Index	(D−F) Diff.	(E−F) Diff.
Unirradiated	−56	−6	−4	52	2	---	---	---	---	---
SSC-1	49	83	78[a]	29[a]	−5[a]	105	89	82[a]	23[a]	7[a]
SSC-2	62	87	90	28	3	118	93	94	24	−1
Wall-1	46	64	77	31	13	102	70	81	21	−11
Wall-2	36	56	63	27	7	92	62	67	25	−5
Wall-3	22	55	46	24	−9	78	61	50	28	11
(average)				(31.8)	(1.8)				(24.2)	(0.2)

[a] Average of left and right compartment data.

Table 15. Comparison of CT vs. C_v Test Method Assessments of Irradiation Effect to Transition Temperature for A533-B Plate

Irradiation Capsule	Transition Temp. (°C)					Irradiation Elevation (Δ°C)				
	(A) (K_{Jc} 100 MPa$\sqrt{m}$ Index)	(B) ($K_{\beta c}$ 100 MPa$\sqrt{m}$ Index)	(C) 41 J Index	(C-A) Diff.	(C-B) Diff.	(D) (K_{Jc} 100 MPa$\sqrt{m}$ Index)	(E) ($K_{\beta c}$ 100 MPa$\sqrt{m}$ Index)	(F) 41 J Index	(D-F) Diff.	(E-F) Diff.
Unirradiated	-23	27	-1	22	-28	---	---	---	---	---
SSC-1	49	74	60	11	-14	72	47	61	11	-14
SSC-2	74	100	80	6	-20	97	73	81	16	-8
Wall-1	57	79	74	17	-5	80	52	75	5	-23
Wall-2	36	66	68	32	+2	59	39	69	-10	-30
Wall-3	33	61	52	19	-9	56	34	53	3	-19
(average)				(17.0)	(-12.3)				(5.0)	(-18.8)

One observation from Figure 9.1 is that the 41 J temperature elevation has a tendency to be less than the 100 MPa$\sqrt{m}$ temperature elevation from K_{Jc} tests. The trend is most apparent for the A302-B plate. For this material, the 41 J temperature elevation is, on average, about 24°C smaller than the 100 MPa$\sqrt{m}$ temperature increase (see Tables 14 and 15). With the A533-B plate, the 41 J temperature elevations are lower by 3 to 16°C except for capsule Wall-2 (discussed below). For purposes of this discussion, agreement within 8°C is considered indicative of a 1:1 correspondence. This assumption is felt to be realistic in view of the data scatter tendencies of the materials, the limited number of tests conducted for each capsule, and the probability for a fluence difference between the C_v and CT specimen groups due to their particular locations in the capsule (See Figs. 5.1 - 5.5).

The reason(s) for the noted dissimilarities of the C_v and CT irradiation effect indications is not yet clear. Analysis of the data, moreover, reveals points of inconsistency. For example, the A302-B data of Table 14 describe a uniform trend. The results for the A533-B plate, on the other hand, are mixed. Here the 41 J temperature elevation is less than the 100 MPa$\sqrt{m}$ temperature elevation for both SCC capsule irradiations, but for the wall capsules the 41 J temperature elevation is either within 5°C of the 100 MPa$\sqrt{m}$ temperature increase or greater by 10°C. To further cloud the issue, earlier tests of the A302-B plate (Ref. 15) after 3.6 x 10^{19} n/cm^2 at 288°C did show close agreement of the two temperature elevations (within 7°C) for the same test orientation (LT) used here. At the same time, a 39°C disagreement was observed when the plate was tested in the TL orientation at a somewhat lower fluence of 2.7 x 10^{19} n/cm^2. A specimen orientation dependence has been ruled out. The early tests (Ref. 15) also produced comparisons of transition temperature elevation for two other A533-B plates, an A508-2 forging and four submerged arc welds. In seven out of eleven irradiation tests made, the 100 MPa$\sqrt{m}$ temperature elevation was found to be much larger than the 41 J temperature elevation. To summarize, the indications of both studies, the 41 J temperature elevation frequently does not provide a conservative estimate of the measured 100 MPa$\sqrt{m}$ temperature elevation by irradiation, from K_{Jc} tests.

Close examination of the data for the A302-B plate suggests that 288°C irradiation decreases the temperature spread between the C_v and K_{Jc} data. In the irradiated condition (Table 14), the 41 J temperature in all cases is about 28°C higher than the K_{Jc} 100 MPa$\sqrt{m}$ temperature. For the unirradiated condition, the difference is 52°C or a factor of two greater. For the A533-B plate (Table 15), on the other hand, the preirradiation and postirradiation differences are nearly the same, i.e., about 17°C. The 6°C difference for capsule SSC-2 and 32°C difference for the capsule Wall-2 are somewhat anomalous in view of the companion results for this plate.

After the application of the β_{Ic}-correction, the comparison of CT and C_v transition temperature shifts does change. As indicated in Fig. 9.2, in all but two cases the 100 MPa$\sqrt{m}$ transition temperature shift is <u>less</u> than the related increase at 41 J. With the 75 MPa$\sqrt{m}$ index, the $K_{\beta c}$ temperature shift for the A302-B material is greater than the 41 J shift, while for the A533-B plate the 41 J shift is larger in all but one case. From Table 14 and 15, the $K_{\beta c}$ transition temperature shifts (at 100 MPa$\sqrt{m}$) are ~ 23°C less on average than the corresponding K_{Jc} shift (at 100 MPa$\sqrt{m}$)

for each material. These decreases are a direct function of the greater increase in temperature at the 100 MPa$\sqrt{m}$ level of the unirradiated curve due to the β_{Ic}-correction as compared to the increase of the irradiated curve.

The cumulative effect of the β_{Ic}-correction is to take K_{Jc} data which indicates that C_v data are an unconservative indicator of irradiation embrittlement, and give $K_{\beta c}$ data which indicates that C_v data are not an unconservative indicator of irradiation embrittlement, at least for these two plates. For the A302-B plate, the $K_{\beta c}$ data (at 100 MPa$\sqrt{m}$) match the C_v 41 J data very closely, while for the A533-B plate the K_{Jc} data (at 100 MPa$\sqrt{m}$) match the C_v 41 J transition temperature increase better than the $K_{\beta c}$ data. The concern now is to determine whether the $K_{\beta c}$ data or the K_{Jc} data are the better approximation of the actual K_{Ic} behavior of the material. In particular, a difference of 23°C in transition temperature elevation could be quite significant to certain older plants. For example, that change in temperature translates to 2.5 - 4 years of reduced operation for some older plants approaching end-of-life K_{IR} temperatures.

Inspite of the above uncertainty, it is encouraging that the adjustment of the K_{IR} curve by the postirradiation elevation of the 41 J temperature proved very conservative when compared against actual CT ($K_{\beta c}$) test data (see Section 8). However, a similar conclusion does not hold for adjustments in terms of the ASME Sec. XI K_{Ic} curve.

A correlation assessment of the C_v and CT methods for the upper shelf regime was not possible. The CT specimens were side-grooved for the unirradiated condition tests but not for the irradiated condition tests; it has been established that side-grooved specimens typically exhibit a lower upper shelf than nonside-grooved specimens (Ref. 15). The one specimen postirradiation tested at 110°C with side-grooves, however, did indicate a 25 percent decrease in upper shelf toughness, in terms of J_{Ic}. The reader is referred to the studies by Loss and co-workers for information on the tentative correlation between J_{Ic} and C_v energy and the correlation between the average tearing modulus and C_v energy (Refs. 15 and 23).

10. DISCUSSION

The C_v and tension tests of the remaining materials should provide valuable reinforcement of the notch ductility and strength trends observed here for through-wall and surveillance locations. The materials (two forgings and two submerged arc welds) as a group represent a relatively broad range of radiation sensitivities. Unfortunately, capsule space limitations precluded the irradiation of CT specimens from these materials as stated above. Current concerns over weldment performance for older vessels, raised by pressurized thermal shock (PTS) analyses and by low upper shelf material analyses, are indicative of a need for through-wall CT data for representative welds. In particular, high copper-high nickel content welds can experience much larger transition temperature elevations than those seen here for the A302-B and A533-B reference plates.

A relatively small difference between embrittlement levels of wall surface and mid-wall positions was expected for the particular fluence range examined. The embrittlement (ΔT trend) developed for the A302-B plate through in-core 288°C irradiation tests (see Fig. 6.13) shows that the rate of embrittlement accrual is higher for fluences below 1-1.5 x 10^{19} n/cm^2 than for fluences above this level. The emphasis of the present PSF study on the higher of the two fluence regimes is consistent with its primary objective of evolving or refining physics-dosimetry-metallurgy correlations for near end-of-life (EOL) vessel conditions. EOL fluences on the inner wall in many instances will range from 4 to 6 x $10^{19}n/cm^2$. Once the data for all six materials are analyzed, and depending on the direction of the PTS analyses, the performance of a second set of experiments examining in depth embrittlement for fluences below the knee of the embrittlement trend curve may be in order.

The potential benefit of radiation effects attenuation with wall thickness, seen as a retention of a tough outer wall ligament, would appear strongest for the more radiation sensitive materials. Figure 10.1 , taken from an earlier study (Ref. 28) illustrates this difference. The analysis shown was developed on the basis of experimentally defined or projected embrittlement trend curves for medium and high sensitivity cases. Within this framework, high copper content welds would follow the "high sensitivity" trend curves. The ASTM A302-B reference plate of Fig. 10.1 is the Code F23 material studied here. As noted, the crack arrest transition (CAT) occurs closer to the wall surface for the "high sensitivity" case than for the "medium sensitivity" case because of the dissimilar gradients of embrittlement. The crack arrest transition (CAT), by definition is the fracture transition elastic (FTE) temperature, taken to be 33°C (60°F) above the drop weight nil-ductility transition (NDT) temperature. The relationships in Fig. 10.1 obviously are not the same for fluence intervals below 1.5 x 10^{19} n/cm^2 where rates of embrittlement accrual tend to be higher.

Two somewhat unexpected observations were the difference in relative embrittlement between the A302-B vs. A533-B plates for short vs. long term irradiation times, and the inconsistency of upper shelf energy vs. upper shelf lateral expansion reductions with increasing fluence. Forthcoming results from the forging and weld materials should help resolve these observations.

11. CONCLUSIONS

Primary conclusions and observations from this study are enumerated.

1. The surveillance capsule results indicate reasonably well the irradiation effects to wall surface and quarter wall thickness locations. C_v surveillance data were conservative where significant (> 10°C) differences were observed; predictions of the 41 J transition temperature elevation were within 15°C.

2. Adjustment of the ASME Section III (Appendix G) toughness curve by the radiation-induced elevation of the C_v 41 J temperature proved conservative when compared against experimentally derived, K_{Jc} data.

3. Adjustment of the ASME Section XI (Appendix A), lower bound K_{Ic} toughness curve for A533-B steel by the 41 J and 100 MPa $\sqrt{m}$ temperature elevations, proved unconservative in some cases when compared against experimentally derived K_{Jc} data for the A533-B reference plate. The maximum disparity, however, was only 15°C.

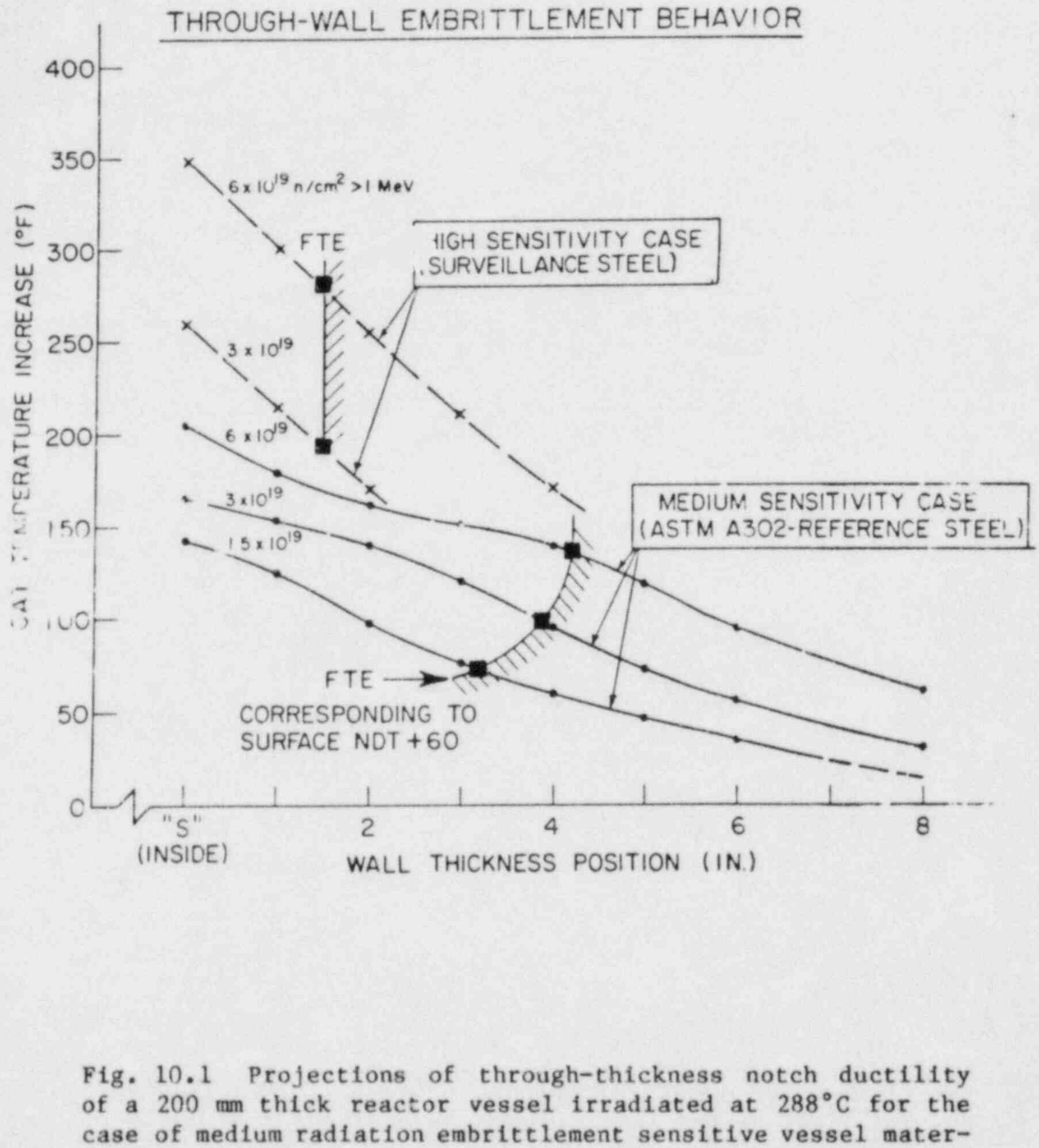

Fig. 10.1 Projections of through-thickness notch ductility of a 200 mm thick reactor vessel irradiated at 288°C for the case of medium radiation embrittlement sensitive vessel materials (depicted by ASTM A302-B reference plate) and for the case of high radiation embrittlement sensitive materials (depicted by the surveillance steel). The loci of the FTE position when the vessel temperature equals the inside surface NDT plus 33°C(60°F) temperature is indicated for each fluence.

4. The in-wall toughness gradient produced by the irradiation indexed to the transition temperature, was small for both materials. The difference in 41 J temperatures between wall surface and mid-thickness positions was 31°C for the A302-B plate and 22°C for the A533-B plate. The variation between measured K_{Jc} 100 MPa $\sqrt{m}$ temperatures was 24°C for the A302-B plate and for the A533-B plate.

5. The postirradiation 41 J temperature elevation was in close agreement with the 68 J temperature elevation (within 6°C in most cases) and with the 0.89mm temperature elevation (within 8°C in all cases).

6. The 41 J temperature elevations with irradiation tend to be less than the corresponding temperature elevations in K_{Jc} at the 100 MPa $\sqrt{m}$ level.

7. The $K_{\beta c}$ 100 MPa $\sqrt{m}$ temperature elevations were ~23°C less than the K_{Jc} elevation at that same level. In turn, the $K_{\beta c}$ elevations tended to be less than the 41 J temperature elevation.

8. Results for the 0.5T-CT and 1T-CT specimens do not show a significant effect of specimen size on the temperature location of the toughness transition.

9. Postirradiation C_v data for the A302-B plate show an anomalous difference traceable to specimen thickness location in the original plate. The anomaly was most evident in the upper shelf temperature regime with specimens irradiated in capsule SSC-1. Good properties uniformity was observed in preirradiation (reference) condition data, however.

REFERENCES

1. C. Z. Serpan, "NRC Light-Water Reactor Pressure Vessel Surveillance Dosimetry Improvement Program," Nuclear Safety, Volume 22, No. 1, July-Aug. 1981.

2. C. Z. Serpan, "USNRC Surveillance Dosimetry Improvement Program," Proceedings of the 6th MPA - Seminar, Safety of the Pressure Boundary of Light Water Reactors, Staatliche Materialprunfungsantalt-Universitat Stuttgart, 9/10, Oct. 1980.

3. U. Potapovs and J. R. Hawthorne, "The Effect of Residual Elements on 550°F Irradiation Response of Selected Pressure Vessel Steels and Weldments," Nuclear Applications, Vol. 6, No. 1, Jan. 1969, pp.27-46.

4. J. R. Hawthorne, J. J. Koziol, and S. T. Byrne, "Evaluation of Commercial Production A533-B Steel Plates and Weld Deposits with Extra-Low Copper Content for Radiation Resistance, "Effects of Radiation on Structural Materials, ASTM STP 683, Am. Soc. for Testing and Materials, Philadelphia, PA., 1979, pp. 278-294.

5. ASTM E 185-79, Standard Practice for Conducting Surveillance Tests for Light-Water Cooled Nuclear Power Reactor Vessels, ASTM Book of Standards, Part 45, 1980, p. 865.

6. J. R. Hawthorne, "Status of Knowledge of Radiation Embrittlement in U.S.A. Reactor Pressure Vessel Steels," USNRC Report NUREG/CR-2511, Feb. 1982.

7. W. N. McElroy, et. al., "LWR Pressure Vessel Surveillance Dosimetry Improvement Program - 1982 Annual Report," USNRC Report NUREG/CR-2805, Vol. 3, also Hanford Engineering Development Laboratory Report HEDL-TME 82-20, Jan. 1983.

8. W. N. McElroy, et. al., "LWR Pressure Vessel Surveillance Dosimetry Improvement Program - 1979 Annual Report," USNRC Report, NUREG/CR-1291, also Hanford Engineering Development Laboratory Report HEDL-SA 1949, 1980.

9. W. N. McElroy, et. al., "LWR Pressure Vessel Surveillance Dosimetry Improvement Program - 1980 Annual Report," USNRC Report NUREG/CR-1747, also Hanford Engineering Development Laboratory Report HEDL-TME 80-73, 1981.

10. W. N. McElroy, et. al., "LWR Pressure Vessel Surveillance Dosimetry Improvement Program - 1981 Annual Report," USNRC Report NUREG/CR-0029, also Hanford Engineering Development Laboratory Report HEDL-SA-2546, 1982.

REFERENCES

11. W. N. McElroy, et. al., "LWR Pressure Vessel Surveillance Dosimetry Improvement Program: PCA Experiments and Blind Test," USNRC Report NUREG/CR-1861, also Hanford Engineering Development Laboratory Report HEDL-TME 80-87, July 1981.

12. J. R. Hawthorne, "Radiation Effects Information Generated on the ASTM Reference Correlation-Monitor Steels," ASTM DS 54, American Society For Testing and Materials, July 1974.

13. C. E. Childress, "Manual for ASTM A-533 Grade B Class 1 Steel (HSST Plate 03) Provided to the International Atomic Energy Agency," Oak Ridge National Laboratory Report, ORNL-TM-3193, March 1971.

14. W. L. Server and W. Oldfield, "Nuclear Pressure Vessel Steel Data Base," NP-933, EPRI Research Project 886-1, Fracture Control Corporation, Goleta, CA, Dec. 1979.

15. J. R. Hawthorne, Ed., "Evaluation and Prediction of Neutron Embrittlement in Reactor Pressure Vessel Materials," NP-2782, EPRI Research Project 886-2, Naval Research Laboratory, Washington, D. C., Dec. 1982.

16. Metal Properties Council, "Prediction of the Shift in the Brittle/Ductile Transition Temperature of LWR Pressure Vessel Materials," ASTM Journal of Testing and Evaluation," July 1983 (To be published).

17. "Coordinated Research Program on Analysis of the Behavior of Advanced Reactor Pressure Vessel Steels Under Neutron Irradiation," IWG RRPC-78/81. International Atomic Energy Agency, Vienna, Austria, 17-18 Oct. 1977.

18. J. R. Hawthorne, "Notch Ductility Degradation of Low Alloy Steels with Low-to-Intermediate Neutron Fluence Exposures," USNRC Report NUREG/CR-1053, Jan. 14, 1980.

19. J. R. Hawthorne, "Evaluation of IAEA Coordinated Program Steels and Welds for 288°C Radiation Embrittlement Resistance," USNRC Report NUREG/CR-2487, Feb. 1982.

20. J. R. Hawthorne, "Significance of Nickel and Copper Content to Radiation Sensitivity and Postirradiation Heat Treatment Recovery of Reactor Vessel Steels," USNRC Report NUREG/CR-2948, Also Materials Engineering Associates Report, MEA-2006, Nov. 1982.

21. ASTM E 399-81 "Standard Method for Plane-Strain Fracture Toughness of Metallic Materials," ASTM Book of Standards, Part 10, 1981, p. 589.

REFERENCES

22. F. J. Loss, B. H. Menke, and R. A. Gray, "Development of J-R Curve Procedures," in The NRL-EPRI Research Program (RP886-2), Evaluation and Prediction of Neutron Embrittlement in Reactor Pressure Vessel Materials Annual Report For CY 1978, Naval Research Laboratory, Report 8327, Aug. 30, 1979, pp. 30-57.

23. F. J. Loss, et. al, "J-R Curve Characterization of Irradiated and Annealed Weld Deposits," Structural Integrity of Water Reactor Pressure Boundary Components, Annual Report, Fiscal Year 1979, USNRC Report NUREG/CR-1128, also Naval Research Laboratory Memorandum Report 4122, Dec. 31, 1979, pp. 4-36.

24. H. A. Ernst, "Material Resistance and Instability Beyond J-Controlled Crack Growth," Scientific Paper 81-1D7-J1NTF-P6, Westinghouse R & D Center, Dec. 3, 1981.

25 ASTM E 813-81, "Standard Test for J_{Ic}, A Measure of Fracture Toughness," ASTM Book of Standards, Part 10, 1981, pp. 810-828.

26. G. R. Irwin, "Fracture Mode Transition for a Crack Transversing a Plate," J. of Basic Eng., ASME, 82 (2), 1960, pp. 417-425.

27. J. G. Merkle, "New Method for Analyzing Small Scale Fracture Specimen Data in the Transition Zone," Tenth Water Reactor Safety Research Information Meeting, USNRC Report NUREG/ CP-0041, Washington, D. C., Oct. 1982, pp. 307-315.

28. F. J. Loss, J. R. Hawthorne, C. Z. Serpan, Jr., and P. P. Puzak, "Analysis of Radiation-Induced Embrittlement Gradients on Fracture Characteristics of Thick-Walled Pressure Vessel Steels," ASME Journal of Engineering for Industry, Nov. 1971, pp. 1007-1015.

APPENDIX A

TABLES OF INDIVIDUAL CHARPY-V TEST RESULTS FROM PSF IRRADIATIONS

APPENDIX A

Table 1A Charpy-V Test Results for A302-B PLate (ASTM Reference) (Code F23)

SPECIMEN NUMBER	TEST TEMPERATURE °C	(°F)	CHARPY ENERGY J	(ft-lb)	LATERAL EXPANSION mm	(mils)
			UNIRRADIATED CONDITION			
Layer 1						
6	-40	(-40)	9	(7)	0.102	(4)
23	-18	(0)	33	(24)	0.483	(19)
43	-1	(30)	41	(30)	0.762	(30)
75	16	(60)	57	(42)	0.940	(37)
82	38	(100)	88	(65)	1.372	(54)
143	82	(180)	110	(81)	1.676	(66)
89	93	(200)	115	(85)	1.753	(69)
90	138	(280)	107	(79)	1.626	(64)
136	177	(350)	99	(73)	1.473	(58)
83	177	(350)	106	(78)	1.676	(66)
137	260	(500)	110	(81)	1.575	(62)
Layer 2						
107	-40	(-40)	14	(10)	0.203	(8)
16	-1	(30)	45	(33)	0.762	(30)
168	21	(70)	71	(52)	1.168	(46)
68	38	(100)	95	(70)	1.448	(57)
114	60	(140)	95	(70)	1.499	(59)
103	60	(140)	99	(73)	1.524	(60)
48	93	(200)	107	(79)	1.626	(64)
161	138	(280)	111	(82)	1.524	(60)
115	177	(350)	104	(77)	1.651	(65)
100	177	(350)	107	(79)	1.626	(64)
162	260	(500)	118	(87)	1.600	(63)
			CAPSULE SSC-1			
Group 1, Left						
F23-1	138	(280)	92	(68)	1.346	(53)
F23-8	104	(220)	92	(68)	1.448	(57)
F23-25	288	(550)	91	(67)	1.473	(58)
F23-45	38	(100)	22	(16)	0.279	(11)
F23-77	204	(400)	95	(70)	1.397	(55)
F23-84	88	(190)	47	(35)	0.711	(28)
F23-91	71	(160)	41	(30)	0.686	(27)
F23-138	99	(210)	99	(73)	1.346	(53)
Group 2, Right						
F23-11	204	(400)	76	(56)	1.168	(46)
F23-18	82	(180)	41	(30)	0.635	(25)
F23-50	104	(220)	66	(49)	1.041	(41)
F23-70	149	(300)	77	(57)	1.168	(46)
F23-102	110	(230)	77	(57)	1.194	(47)
F23-116	54	(130)	27	(20)	0.381	(15)
F23-163	288	(550)	73	(54)	1.270	(50)
F23-170	10	(50)	11	(8)	0.076	(3)

Table 1A Continued

SPECIMEN NUMBER	TEST TEMPERATURE °C	(°F)	CHARPY ENERGY J	(ft-lb)	LATERAL EXPANSION mm	(mils)
			CAPSULE SSC-2			
Group 1, Left:						
Layer 1						
22	116	(240)	83	(61)	1.295	(51)
42	288	(550)	79	(58)	1.448	(57)
74	104	(220)	73	(54)	1.194	(47)
81	204	(400)	72	(53)	1.194	(47)
88	88	(190)	38	(28)	0.584	(23)
142	66	(150)	22	(16)	0.381	(15)
76	154	(310)	73	(54)	1.219	(48)
Group 2, Right:						
Layer 2						
15	204	(400)	65	(48)	1.143	(45)
47	93	(200)	42	(31)	0.762	(30)
67	104	(220)	65	(48)	1.168	(46)
99	154	(310)	73	(54)	1.168	(46)
106	77	(170)	23	(17)	0.483	(19)
113	121	(250)	76	(56)	1.092	(43)
120	288	(550)	73	(54)	1.295	(51)
167	24	(75)	7	(5)	0.001	(3)
101	46	(115)	18	(13)	0.254	(10)
			CAPSULE WALL NO. 1 (SURFACE)			
Group 1, Left						
2	149	(300)	85	(63)	1.422	(56)
9	116	(240)	84	(62)	1.295	(51)
39	91	(195)	65	(48)	—	—
71	102	(215)	81	(60)	1.295	(51)
78	204	(400)	91	(67)	1.372	(54)
85	88	(190)	46	(34)	—	—
139	66	(150)	33	(24)	0.483	(19)
7	49	(120)	23	(17)	0.584	(23)
Group 2, Right						
12	204	(400)	77	(57)	1.245	(49)
19	93	(200)	53	(39)	0.838	(33)
64	71	(160)	46	(34)	0.711	(28)
96	154	(310)	76	(56)	1.219	(48)
103	77	(170)	49	(36)	0.838	(33)
110	121	(250)	73	(54)	1.194	(47)
117	60	(140)	31	(23)	0.457	(18)
164	21	(70)	15	(11)	0.178	(7)
17	43	(110)	18	(13)	0.381	(15)

Table 1A Continued

SPECIMEN NUMBER	TEST TEMPERATURE °C	(°F)	CHARPY ENERGY J	(ft-lb)	LATERAL EXPANSION mm	(mils)
			CAPSULE WALL NO. 2 (QUARTER T)			
Group 1, Left						
3	2	(35)	5	(4)	0.000	(0)
10	104	(220)	85	(63)	1.346	(53)
40	288	(550)	80	(59)	1.524	(60)
72	43	(110)	49	(36)	0.711	(28)
79	204	(400)	88	(65)	1.499	(59)
86	49	(120)	26	(19)	0.483	(19)
93	71	(160)	47	(35)	0.813	(32)
140	149	(300)	80	(59)	1.321	(52)
24	27	(80)	27	(20)	0.406	(16)
Group 2, Right						
13	204	(400)	73	(54)	1.245	(49)
20	82	(180)	71	(52)	1.118	(44)
65	32	(90)	30	(22)	0.508	(20)
97	71	(160)	43	(32)	0.737	(29)
104	127	(260)	73	(54)	1.270	(50)
118	54	(130)	42	(31)	0.610	(24)
165	288	(550)	71	(52)	1.245	(49)
49	10	(50)	8	(6)	0.076	(3)
			CAPSULE WALL NO. 3 (HALF T)			
Group 1, Left						
4	121	(250)	84	(62)	1.499	(59)
21	60	(140)	52	(38)	0.914	(36)
41	288	(550)	81	(60)	1.397	(55)
73	43	(110)	39	(29)	0.559	(22)
80	204	(400)	84	(62)	1.372	(54)
94	77	(170)	64	(47)	1.067	(42)
141	93	(200)	88	(65)	1.372	(54)
44	10	(50)	14	(10)	0.229	(9)
Group 2, Right						
14	93	(200)	69	(51)	1.067	(42)
46	54	(130)	45	(33)	0.762	(30)
66	204	(400)	80	(59)	1.448	(57)
98	121	(250)	76	(56)	1.270	(50)
105	38	(100)	35	(26)	0.533	(21)
112	27	(80)	27	(20)	0.483	(19)
119	66	(150)	60	(44)	0.914	(36)
166	288	(550)	80	(59)	1.422	(56)
69	-1	(30)	11	(8)	0.152	(6)

Table 2A Charpy V Test Results for A533-B HSST Plate 03
(Code 3PS, 3 PT, 3 PU)

SPECIMEN NUMBER	TEST TEMPERATURE °C	(°F)	CHARPY ENERGY J	(ft-lb)	LATERAL EXPANSION mm	(mils)
			UNIRRADIATED CONDITION			
Layer 2						
3PT-16	-40	(-40)	15	(11)	0.305	(12)
3PT-11	-12	(10)	37	(27)	1.016	(40)
3PT-12	27	(80)	79	(58)	1.245	(49)
3PT-15	66	(150)	110	(81)	1.981	(78)
3PT-13	121	(250)	146	(108)	1.905	(75)
3PT-14	204	(400)	152	(112)	2.159	(85)
3PT-32	-40	(-40)	12	(9)	0.305	(12)
3PU-16	4	(40)	42	(31)	0.635	(25)
Layer 3						
3PU-32	149	(300)	134	(99)	1.905	(75)
Layer 4						
3PT-27	-12	(10)	27	(20)	0.635	(25)
3PT-28	27	(80)	65	(48)	1.067	(42)
3PT-31	66	(150)	115	(85)	1.727	(68)
3PT-29	121	(250)	159	(117)	2.184	(86)
3PT-30	204	(400)	146	(108)	2.235	(88)
			CAPSULE SSC-1			
Group 1, Left						
3PU-1	210	(410)	133	(98)	1.727	(68)
3PU-2	43	(110)	27	(20)	0.406	(16)
3PU-3	71	(160)	50	(37)	0.737	(29)
3PU-4	99	(210)	81	(60)	1.143	(45)
3PU-5	177	(350)	113	(83)	1.905	(75)
Group 2, Right						
3PU-17	160	(320)	111	(82)	1.600	(63)
3PU-18	71	(160)	28	(21)	0.406	(16)
3PU-19	116	(240)	108	(80)	1.499	(59)
3PU-20	82	(180)	56	(41)	0.838	(33)
3PU-21	210	(410)	119	(88)	1.702	(67)
			CAPSULE SSC-2 (Code 3PT)			
Group 1, Left						
6	216	(420)	103	(76)	1.778	(70)
7	77	(170)	41	(30)	0.559	(22)
8	93	(200)	49	(36)	0.813	(32)
9	121	(250)	83	(61)	1.397	(55)
10	43	(110)	14	(10)	0.279	(11)
Group 2, Right						
22	113	(235)	79	(58)	1.270	(50)
23	66	(150)	33	(24)	0.508	(20)
24	149	(300)	103	(76)	1.626	(64)
25	104	(220)	49	(36)	0.889	(35)
26	216	(420)	110	(81)	1.803	(71)

Table 2A Continued

SPECIMEN NUMBER	TEST TEMPERATURE °C	(°F)	CHARPY ENERGY J	(ft-lb)	LATERAL EXPANSION mm	(mils)
	CAPSULE WALL NO. 1 (SURFACE) (Code 3PU)					
Group 1, Left						
6	154	(310)	108	(80)	1.651	(65)
7	77	(170)	50	(37)	0.737	(29)
8	93	(200)	64	(47)	0.889	(35)
9	121	(250)	98	(72)	1.549	(61)
10	43	(110)	33	(24)	0.483	(19)
Group 2, Right						
22	82	(180)	41	(30)	0.635	(25)
23	66	(150)	35	(26)	0.559	(22)
24	24	(75)	14	(10)	0.102	(4)
25	104	(220)	62	(46)	1.092	(43)
26	210	(410)	103	(76)	1.524	(60)
	CAPSULE WALL NO. 2 (QUARTER T) Code 3PU)					
Group 1, Left						
11	210	(410)	127	(94)	1.753	(69)
12	43	(110)	22	(16)	0.483	(19)
13	71	(160)	65	(48)	1.041	(41)
14	93	(200)	69	(51)	1.143	(45)
15	66	(150)	41	(30)	0.660	(26)
Group 2, Right						
27	149	(300)	87	(64)	1.499	(59)
28	54	(130)	24	(18)	0.406	(16)
29	116	(240)	98	(72)	1.575	(62)
30	82	(180)	50	(37)	0.686	(27)
31	177	(350)	100	(74)	1.676	(66)
	CAPSULE WALL NO. 3 (HALF T) (Code 3PT)					
Group 1, Left						
1	204	(400)	119	(88)	1.880	(74)
2	16	(60)	20	(15)	0.356	(14)
3	66	(150)	54	(40)	0.838	(33)
4	93	(200)	92	(68)	1.549	(61)
5	54	(130)	42	(31)	0.686	(27)
Group 2, Right						
17	149	(300)	125	(92)	1.880	(74)
18	43	(110)	37	(27)	0.635	(25)
19	104	(220)	100	(74)	1.702	(67)
20	77	(170)	62	(46)	1.118	(44)
21	210	(410)	130	(96)	2.032	(80)

APPENDIX B

ILLUSTRATIONS OF CHARPY-V AND COMPACT TENSION TEST RESULTS FROM PSF IRRADIATIONS

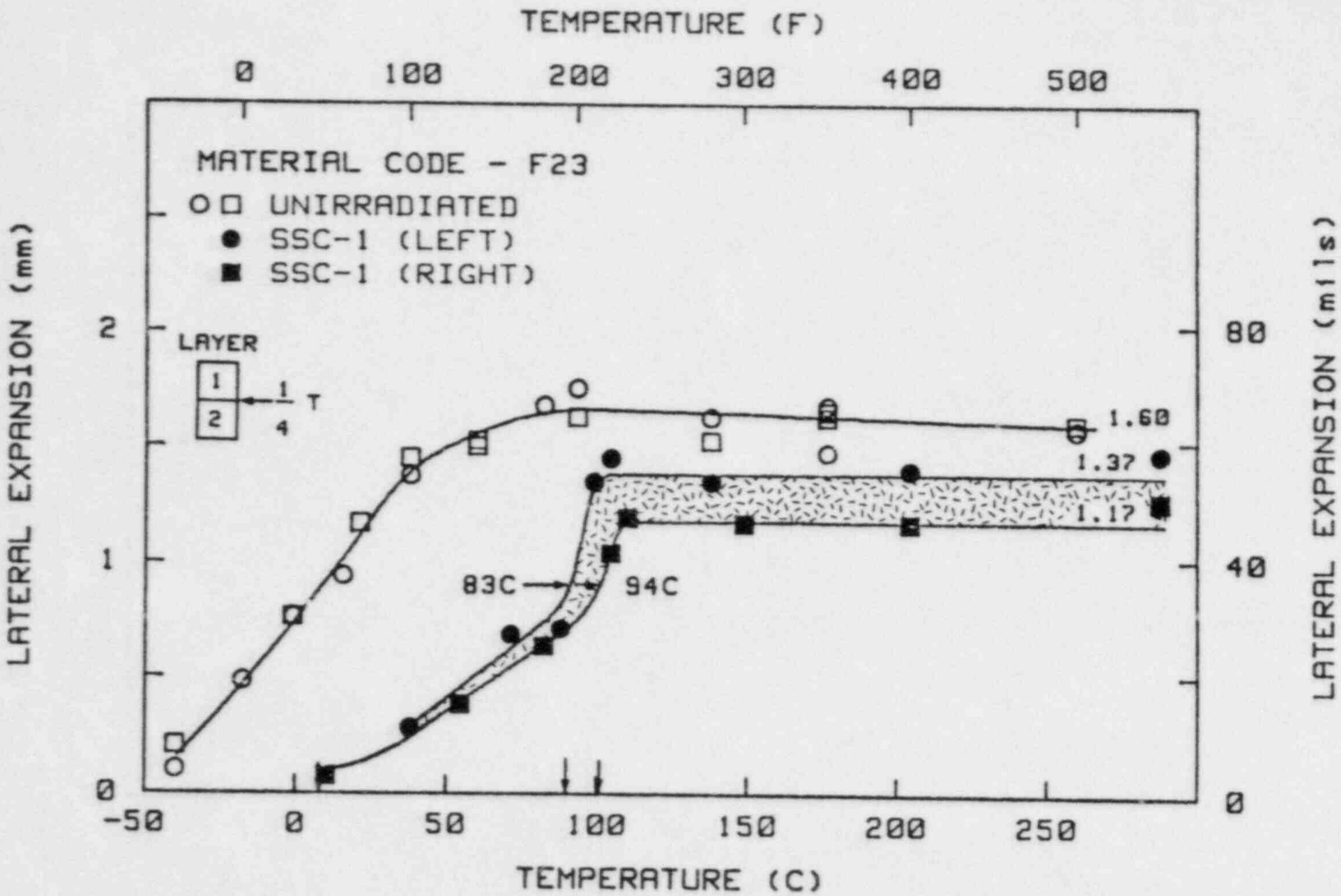

Fig. B.1 Charpy-V lateral expansion measurements for the A302-B reference plate before and after irradiation in capsule SSC-1.

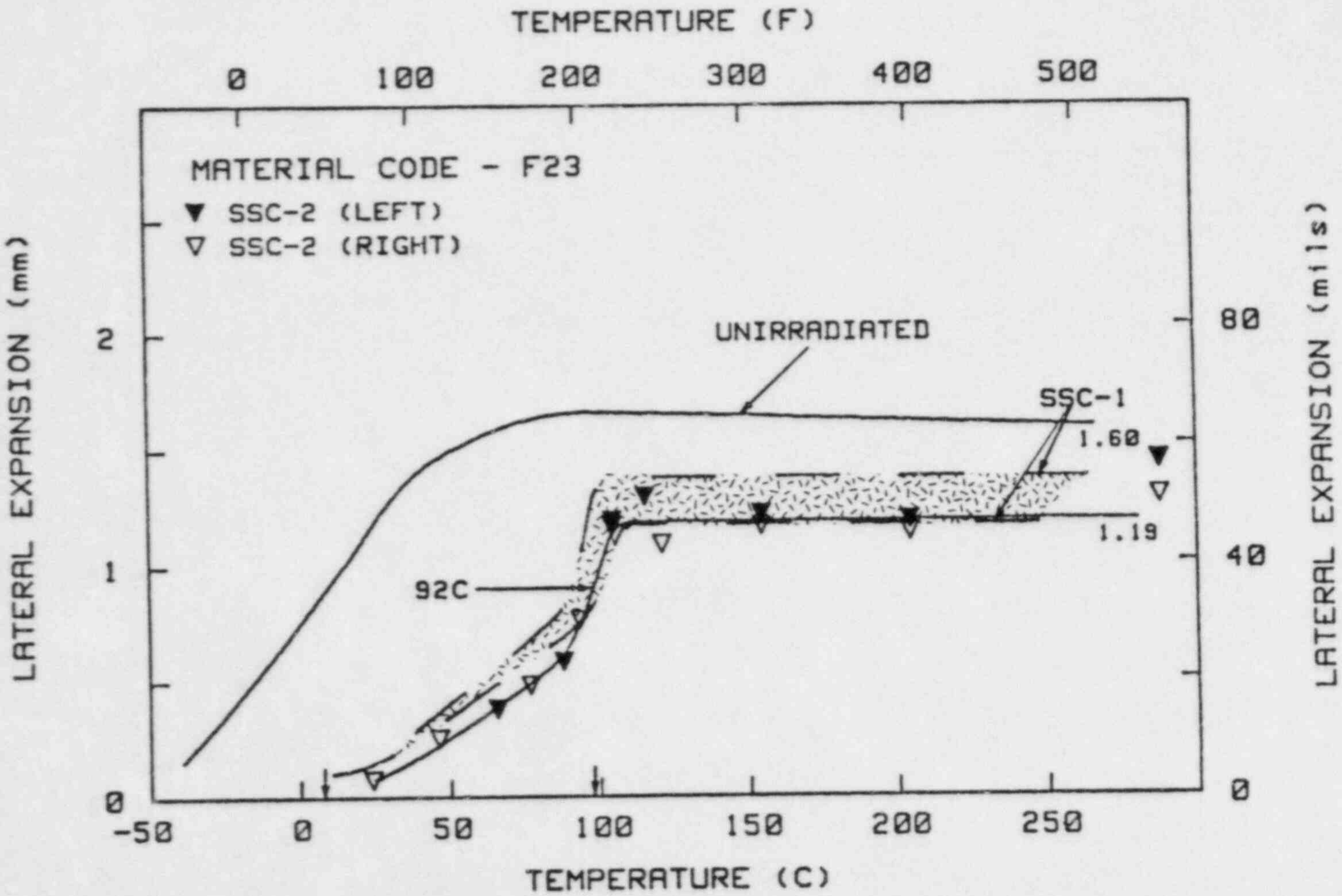

Fig. B.2 Charpy-V lateral expansion measurements for the A302-B reference plate before and after irradiation in capsule SSC-2.

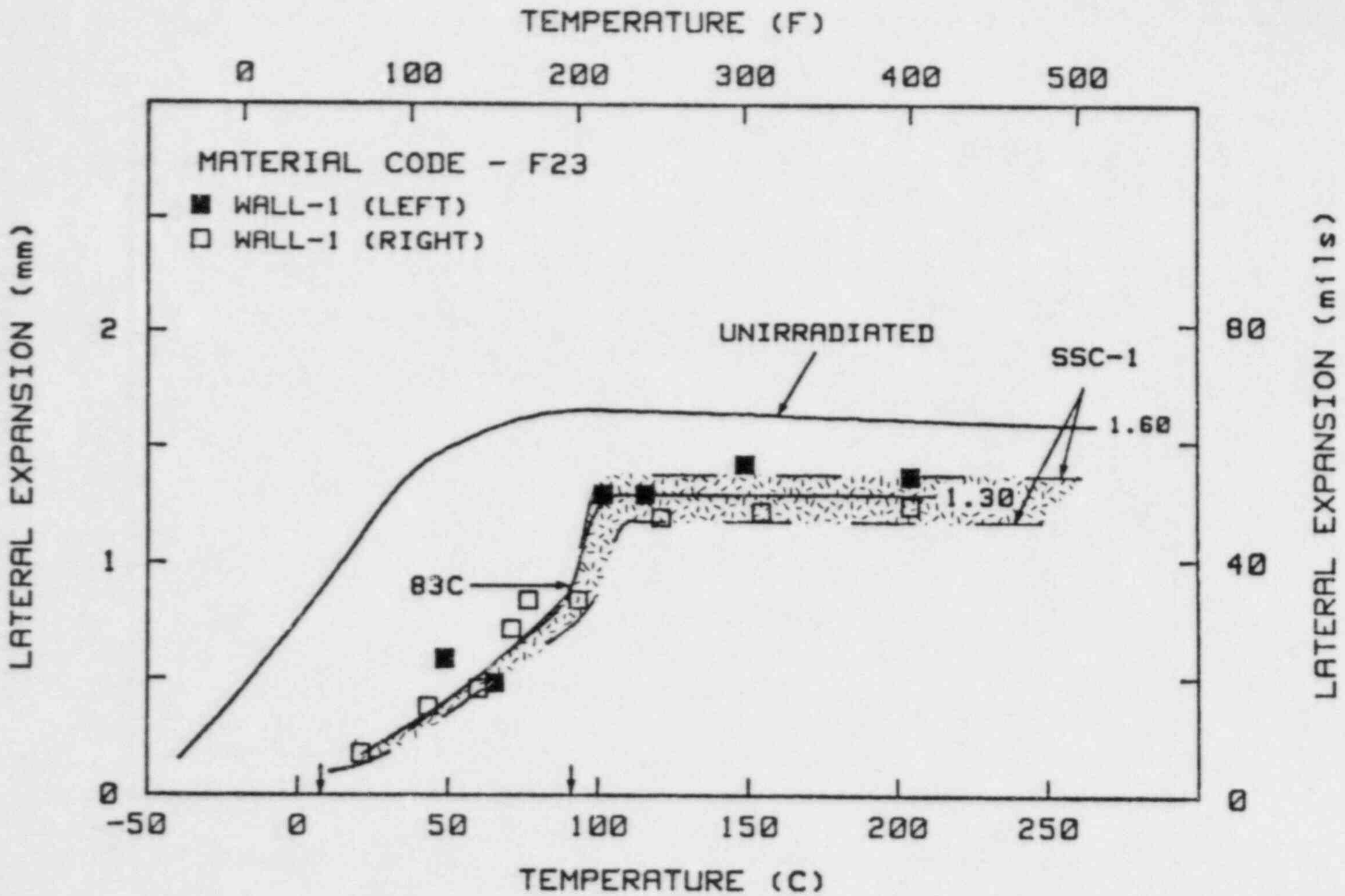

Fig. B.3 Charpy-V lateral expansion measurements for the A302-B reference plate before and after irradiation in capsule Wall-1.

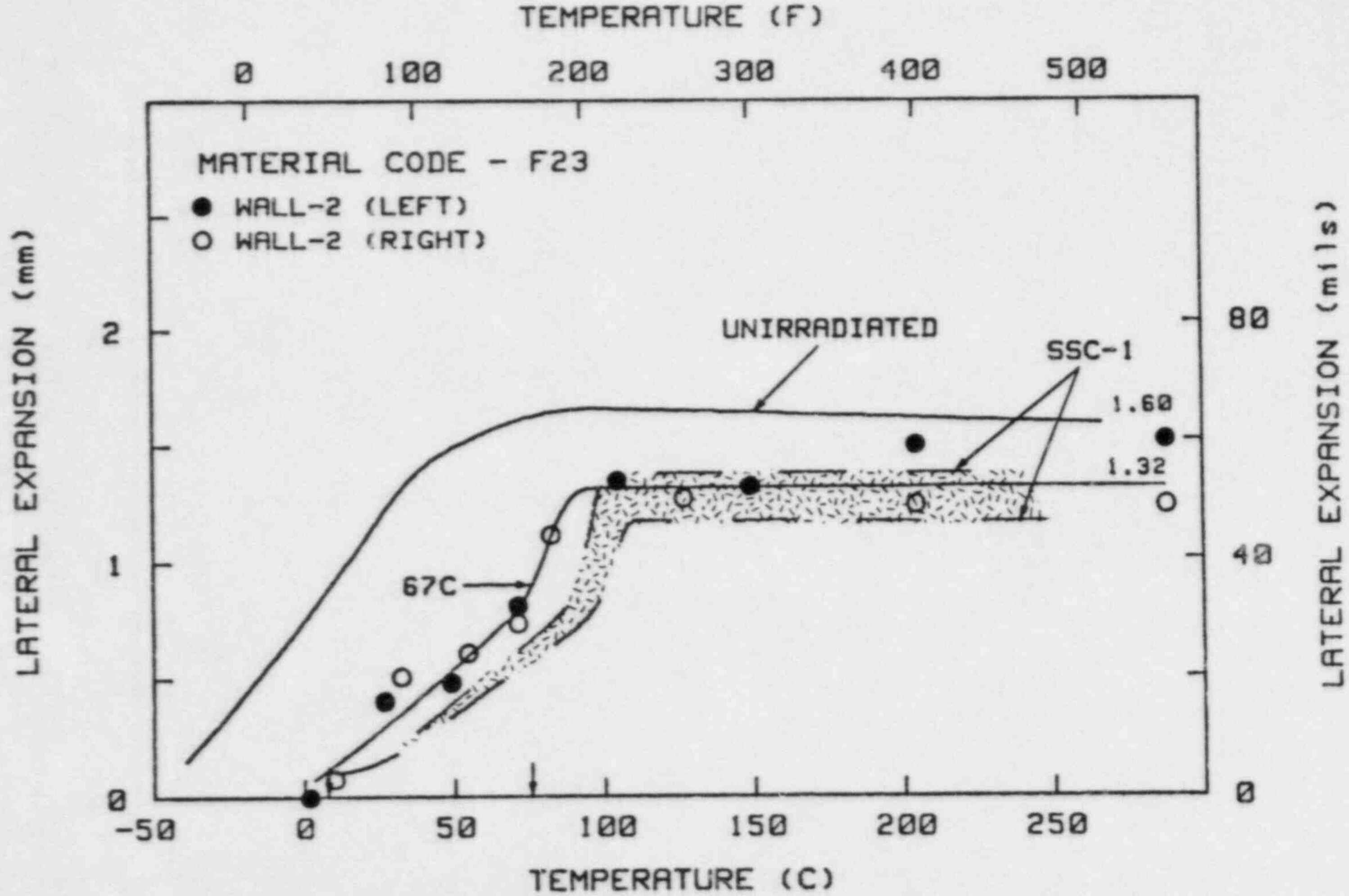

Fig. B.4 Charpy-V lateral expansion measurements for the A302-B reference plate before and after irradiation in capsule Wall-2.

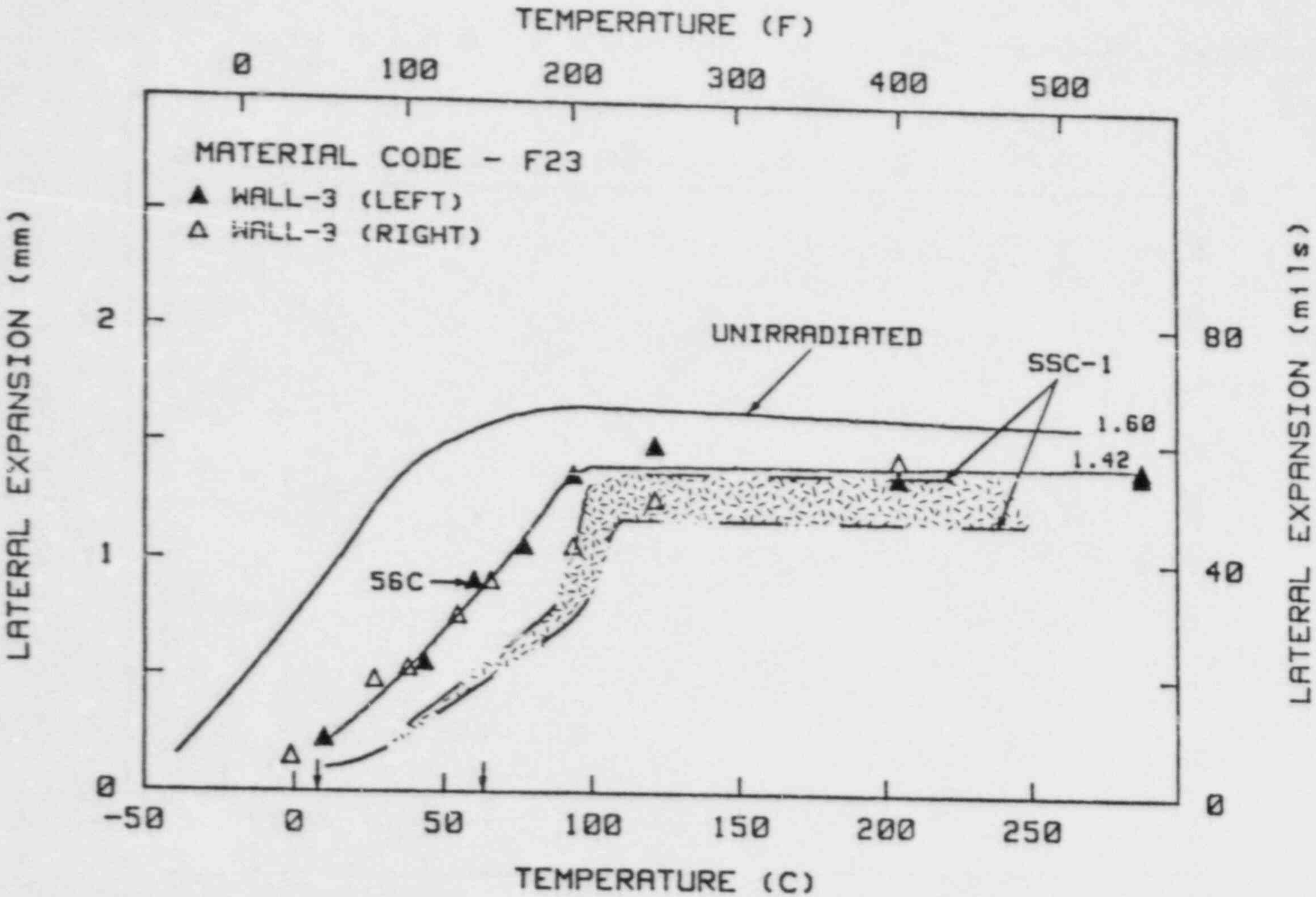

Fig. B.5 Charpy-V lateral expansion measurements for the A302-B reference plate before and after irradiation in capsule Wall-3.

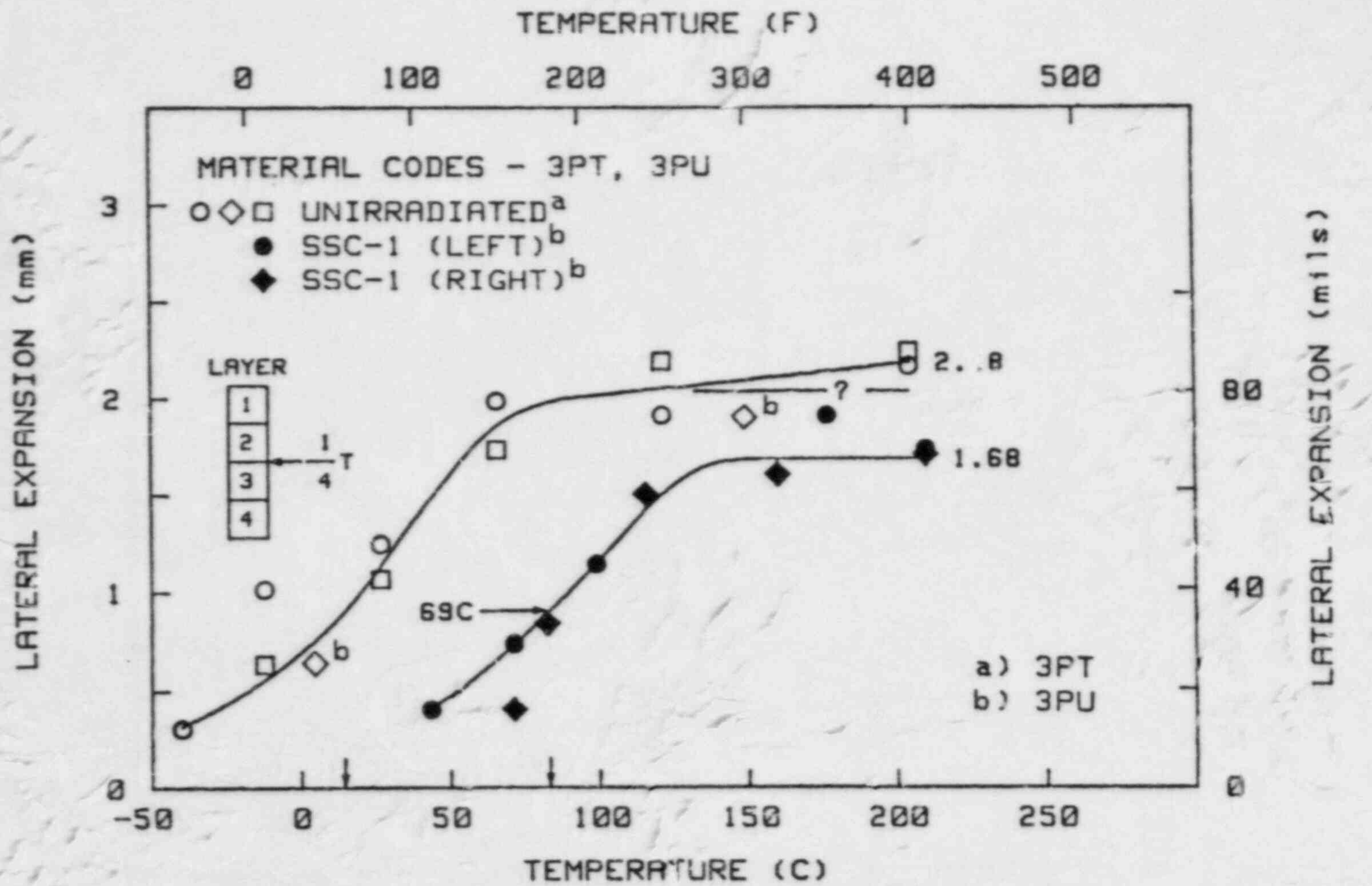

Fig. B.6 Charpy-V lateral expansion measurements for the A533-B reference plate before and after irradiation in capsule SSC-1.

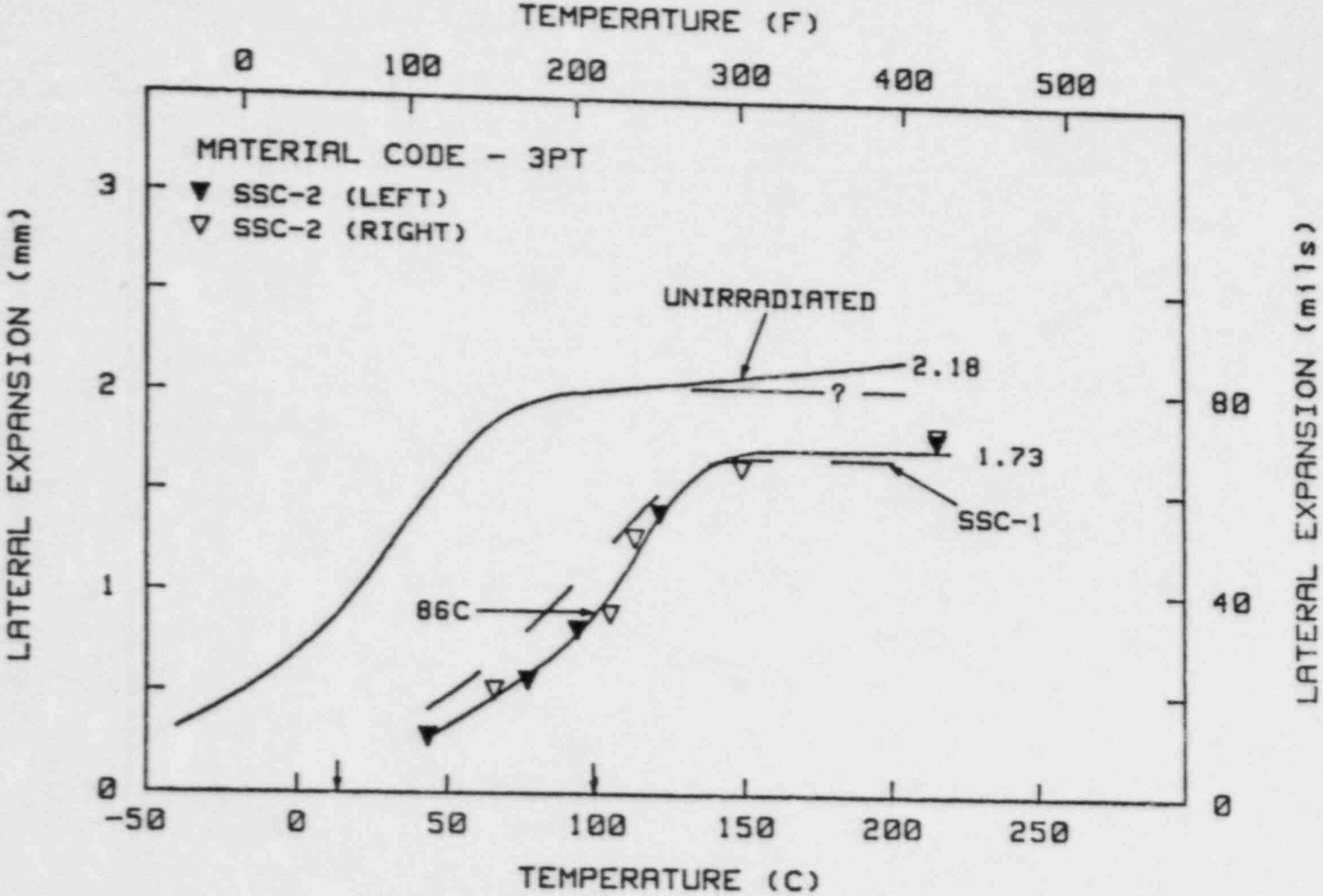

Fig. B.7 Charpy-V lateral expansion measurements for the A533-B reference plate before and after irradiation in capsule SSC-2.

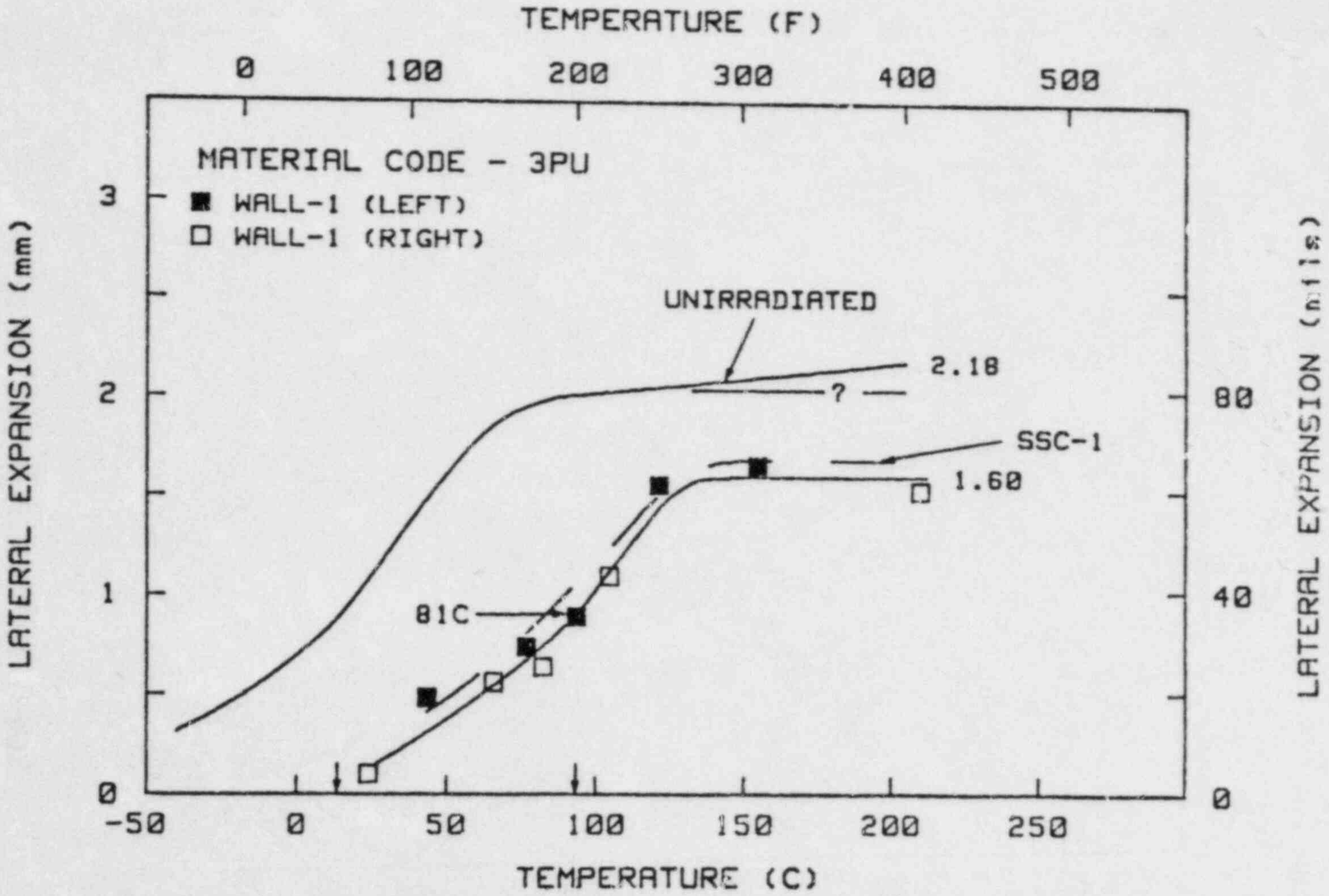

Fig. B.8 Charpy-V lateral expansion measurements for the A533-B reference plate before and after irradiation in capsule Wall-1.

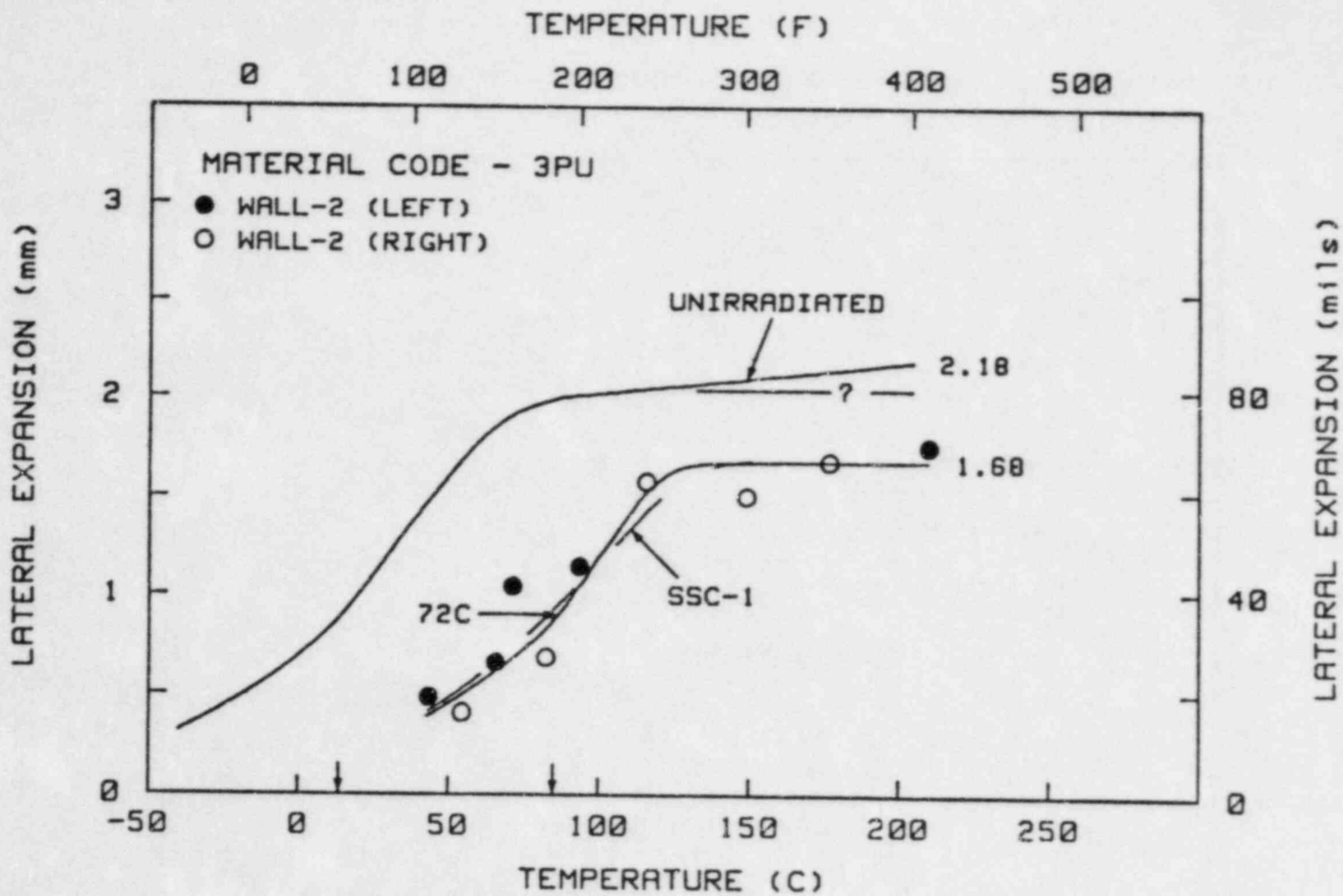

Fig. B.9 Charpy-V lateral expansion measurements for the A533-B reference plate before and after irradiation in capsule Wall-2.

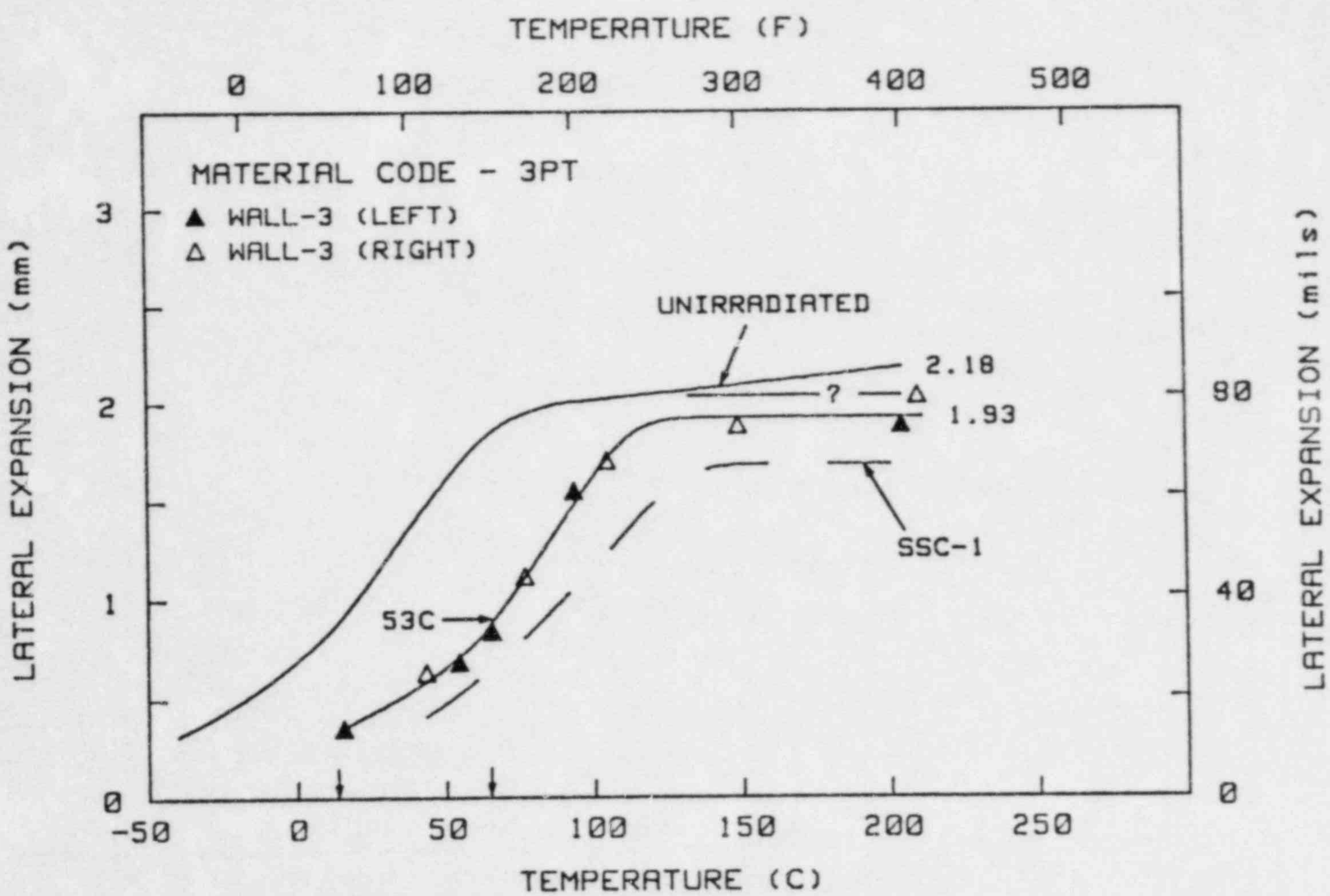

Fig. B.10 Charpy-V lateral expansion measurements for the A533-B reference plate before and after irradiation in capsule Wall-3.

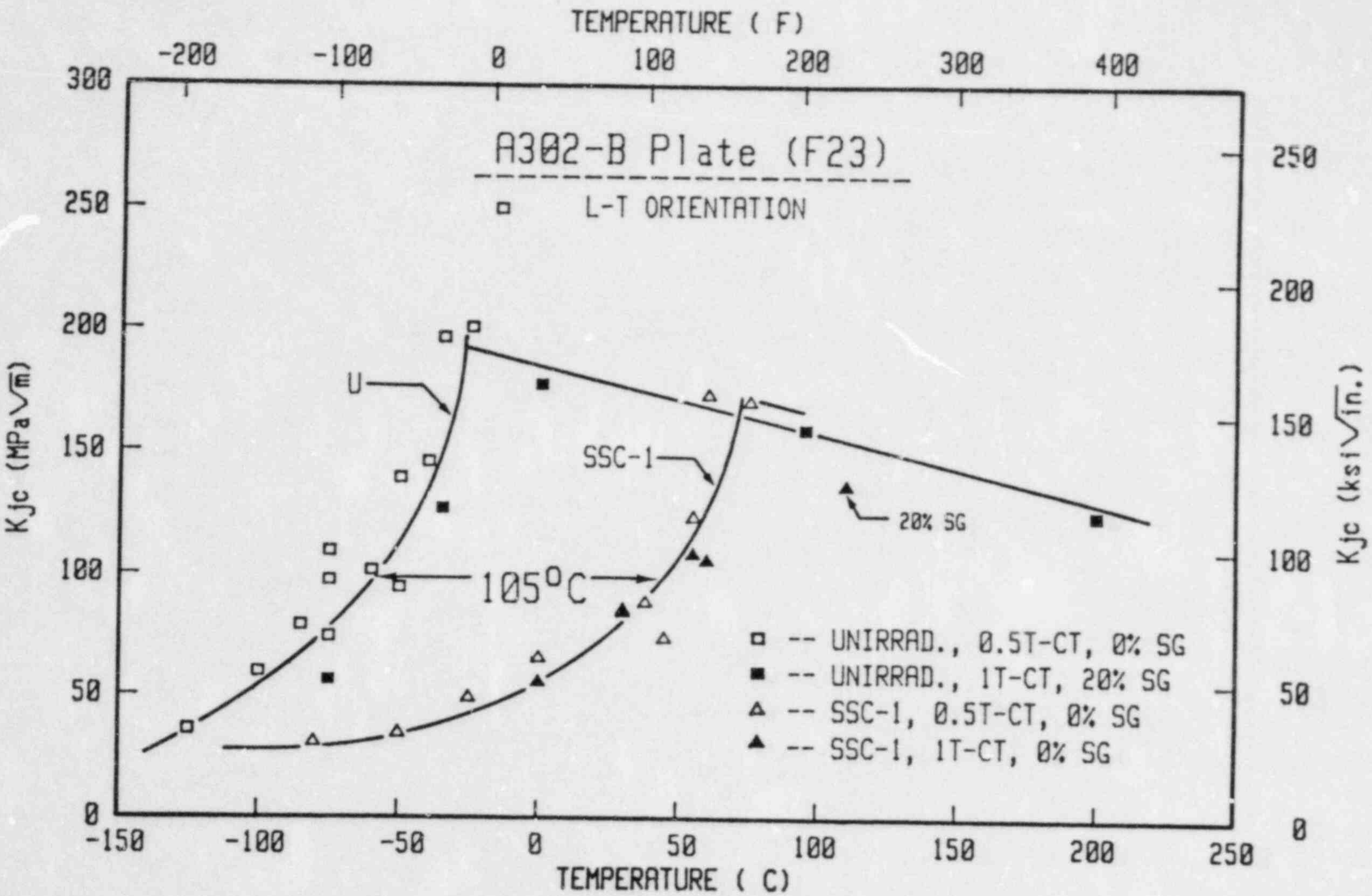

Fig. B.11 Initiation fracture toughness of A302-B plate before and after irradiation in capsule SSC-1.

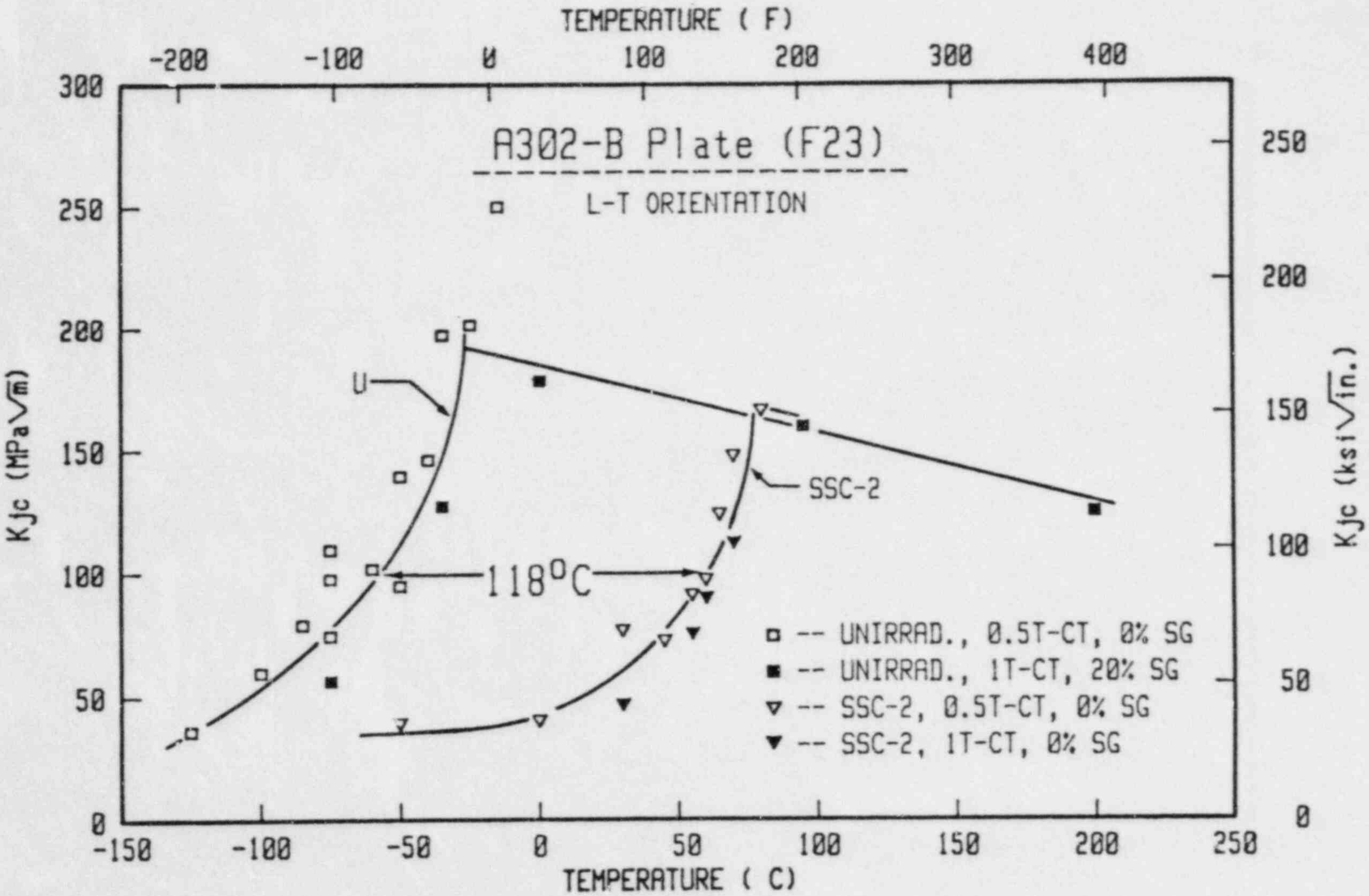

Fig. B.12 Initiation fracture toughness of A302-B plate before and after irradiation in capsule SSC-2.

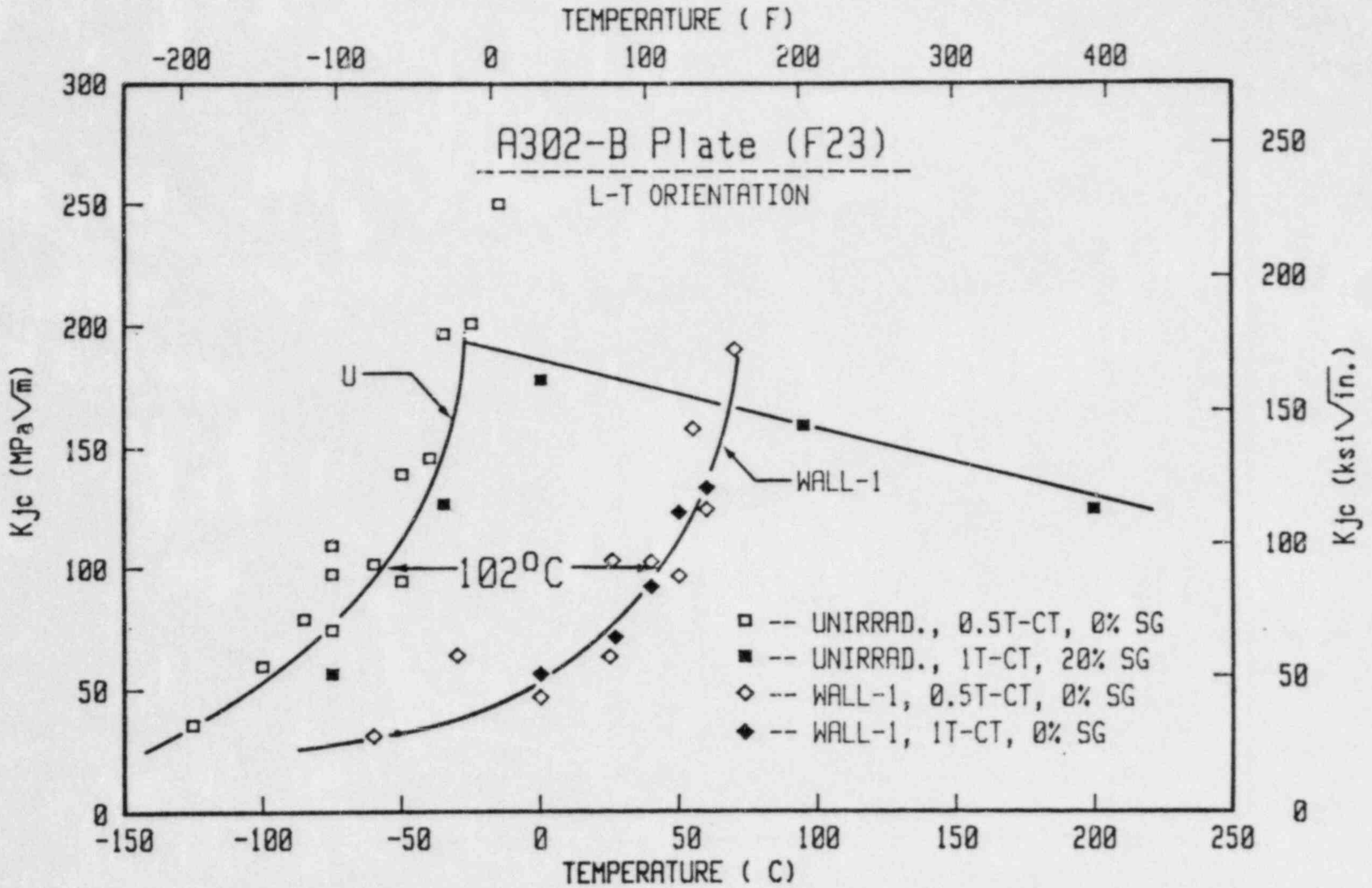

Fig. B.13 Initiation fracture toughness of A302-B plate before and after irradiation in capsule Wall-1.

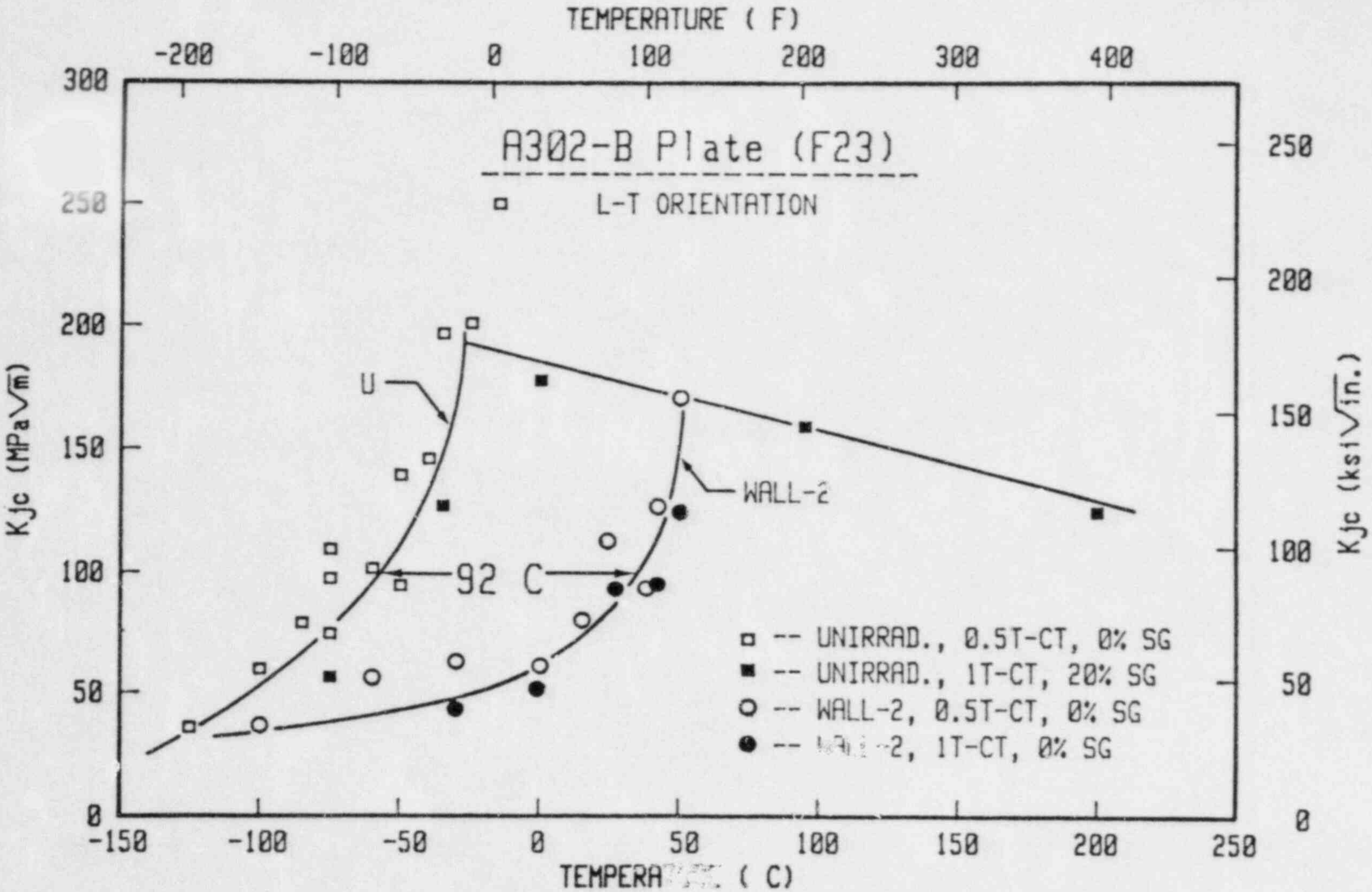

Fig. B.14 Initiation fracture toughness of A302-B plate before and after irradiation in capsule Wall-2.

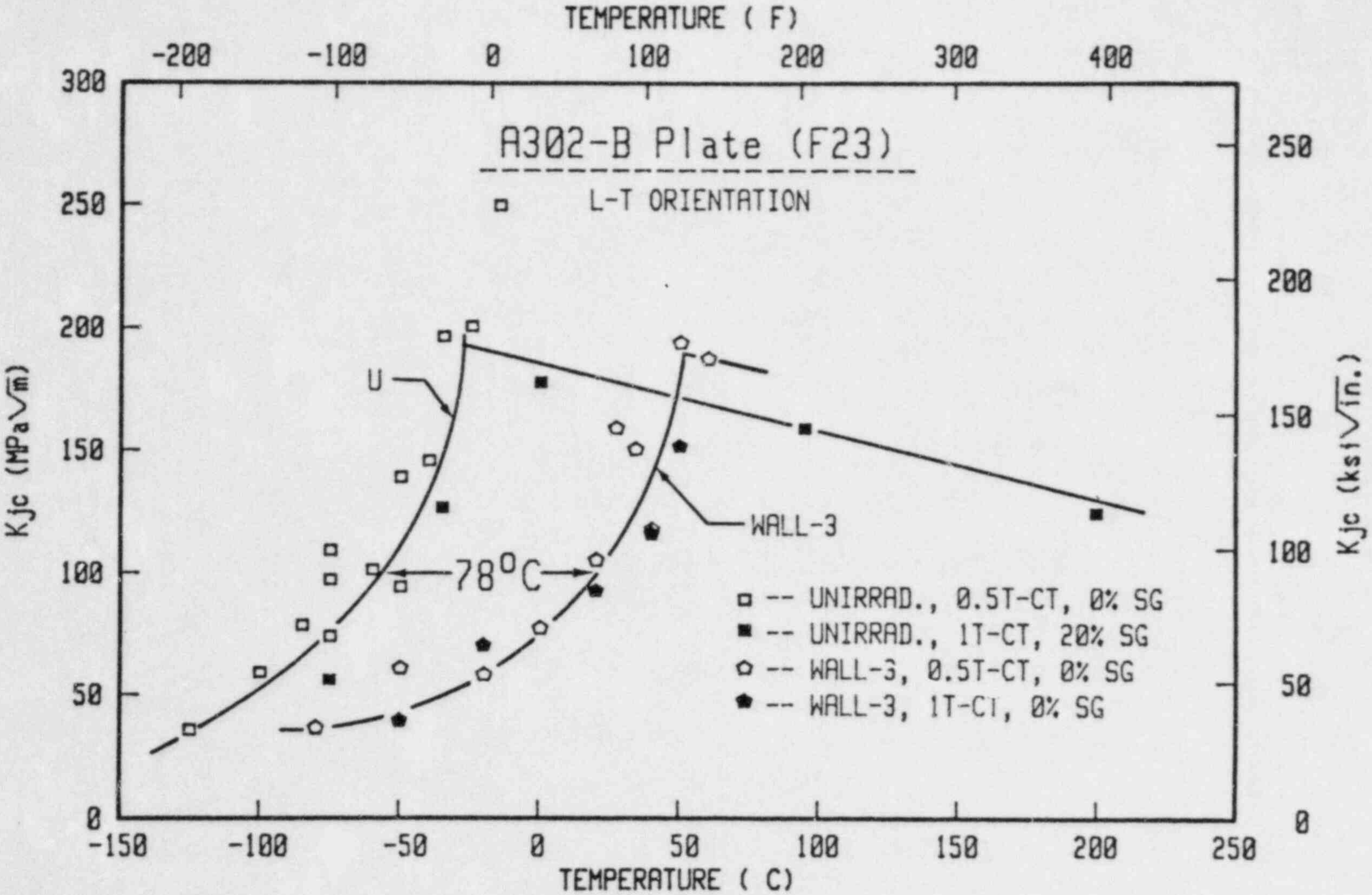

Fig. B.15 Initiation fracture toughness of A302-B plate before and after irradiation in capsule Wall-3.

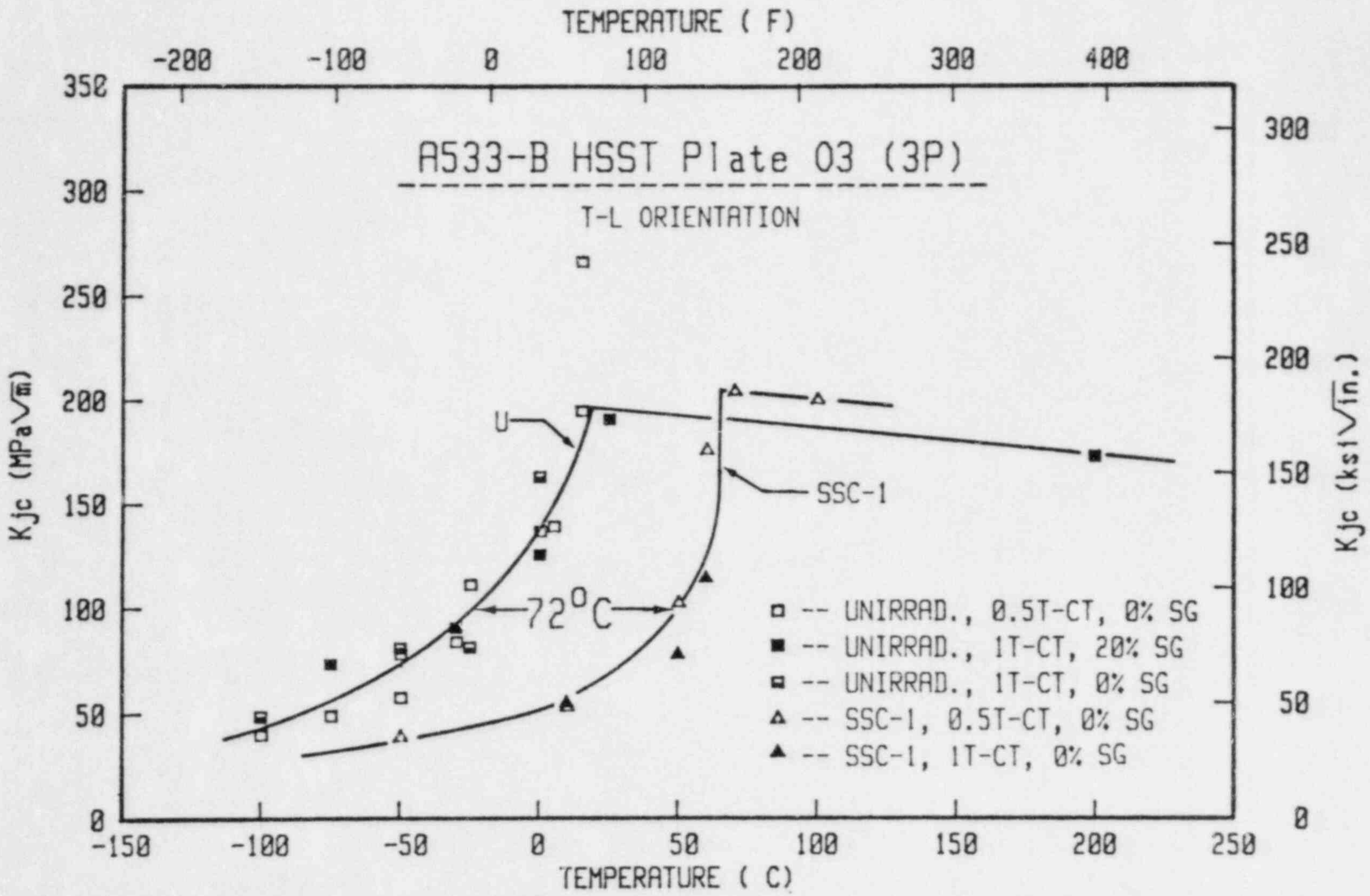

Fig. B.16 Initiation fracture toughness of A533-B plate before and after irradiation in capsule SSC-1.

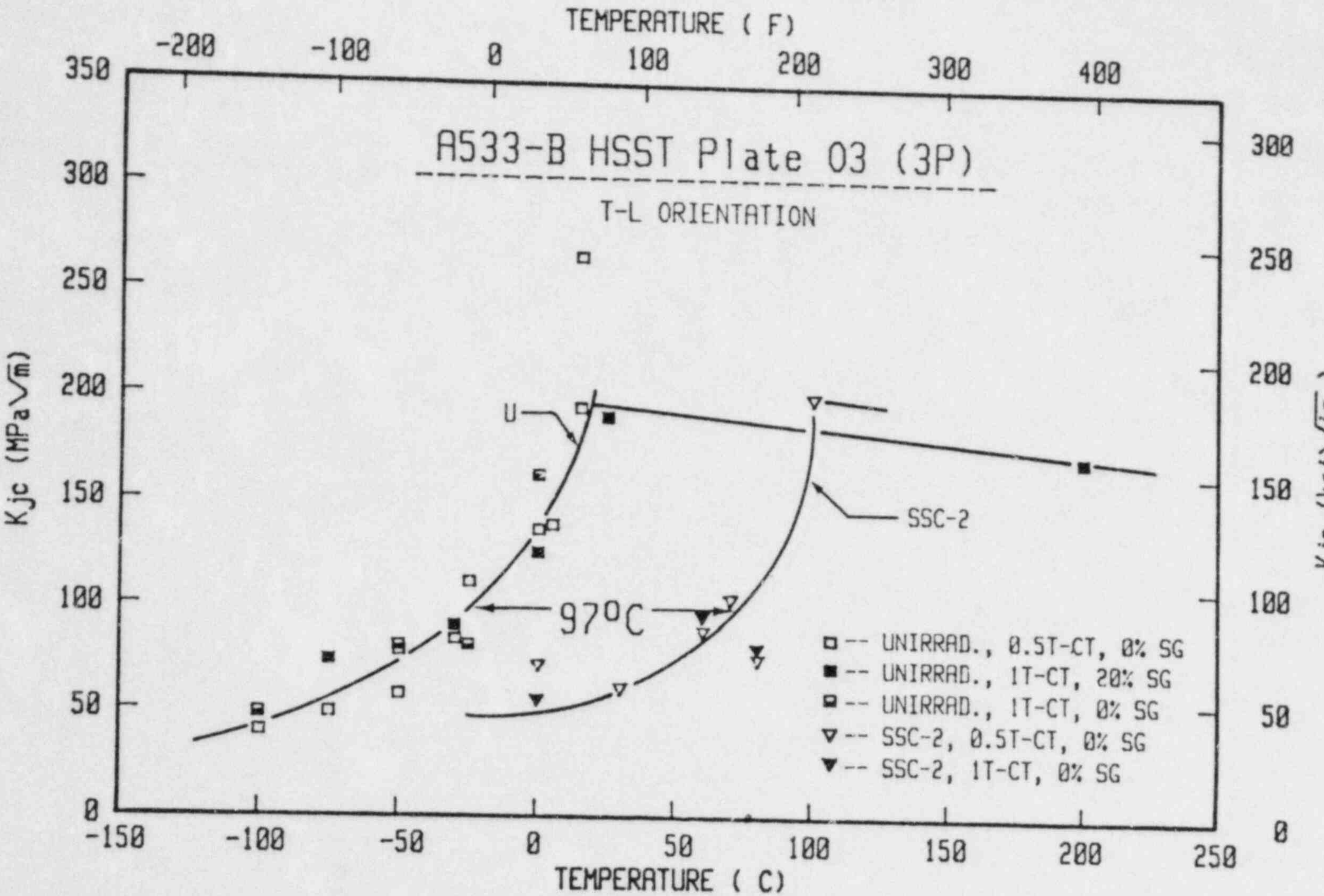

Fig. B.17 Initiation fracture toughness of A533-B plate before and after irradiation in capsule SSC-2.

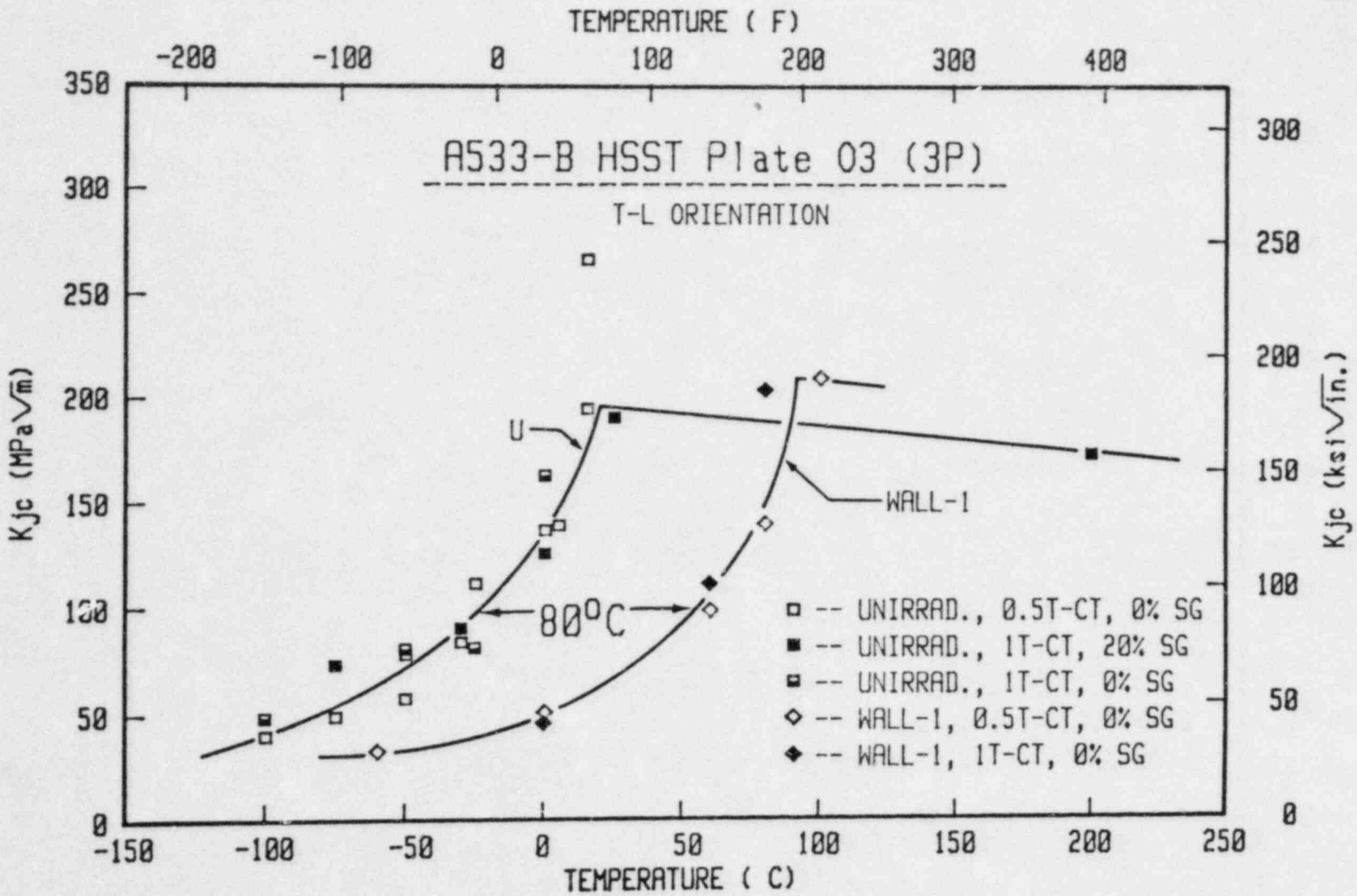

Fig. B.18 Initiation fracture toughness of A533-B plate before and after irradiation in capsule Wall-1.

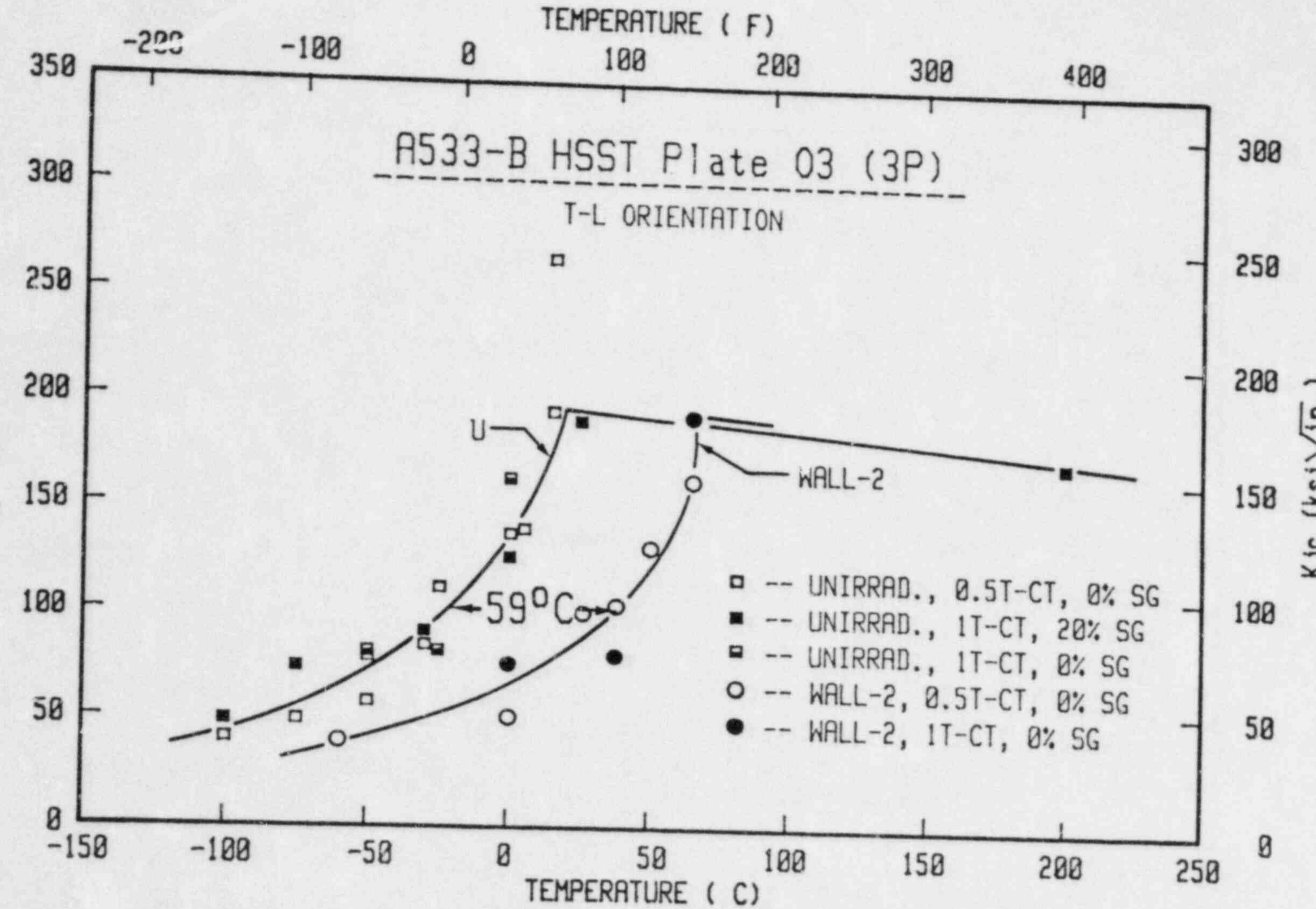

Fig. B.19 Initiation fracture toughness of A533-B plate before and after irradiation in capsule Wall-2.

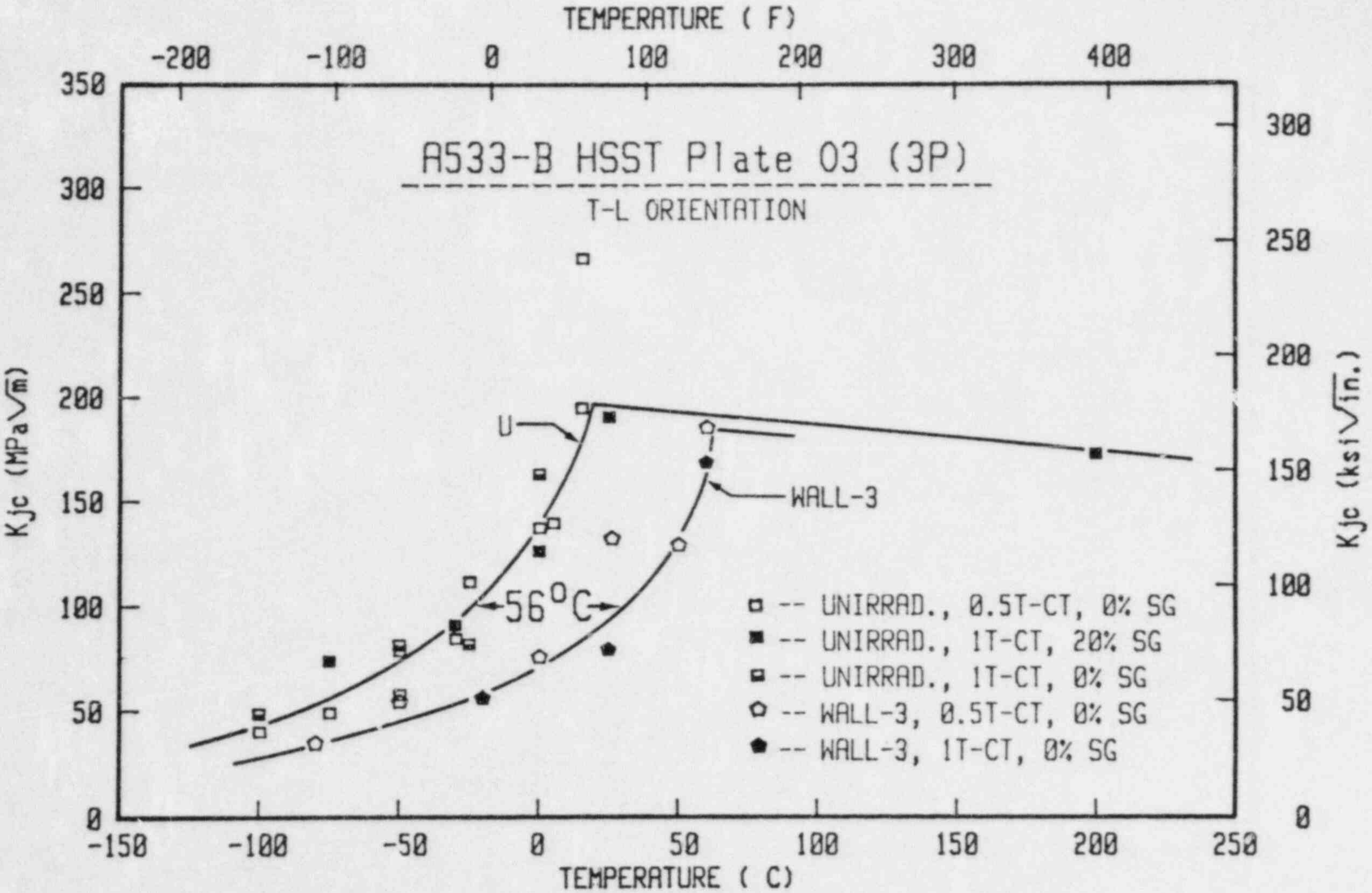

Fig. B.20 Initiation fracture toughness of A533-B plat before and after irradiation in capsule Wall-3.

NRC FORM 335 (11 81)

U.S. NUCLEAR REGULATORY COMMISSION

BIBLIOGRAPHIC DATA SHEET

1. REPORT NUMBER (Assigned by DDC)
NUREG/CR-3295
MEA-2017
Vol. 1

2. (Leave blank)

3. RECIPIENT'S ACCESSION NO.

4. TITLE AND SUBTITLE (Add Volume No., if appropriate)
Light Water Reactor Pressure Vessel Surveillance Dosimetry Improvement Program: Notch Ductility and Fracture Toughness Degradation of A302-B and A533-B Reference Plates from PSF Simulated Surveillance and Through-Wall Irradiation Capsules

5. DATE REPORT COMPLETED
MONTH May YEAR 1983

7. AUTHOR(S)
J. R. Hawthorne, B. H. Menke, and A. L. Hiser

DATE REPORT ISSUED
MONTH April YEAR 1984

9. PERFORMING ORGANIZATION NAME AND MAILING ADDRESS (Include Zip Code)
Materials Engineering Associates, Inc.
9700B George Palmer Highway
Lanham, Maryland 20706

UNDER SUBCONTRACT TO:
ENSA, Inc.
3320 Bailey Avenue
Buffalo, New York 14215

6. (Leave blank)

8. (Leave blank)

12. SPONSORING ORGANIZATION NAME AND MAILING ADDRESS (Include Zip Code)
Division of Engineering Technology
Office of Regulatory Research
U.S. Nuclear Regulatory Commission
Washington, D. C. 20555

10. PROJECT/TASK/WORK UNIT NO.

11. FIN NO.
NRC FIN B8133

13. TYPE OF REPORT
Technical Report

PERIOD COVERED (Inclusive dates)

15. SUPPLEMENTARY NOTES

14. (Leave blank)

16. ABSTRACT (200 words or less)
The NRC's Light Water Reactor-Pressure Vessel Surveillance Dosimetry Program has irradiated Charpy-V (C_v), compact tension (CT) and tension test specimens of selected steels at 288°C in a pressure vessel wall/thermal shield mock-up known as the Pool Side Facility. Objectives include the study of through-wall toughness gradients produced by irradiation, the relative irradiation effect at surveillance capsule vs. in-wall locations and the correspondence of C_v vs. CT fracture toughness test methods in their independent descriptions of radiation-induced embrittlement. This report presents properties data developed for two steels: the ASTM A302-B reference plate and the HSST Program A533-B Plate 03.

Irradiation at the simulated surveilance location reproduced reasonably well the irradiation degradation developed at the vessel inner surface and quarter wall thickness locations. The radiation-induced toughness gradient was small; the difference between transition temperatures at the inner surface vs. mid-wall locations was 31°C or less, independent of the test method. The temperature elevation of the C_v curve (41 J level) with irradiation was generally less than that defined by fracture toughness tests (100 MPa$\sqrt{m}$ level) but greater than defined by "β_{Ic}-corrected" data.

17. KEY WORDS AND DOCUMENT ANALYSIS

A302-B Steel
A533-B Steel
Fracture Resistance
Fracture Toughness
Low Alloy Steels
Notch Ductility

17a. DESCRIPTORS

Nuclear Reactor Pressure Vessels
J-R Curve
Radiation Embrittlement
Radiation Sensitivity
Reactor Vessel Surveillance
Specimen Size Effects

17b. IDENTIFIERS/OPEN-ENDED TERMS

18. AVAILABILITY STATEMENT
Unlimited

19. SECURITY CLASS (This report)
Unclassified

20. SECURITY CLASS (This page)
Unclassified

21. NO. OF PAGES

22. PRICE
S

NRC FORM 335 (11 81)

UNITED STATES
NUCLEAR REGULATORY COMMISSION
WASHINGTON, D.C. 20555

OFFICIAL BUSINESS
PENALTY FOR PRIVATE USE, $300

FOURTH CLASS MAIL
POSTAGE & FEES PAID
USNRC
WASH D C
PERMIT No G 67